Study on the formation behavior of FeN nano-structure on surface of Si(111)-7×7-CH_3OH

Si(111)-7×7-CH_3OH 表面における FeN ナノ構造の形成過程に関する研究

Wenxin Li

Saitama Institute of Technology

February, 2019

Table of Contents

Abstract

In recent years, metal clusters and metallic compounds grow on the surface of silicon which are promising for low cost high density devices. In this study, Fe atoms were deposited on the Si(111)-7×7 surface, which has been saturated with the CH_3OH molecules. Atomic linear structure was composed of stable clusters and in-situ observed by the scanning tunneling microscopy (STM). Then, aim to greatly enhance the magnetic strength of the memory units, nitriding experiments were implemented on the existing Fe clusters. This study has three main purposes: (a) Explore the specific adsorption process of methanol as an intermediate layer, as well as establish its suitable model for metal adsorption; (b) Establish several pure iron cluster models, and identify their properties like magnetic and stability; (c) Adjust the nitriding process, further optimize iron-nitride clusters as applied magnetic storage units. The first chapter discusses the background of the atomic level technologies and smart materials industry. Introduce Si(111)-7×7 as important substrate material, and expounds the existing problems and the research purpose of this paper. In the second chapter, by comparing and analyzing the adsorption of various alcoholic gases, the optimal model of the intermediate layer was established, which laid the foundation for metal deposition later. Chapter 3 focuses on the Fe clusters. Different cluster structures were adjusted by different steaming temperature, and their performance were analyzed and evaluated, respectively. In Chapter 4: After the initial nitridation, the formation process of magnetic units was adjusted and optimized according to the observed deficiencies. Several iron-nitride models were established, which laid the foundation for high-density storage. Finally, conclusions and exposition of the dissertation were given in Chapter 5, and some future research directions were also proposed.

Chapter 1 Introduction

1.1 Development of atomic level technologies and smart materials industry

In the process of human social development, the level of material development has always been a sign of age and social civilization. With the rapid development of the smart materials industry, the size of electronic components and devices becomes smaller and smaller [1,2]. Accordingly, thin film materials are given high expectations, such as the regular structure of metal clusters and the high-density of memory units [3-5]. In recent years, atomic level technologies have increased the interest of researchers [6]. The 2016 Nobel Prize in chemistry was awarded to Jean-Pierre Sauvage, J. Fraser Stoddart and Bernard L. Feringa for "inventing molecular machines that can move in a controlled manner and perform tasks when given energy" [7]. The development of atomic level technology has led to the miniaturization of the technological revolution. That year's Nobel Prize in chemistry has brought Physical/Chemistry research into a new field. Using energy to control the movement of molecules, atomic technology has made scientific research out of the stalemate. From a developmental point of view, molecular machines for us are like motors for people in the nineteenth century. They didn't know that these coils and magnets would become trams, washing machines, fans and so on. Molecular machines can be useful in future new materials, sensors and energy storage systems.

According to the basic principles of material science and related disciplines, the parameters and processes of material preparation are designed and simulated, so as to figure out the relationship between macro performance and micro structure. At the macro level, if millions of molecular components work together, several typical properties of the material can indeed be altered [8, 9]. New smart materials will be embedded with molecular switches as well as similar molecular system, so as to step

into business applications. For example, the Nissan scratch-proof iPhone case [10], introduced in 2012, is based on work of professor Ito Kozo in the university of Tokyo. The material it used is made from a polymer chain that passes through a number of the rings, forming an "eight" shape. When a common polymer coating is subjected to pressure, the connections between the polymer chains are broken, resulting in scratches. But in this material, the cyclodextrins allow the polymer chain to slide smoothly under stress without damage. A film made of this material can even keep the phone's screen from breaking under the hammer. All of these cases mean that the molecular parts of atomic technology are mature enough to apply. Since the research of this field has experienced a long way, now it is the time to prove that they are useful to the world.

Based on the characteristics of the surface properties and the types of surface information to be obtained, surface analysis can be divided into: surface topography analysis, surface composition analysis, surface structure analysis, electronic state analysis and atomic state analysis. There may be several methods for the same analysis purpose, and each method has its own characteristics (advantages and disadvantages). With the progress of surface testing technology, especially the application of scanning tunneling microscope (STM) and atomic force microscope (AFM) [11, 12], more and more interesting dynamic phenomena on the solid surface have been found. The basic principle of scanning tunneling microscopy (STM) is to use a very fine probe (atomic level) and the surface of the studied material as two electrodes. When the distance between the sample and the probe tip is very close (usually less than 1nm), electrons will pass through the barrier between the two electrodes under the influence of the electric field. Atomic force microscopy (AFM) is a kind of microscopic technology similar to STM [13-15]. The height of the sample surface can be directly converted by the force value of the microprobe, and the surface topography of the sample can be obtained. As shown in Tab. 1.1, the main difference between them is that the scanning tunneling microscopy detects the tunnel current between the tip and the sample, while the atomic force microscopy detects the force between the tip and the sample.

Table. 1.1 Comparison of several detection equipments and their functions

Equip ment	Resolution	Working environment	Operating temperature	Sample damage	Detecting depth
STM	Atoms can be observed directly. Horizontal resolution: 0.1 nm Vertical resolution: 0.01 nm	Atmosphere, solution, vacuum	Low temperature, room temperature, high temperature	None	1-2 atomic layer
TEM	Horizontal resolution: 0.3-0.5 nm Horizontal lattice resolution: 0.1 nm - 0.2 nm Vertical resolution: none	High vacuum	Low temperature, room temperature, high temperature	Medium	Equal to sample thickness (<100 nm)
SEM	Using secondary electron imaging. Horizontal resolution: 1-3 nm Vertical resolution: low	High vacuum	Low temperature, room temperature, high temperature	Slight	1 μm
FIM	Horizontal resolution: 0.2 nm Vertical resolution: low	Ultra high vacuum	30-80 K	Serious	Atomic thickness
AES	Horizontal resolution: 6-10 nm Vertical resolution: 0.5 nm	Ultra high vacuum	Low temperature, room temperature	Serious	2-3 atomic layer

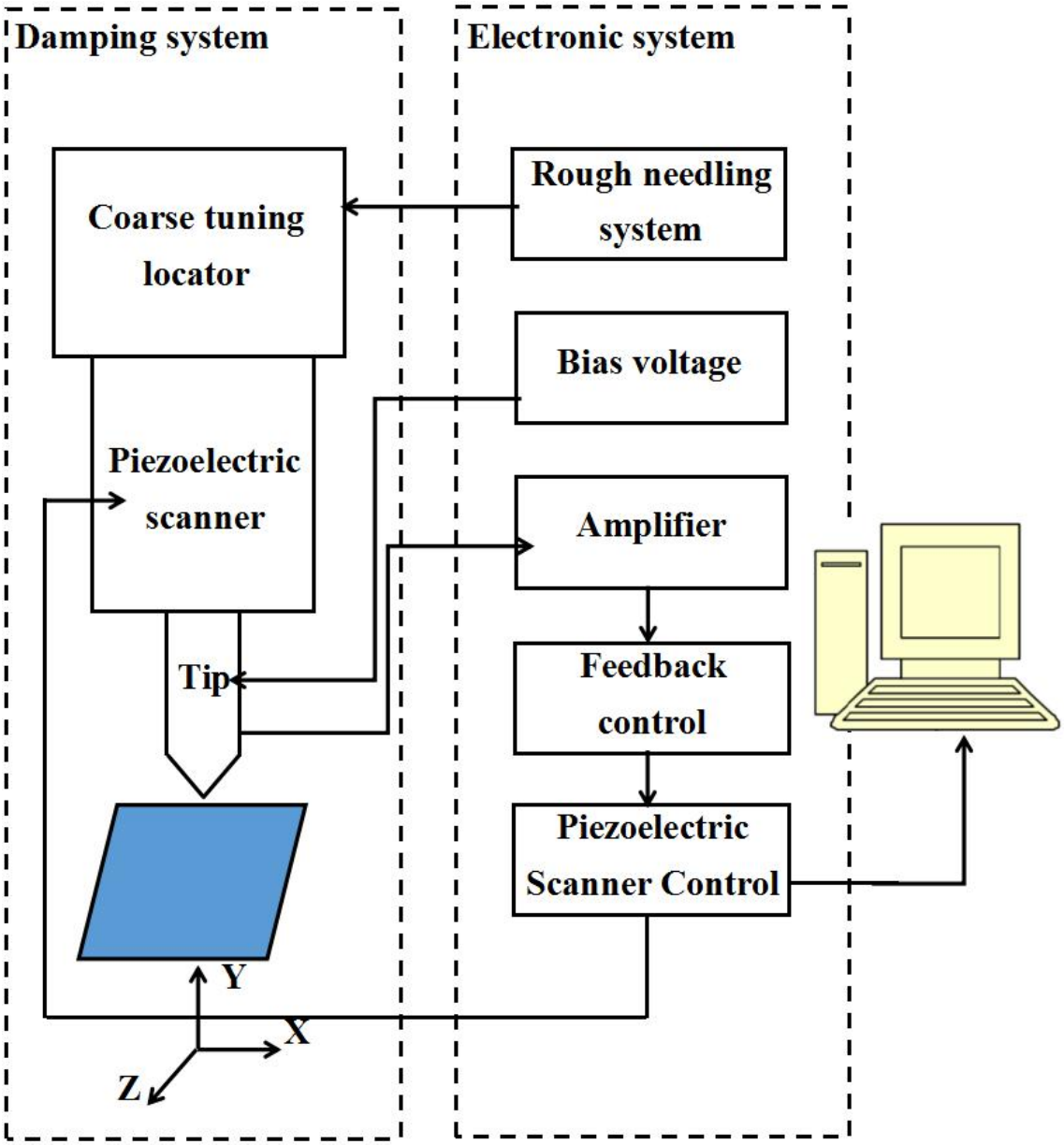

Fig. 1.1 The basic structure diagram of STM

Compared with the analysis technology such as TEM, SEM [16, 17], scanning tunneling microscopy (STM) has the following features:

(1) The system of STM has a simple structure.

(2) Experiments can be carried out in a variety of environmental, such as atmosphere, ultra high vacuum or liquid (including in the insulating fluid and electrolyte).

(3) A wide working temperature range, which can be changed from mK to 1100 k.

This wide range is any other kinds of microscopy techniques unable to achieve at present.

(4) High resolution. The scanning tunneling microscope has horizontal/vertical resolution of 0.1 nm and 0.01 nm, respectively. Therefore, individual atoms on the surface of the material can be directly observed, as well as their three-dimensional image.

(5) In the observation process of material surface structure, the sample can also be studied with scanning tunneling spectroscopy (STS). So that, chemical structure and electronic state of the material surface can be known.

(6) Unable to detect deep information and can not observe insulators directly.

A sharp metal probe is used to scan the sample surface. By using the quantum tunneling effect of the nanometer gap between the tip and sample, the tunnel current and the gap size show an exponential relationship, and the surface topography features of atomic samples are obtained. Scanning tunneling microscopy (STM) can be used to directly observe whether the surface atoms of materials have periodic surface structural characteristics, surface reconstruction and structural defects (Fig. 1.2).

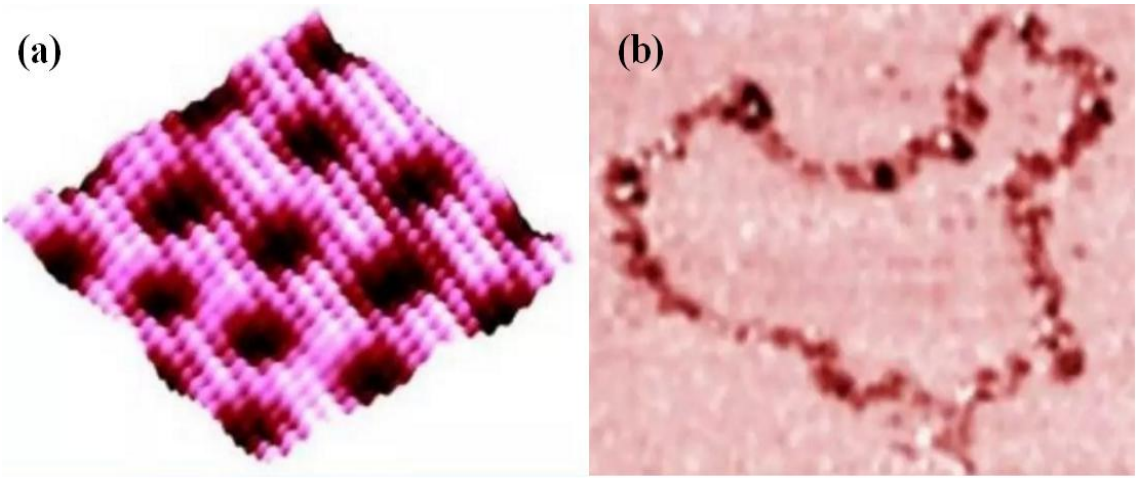

Fig. 1.2 (a) STM image of sulfate ions adsorbed on the surface of single copper crystal (111) in electrolyte; (b) A map of China using graphite processing technology to remove carbon atoms on the surface of graphite.

The future development of this field should start from two aspects: At the micro level, these molecular machines can complete the tasks that cannot be completed by other means; At the macro level, trillions of atomic-scale components are used to reshape material properties. For example, some components are made to raise something much heavier than themselves, like ants. So that, when the concentration of metal atomic adsorption was low, researchers usually explored the single atom mechanism on the substrate (Fig. 1.3) [18, 19]. By contrast, the application of thin film adsorption was studied at higher concentration [20]. Since the specific cluster models were not clear, the formation process between the two subjects could not be accurately controlled [21]. In recent years, researches around the different compounds or clusters have increased the interest of researchers [22].

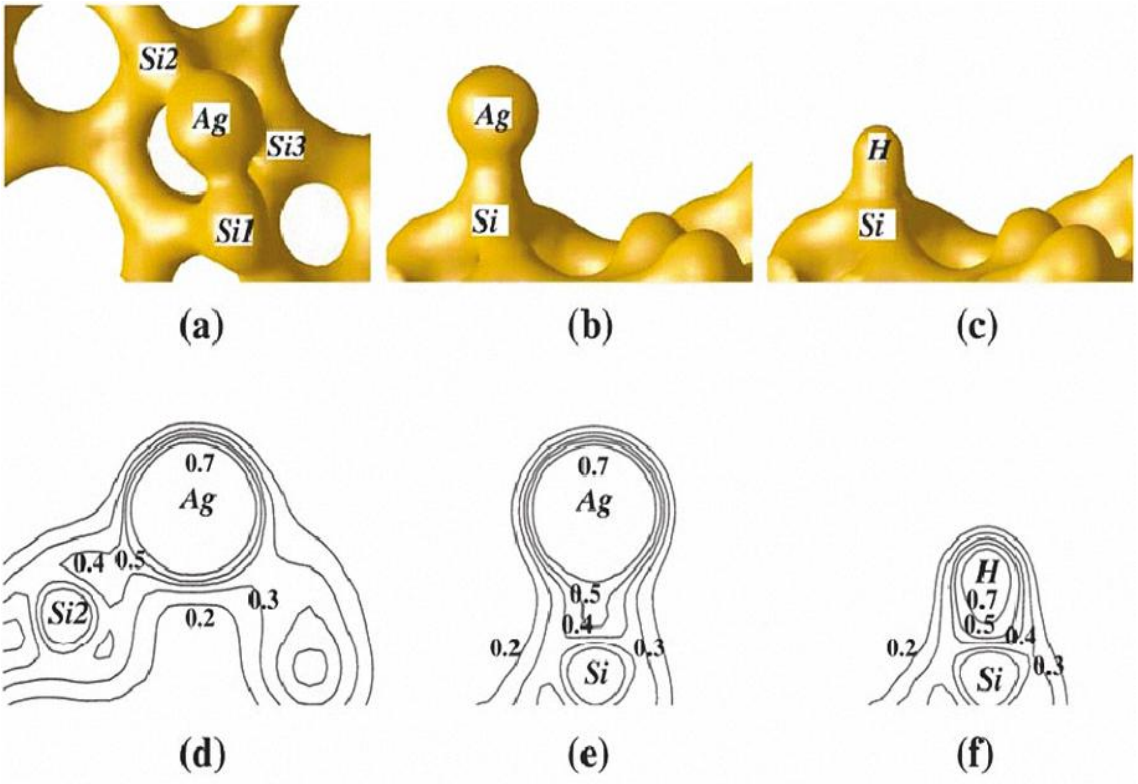

Fig. 1.3 (a) and (b) are schematic diagrams of the positions of individual silver atoms above different silicon substrate. (c) is a schematic diagram of the position of hydrogen atoms on the Si(111) surface. (d) – (f) are the corresponding charge density contours in the cross section of the bonds (e/Å^3).

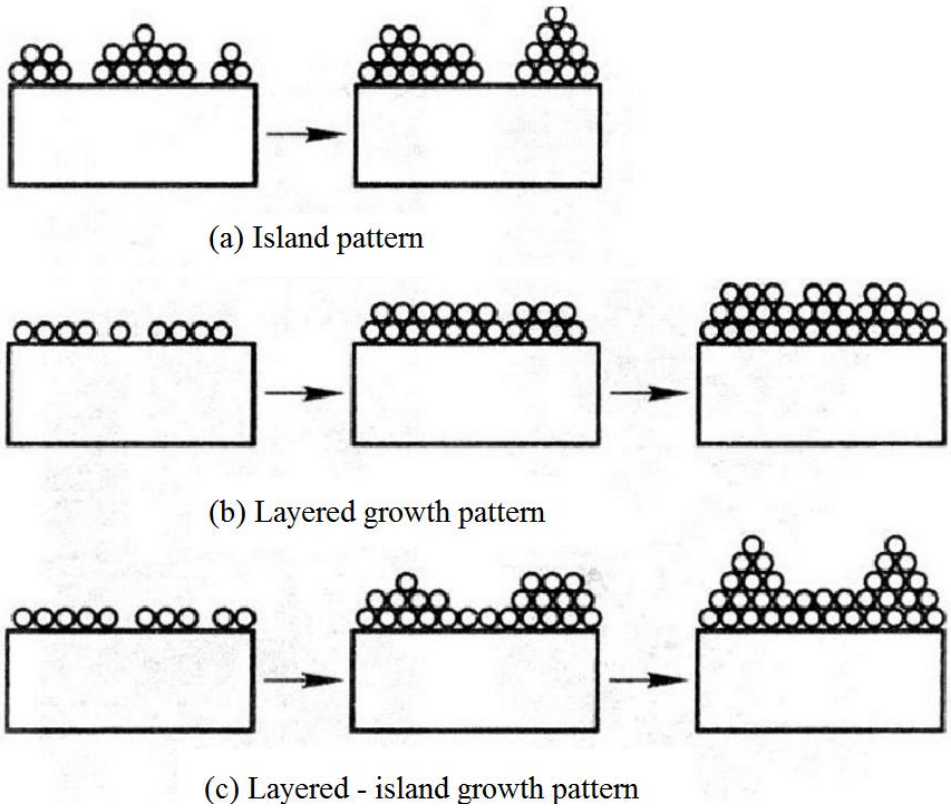

Fig. 1.4 Three different film growth patterns

Unlike the bulk material, thin film material is a layer of material deposited or prepared on the surface by special methods, as shown in Fig. 1.4. Thin film materials are valued because it usually has special performance or combination performance [23, 24]. The key part of film science is the study of the growth process of film, which can be divided into three patterns [25, 26].

(1) Island pattern

At the initial stage of film formation, the core is formed according to the three-dimensional nucleation mode, and the stable core grows into isolated islands. The islands are then merged into continuous films, such as Au films on SiO_2 substrate. In this growth mode, atoms or molecules of sediment tend to bond with each other rather than with substrate atoms. That is, the wettability between the deposited material and the substrate is weak.

(2) Layered growth pattern

When the wettability between the deposition and the substrate is good, the atoms tend to bond with the substrate atoms. From the initial stage of film formation, the films have been grown in a two-dimensional expansion mode, such as Si films on Si substrates. In this mode, there is no significant stage of nucleation. Each layer is automatically spread on the surface of the substrate or film to reduce the total energy of the system.

(3) Layered - island growth pattern

In the initial stage of film formation, several layers were formed according to the two-dimensional layered growth. After that, the growth mode was transformed into island mode, such as Ag films on Si substrates. The physical mechanism leading to this mode transition is quite complex, and the fundamental reason can be attributed to the growth and decline of various energy in the process of film growth. For example, due to the mismatch of lattice constants between thin films and substrates, in order to reduce strain energy, island mode is transformed into island mode, and so on.

World's new material industry is at a stage of development from low level to high level, with a wide range of application scope [27-29]. In the process of communication and cooperation, smart materials industry presents a rapid development trend, especially in some key areas. Significant results have been achieved in development potential, environmental protection and resource utilization. With the rapid development of the world's social economy, emerging industries have been constantly optimized and upgraded. As a result, the demand for new smart materials is constantly expanding in all markets. At present, new materials have accounted for 15-20% of the output value of high-tech industries in developed countries. Its research/development capacity and industrialization scale have evolved into the important measurement of one country's overall economic and social development as well as national defense strength. However, there are still serious problems in the innovation process of new materials.

In this paper, a cross-section of new material, namely nanomaterial, is selected to specifically discuss the problems in the innovation process [30, 31].

(1) Definition of smart material industry

As the smart material industry was initially formed in the middle and late last century and newly developed in the beginning of this century, there is no clear and stable concept definition of new material industry. However, there should be a relatively unified and rigorous logical starting point for research. In this paper, intelligent material was divided into two categories:

(Ⅰ) Embedded smart materials, also known as smart material structure or intelligent material system. On the substrate material, three types of materials are embedded, including sensor, motion and control functions. Sensor components collect and detect the information given by the external environment. The control processor is responsible for directing and motivating the motion components, so the corresponding actions are executed.

(Ⅱ) The micro-structure itself has intelligent features. The performance can be carried out with changes in environment, time and so on. For example, a smart gel based on light/chemical signals may be used to produce an adjustable lens or sensor. Some similar products are also popular, such as filters, InP semiconductors, etc.

(2) Comparison between materials and smart materials

It is particularly important to note the differences between materials and new materials. Materials are substances that can be directly used to make objects, components or devices [32]. Compared with traditional materials, new materials industry is characterized by high technology density, high investment in research and development, high added value of products, strong international production and market, wide application range and good development prospect. etc. Smart materials industry, including new materials and related technical products/equipments. Specifically, it mainly includes three aspects: (Ⅰ) the industry formed by new materials itself; (Ⅱ) the manufacturing of new materials technology and equipment; (Ⅲ) the improvement of traditional materials technology Industry, etc.

(3) Nano-material technology and its innovation process

In addition to develop the basic research, some nano-material technologies have

begun to enter the stage of industrialization, especially in the transformation of traditional and nano-composite materials. At the same time, the transformation of nano-material technology from manufacturing to industrialization has been realized step by step. The innovation process of nano-material industry and even the whole smart material industry is different from that of general industry. It is not only a progressive innovation in a certain field, but also a process of bringing new changes to multiple applications. With the development of technology, nanotechnology has gradually stepped down from the altar of gods. From the initial advanced industry, nanomaterial gradually expands to the field of cosmetics, textiles and the like, which is more closely related to the life of people.

Magnetic storage or magnetic recording stores data on magnetized media [33,34]. Using different patterns of magnetisation in a magnetisable material, it can be designed as a form of non-volatile memory [35, 36]. Moreover, the information is accessed by using one or more read/write heads. As of 2017, magnetic storage media (mainly hard disks) are widely used to store computer data, audio and video signals. Especially in the field of computing field, magnetic storage is preferred. The read-and-write head is used to detect and modify the magnetisation of the storage unit immediately. Based on the phenomenological theory of ferromagnetic material, the conception of magnetic domain was first proposed in 1907 [37]. And the structure of magnetic domain based on the interaction of the magneto-static energy was proposed by L. D. Landau and E. M. Lifshitz in 1935 [38]. The magnetic surface is conceptually divided into many small sub-micrometer-sized magnetic regions, referred to as magnetic domains. Although not in a rigorous physical sense, these magnetic domains have a mostly uniform magnetisation. Due to the polycrystalline property of the magnetic material each of these magnetic regions is composed of a few hundred magnetic grains. Magnetic grains are typically 10 nm in size, forming a single magnetic domain. As a result, each magnetic region would form a magnetic dipole, producing a magnetic polarity.

There are two magnetic polarities, which is used to represent 0 or 1, respectively.

In older hard disk drive (HDD) designs, storage areas were oriented horizontally and parallel to the disk surface, as shown in Fig. 1.5. However, since 2005, the direction has been changed to the vertical direction to ensure closer domain spacing [39-41]. When the film is thin enough, it can be seen as a two-dimensional material. Accordingly, under the action of surface effect, it has different properties from bulk material. It was found that when the thickness of magnetic layer decreased to nanometer level, the relation between magnetic strength and temperature of multilayer films gradually transited to linear. Critical temperature increases with the increase of film thickness, which is tending to the value of the block material. With the popularization of computer technology, it is increasingly important to develop mass storage technology [42]. Magnetic storage is the most commonly used method of mass storage. As the information storage material, the most important feature is that the information must be stored for a long time, requiring that the storage state must be stable. The unique vertical anisotropy produced by the magnetic anisotropy of one-dimensional magnetic materials can be recorded in a vertical mode. Since it can overcome the theoretical limit of horizontal recording mode, high-density storage would be realized. After that, nanowire arrays became the focus of research at that time. As a vertical magnetic recording medium, magnetic nanowires need not only vertical anisotropy (that is, the direction of easy magnetization is perpendicular to the surface), but also high coercivity and remanence ratio. Fe, Co, Ni, Cu and their alloys are widely used. Specifically, the hysteresis loop of the material shows a large rectangular ratio. In this way, the influence of the demagnetization between the nanowires is very small. A single nanowire can be designed close to other nanowires without the drawback of demagnetism. Thus, the unit storage density of magnetic recording is greatly improved. So that, it has attracted extensive attention in the academic field.

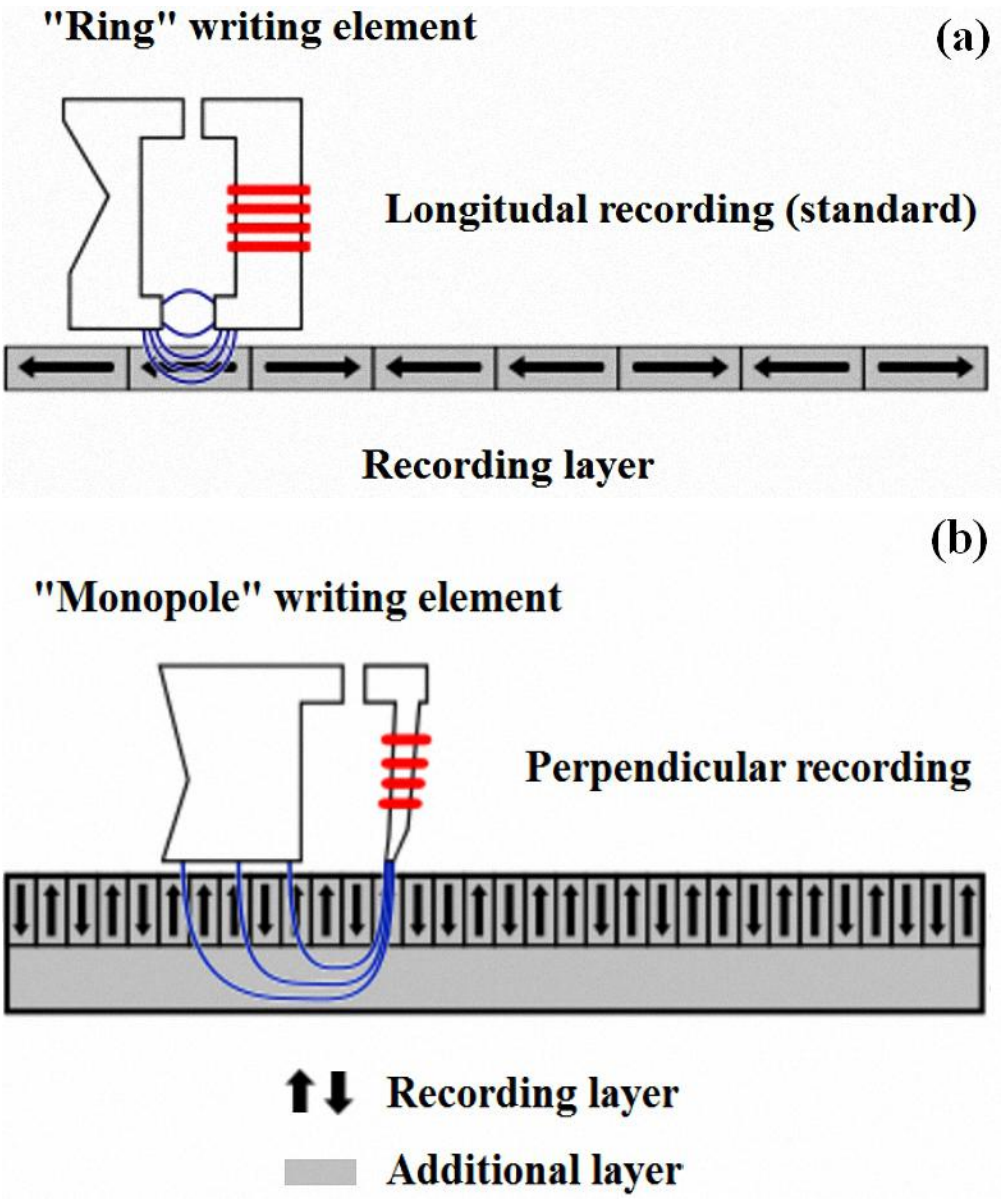

Fig. 1.5 Structure diagrams of (a) longitudal recording and (b) perpendicular recording.

Some achievements have been made in the research of one-dimensional magnetic nanowires, it will also be the development trend of magnetic recording in the future. In recent years, metal films have attracted more and more interest due to their potential applications in ultra-high density magnetic recording medium, magneto-optical recording medium, thin film magnetic head and sensor [43, 44]. Recently, it was found that the particles change to single-domain magnetic clusters by

decreasing their size [45-47]. Accordingly, the preparation of single magnetic domain clusters is an interesting challenge to magnet materials for high-density magnetic recording medium. So far, the reported critical sizes for single magnetic domains were 85 nm for Ni, 40 nm for Fe_3O_4, and 16 nm for α-Fe [45-47], and the cluster with a size lower than the critical value displays super paramagnetism, which could not be applied for the magnetic recording medium. To improve the density of magnetic recording without the restriction of super paramagnetism, it is necessary to prepare the single magnetic domain clusters with limited critical size. Human research on iron nitride material has a long history, which was first discovered in the hardened layer of nitriding treatment on steel surface. The systematic study of gasified iron began in 1928, when the structure of iron-nitride was studied by X-ray diffraction. Subsequently, the magnetism of iron-nitride was experimentally studied in 1930. Finally, in 1946, γ'-Fe_4N was found to have a large saturation magnetic moment after. The series of iron-nitride compounds began to attract widespread attention. From this view point, FeN single magnetic domain clusters have become the research focus, which could be analyzed for the spin in physics, ontrollable surface reaction in chemistry, for example, FeN and FeOx with the critical size lower than 10 nm.

1.2 Purpose of this research

Nano-magnetic materials are one of the most important research fields in the world. At present, there are many kinds of nano-magnetic materials, such as ferrite, γ-Fe_2O_3, Fe_3O_4, $BaFe_{12}O_9$, metal magnetic powder, rare earth alloy and iron-nitride have been successfully prepared in granular magnetic materials. Crystallizing semiconductor nanowires and thin films at room temperatures by using catalytic behavior of metals has become an increasingly active field of research1. Accordingly, thin film materials are also given higher expectations, such as the thinner thickness of atomic linear structure, the higher density of storage units, etc. In recent years, metal clusters and metallic compound grow on the surface of silicon which are promising for low cost high density devices. In this paper, the meticulous preparation of a

regular structure is desired not only for the fundamental studies, but also for the application of high-density magnetic memory thin film. The Fe clusters were prepared by many techniques [48-51]. Magnetic units are adsorbed on the surface of substrate, forming a stable arrangement. Taking advantage of strong magnetism, the atomic structure of Fe was considered in this study. In order to improve the density of magnetic storage unit, the iron cluster are formed as well as their multi-layer model. However, since the magnetic property of existing Fe compounds is weak, this study tried to nitride it with adsorption gas. Concerning the stability of the iron compound in the nitrogen and oxygen environment, this paper tends to focus on NH_3 gas. Using mass spectrometer and gas adsorption device, the previous hypothesis is confirmed. Methanol and ammonia have similar adsorption mechanism, and the specific process can be defined. As discussed in a previous breaking gas, the ammonia synthesis reaction on Fe catalysts is catalyzed by a cyclic process consisting of the formation of the quasi-compound Fe_xNH_y and its rapid change to Fe_xN. When the concentration is relatively high, although FexN compounds continue to grow steadily on the surface of Si(111)-7×7-CH_3OH, the linearity of them is quite confusing. By adjusting the concentration of ammonia, the preliminary formation stage of iron-nitride compounds has been figured out. In particular, some specific classifications, including the concept of precursor compounds could to be verified and summarized. Different formation mechanism corresponds to different cluster shapes, the most suitable growth pattern could be found with the 3D images of STM. As a result, the thickness of iron clusters was confirmed to be the key to the dissociation process. With the introduction of Ar, the adverse influence of metal deposition was solved effectively. As a result, 2 typical Fe_3N_x models have promoted the formation rate of the stable structure greatly. Finally, considering the growth of each cluster, the interaction of N atom to Fe atoms would be explored. Referring to previous literature and scanning outcomes, the stable width is controlled less than 10 nm. Referring to magnetic result, the relationship between linearity and magnetic intensity should be deduced. It is proved that our new linear iron-nitride clusters can still maintain good stability with the improvement of nitriding efficiency. From the application point of view, the stable linear cluster structure has

replaced the original surface metal structure, laying a good foundation for the development of high-density storage ultrathin film.

Reference

1 Seminario, J.M. Molecular Electronics Approaching Reality. Nat. Mater. 2005, 4, 111–113.

2 Quapp, W. A minimal 2D model of the free energy surface for a unidirectional natural molecular motor. J. Math. Chem. 2018, 56, 1339–1347.

3 Alam, K.; Disseler, S.M.; Ratcliff, W.D.; Borchers, J.A.; Ponce-Pérez, R.; Cocoletzi, G.H.; Smith, A.R. Structural and magnetic phase transitions in chromium nitride thin films grown by RF nitrogen plasma molecular beam epitaxy. Phys. Rev. B 2017, 96, 104433.

4 Zygmanski, P.; Sajo, E. A self-powered thin film radiation detector using intrinsic high energy current. Med. Phys. 2016, 43, 4–15.

5 Bartolomé, J.; Bartolomé, F.; Brookes, N.B.; Sedona, F.; Basagni, A.; Forrer, D. Reversible Fe magnetic moment switching in catalytic oxygen reduction reaction of Fe-phthalocyanine adsorbed on Ag(110). J. Phys. Chem. C 2015, 119, 12488–12495.

6.Warner, B.; Gill, T.G.; Caciuc, V.; Atodiresei, N.; Fleurence, A.; Yoshida, Y.; Hirjibehedin, C.F. Guided Molecular Assembly on a Locally Reactive 2D Material. Adv. Mater. 2017, 29, 1703929.

7 Sauvage, J. P., Stoddart, J. F., & Feringa, B. L. (2016). The noBel prize in chemisTry 2016. The UKRAINIAN, 138.

8 Walsh, C. (2000). Molecular mechanisms that confer antibacterial drug resistance. Nature, 406(6797), 775.

9 Tour, J. M. (2000). Molecular electronics. Synthesis and testing of components. Accounts of Chemical Research, 33(11), 791-804.

10 Ball, P. (2015). Material witness: Concrete mixing for gorillas. Nature materials, 14(5), 472.

11 Y. Sugimoto, Y. Nakajima, D. Sawada, et al., Simultaneous AFM and STM measurements on the Si (111)−(7×7) surface, Phys. Rev. B 81 (2010): 245-322.

12 J. L. Webb, O. Persson, K. A. Dick, et al., High resolution scanning gate

microscopy measurements on InAs/GaSb nanowire Esaki diode devices, NANO. RES. 7.6 (2014): 877-887.

13 Hansma, P. K., Elings, V. B., Marti, O., & Bracker, C. E. (1988). Scanning tunneling microscopy and atomic force microscopy: application to biology and technology. Science, 242(4876), 209-216.

14 Tseng, A. A., Notargiacomo, A., & Chen, T. P. (2005). Nanofabrication by scanning probe microscope lithography: A review. Journal of Vacuum Science & Technology B: Microelectronics and Nanometer Structures Processing, Measurement, and Phenomena, 23(3), 877-894.

15 Magonov, S. N., & Whangbo, M. H. (2008). Surface analysis with STM and AFM: experimental and theoretical aspects of image analysis. John Wiley & Sons.

16 Grabulov, A., Ziese, U., & Zandbergen, H. W. (2007). TEM/SEM investigation of microstructural changes within the white etching area under rolling contact fatigue and 3-D crack reconstruction by focused ion beam. Scripta Materialia, 57(7), 635-638.

17 Stevie, F. A., Vartuli, C. B., Giannuzzi, L. A., Shofner, T. L., Brown, S. R., Rossie, B., ... & Purcell, B. M. (2001). Application of focused ion beam lift‐out specimen preparation to TEM, SEM, STEM, AES and SIMS analysis. Surface and Interface Analysis: An International Journal devoted to the development and application of techniques for the analysis of surfaces, interfaces and thin films, 31(5), 345-351.

18 T. Hashizume, K. Motai, Y. Hasegawa, et al., Alkali metal adsorption on the Si (111) 7×7 surface, J. VAC. SCI. TECHNOL. B 9.2 (1991): 745-747.

19 Q. Liu, Q. Fu, X. Shao, et al., Diffusion of single Au, Ag and Cu atoms inside Si (111)-(7×7) half unit cells: A comparative study, APPL. SURF. SCI. 401 (2017): 225-231.

20 Z. Zhang, M. G. Lagally, Atomistic processes in the early stages of thin-film growth, SCIENCE 276.5311 (1997): 377-383.

21 R. L. Puurunen, Surface chemistry of atomic layer deposition: A case study for the trimethylaluminum/water process, J. APPL. PHYS. 97 (2005): 9.

22 S. V. Sitnikov, A. V. Latyshev, S. S. Kosolobov, Advacancy-mediated atomic steps kinetics and two-dimensional negative island nucleation on ultra-flat Si (111) surface, J. CRYST. GROWTH. 457 (2017): 196-201.

23 Freund, L. B., & Suresh, S. (2004). Thin film materials: stress, defect formation and surface evolution. Cambridge University Press.

24 Eason, R. (2007). Pulsed laser deposition of thin films: applications-led growth of functional materials. John Wiley & Sons.

25 Ohring, M. (2001). Materials science of thin films. Elsevier.

26 Thompson, C. V. (1990). Grain growth in thin films. Annual review of materials science, 20(1), 245-268.

27 Smith, R. C. (2005). Smart material systems: model development (Vol. 32). Siam.

28 Leo, D. J. (2007). Engineering analysis of smart material systems. John Wiley & Sons.

29 Shrouf, F., Ordieres, J., & Miragliotta, G. (2014, December). Smart factories in Industry 4.0: A review of the concept and of energy management approached in production based on the Internet of Things paradigm. In Industrial Engineering and Engineering Management (IEEM), 2014 IEEE International Conference on (pp. 697-701). IEEE.

30 Klabunde, K. J., & Richards, R. M. (Eds.). (2009). Nanoscale materials in chemistry. John Wiley & Sons.

31 Silberglitt, R., Antón, P. S., Howell, D. R., & Wong, A. (2006). The global technology revolution 2020, executive summary: Bio/nano/materials/information trends, drivers, barriers, and social implications. Rand Corporation.

32 Akhras, G. (2000). Smart materials and smart systems for the future. Canadian Military Journal, 1(3), 25-31.

33 Thompson, D. A., & Best, J. S. (2000). The future of magnetic data storage technology. IBM Journal of Research and Development, 44(3), 311.

34 Todorovic, M., Schultz, S., Wong, J., & Scherer, A. (1999). Writing and reading of single magnetic domain per bit perpendicular patterned media. Applied

Physics Letters, 74(17), 2516-2518.

35 Sagawa, M., Fujimura, S., Togawa, N., Yamamoto, H., & Matsuura, Y. (1984). New material for permanent magnets on a base of Nd and Fe. Journal of Applied Physics, 55(6), 2083-2087.

36 Friedrich, H., & Schumann, S. (2001). Research for a “new age of magnesium” in the automotive industry. Journal of Materials Processing Technology, 117(3), 276-281.

37 Weiss P: Hypothesis of the molecular field and ferromagnetic properties.J Phys 1907, 4:661.

38 Landau LD, Lifshitz E: On the theory of the dispersion of magnetic permeability in ferromagnetic bodies. Phys Z Sovietunion 1935, 8:153.

39 Wood, R. (2009). Future hard disk drive systems. Journal of magnetism and magnetic materials, 321(6), 555-561.

40 Piramanayagam, S. N. (2007). Perpendicular recording media for hard disk drives. Journal of Applied Physics, 102(1), 2.

41 Grochowski, E., & Halem, R. D. (2003). Technological impact of magnetic hard disk drives on storage systems. IBM Systems Journal, 42(2), 338-346.

42 Wang, S. X., & Taratorin, A. M. (1999). Magnetic Information Storage Technology: A Volume in the Electromagnetism Series. Elsevier.

43 Werthamer, N. R. (1963). Theory of the superconducting transition temperature and energy gap function of superposed metal films. Physical Review, 132(6), 2440.

44 Neugebauer, C. A., & Webb, M. B. (1962). Electrical conduction mechanism in ultrathin, evaporated metal films. Journal of Applied Physics, 33(1), 74-82.

45 Mills DL, Bland JAC: Nanomagnetism: Ultrathin Films, Multilayers and Nanostructures. Amsterdam: Elsevier BV; 2006.

46 Cullity BD, Graham CD: Introduction to Magnetic Materials. Hoboken: Wiley;2009.

47 Hubert A, Schäfer R: Magnetic Domains: The Analysis of Magnetic Microstructures. Berlin: Springer; 2009.

48 Ruder WC, Hsu CPD, Edelman BD Jr, Schwartz R, LeDuc PR: Biological colloid engineering: self-assembly of dipolar ferromagnetic chains in a functionalized biogenic ferrofluid. Appl Phys Lett 2012, 101:063701.

49 Ching WY, Xu YN, Rulis P: Structure and properties of spinel and comparison to zinc blende FeN. Appl Phys Lett 2002, 80:2904.

50 Šljivančanin Ž, Pasquarello A: Supported Fe nanoclusters: evolution of magnetic properties with cluster size. Phys Rev Lett 2003, 90:247202.

51 Couet S, Schlage K, Rüffer R, Stankov S, Diederich T, Laenens B, Röhlsberger R: Stabilization of antiferromagnetic order in FeO nanolayers. Phys Rev Lett 2009, 103:097201.

Chapter 2 Mechanism of alcohols on a Si(111)-7×7 surface studied by scanning tunneling microscopy

2.1 Introduction of the reconstructed Si(111)-7×7 surface

2.1.1 Introduction of the DAS model

Silicon is an important semiconductor material, and the study on Si surface is always one of the main directions of the surface physical [1, 2]. As we know that the atoms can rearrange on the semiconductor clean surface or adsorption atom layer, in order to reduce the surface energy, which is called the "surface reconstruction". According to different treatment conditions, Si surface reconstruction varies, such as 1×1, 2×1, 2×2, c2×4, c2×8, √3×√3, n×n (n is odd, n>1) [3-6]. However, 7×7 surface reconstruction is one of the most complex surface reconstruction in Si(111). It was studied almost at the same time as the emergence of surface science. For the unreconstructed Si(111) surface, there should be 49 suspension keys in the 7×7 surface. It's a very high-energy surface, very unstable. The atoms will be rearranged and reconstructed into a stable 7×7 structure under certain conditions. Each reconstructed 7×7 cell contains only 19 dangling bonds, distributed over 12 top atoms, 6 stationary atoms and 1 hole atom. The tunneling current in STM scanning process basically comes from these suspension keys.

Many models of its atomic structure have been proposed, which were greatly inconsistent with the experimental results obtained later. Until 1985, Takayanagi et al. proposed a Dimer-Adatom-Stacking fault (DAS) model, which was widely accepted because it was consistent with the experimental results. A series of n×n surface reconstruction on Si(111) surface can be described by DAS atomic structure model. However, its energy increases from 7×7 to both sides. The model established (Fig. 2.1) is in close agreement with that observed in the STM experiments: One large dip at the corner of the 7×7 unit cell, six hills and three shallow dips in each of the triangular

subunits, and two dips on each side of the triangular subunits. The model structure contains 19 dangling bonds (18 dangling bonds for the adatoms and for atoms in the top layer which are not bonded to the adatoms and one dangling bond for the atom below the vacancy at the corner). The number of the dangling bond is the lowest for the present model among the proposed models. The energy barrier of the diffusion from unfaulted-HUC (UHUC) to faulted-HUC (FHUC) along this pathway is 0.79 eV. In the middle of each of these two pathways, there is a metastable adsorption site rendering the diffusion to be a two-step process. The energy barriers of the rate determining processes in UHUC to FHUC diffusion (forward diffusion) and the reverse diffusion (backward diffusion) along these two pathways are about 1 eV.

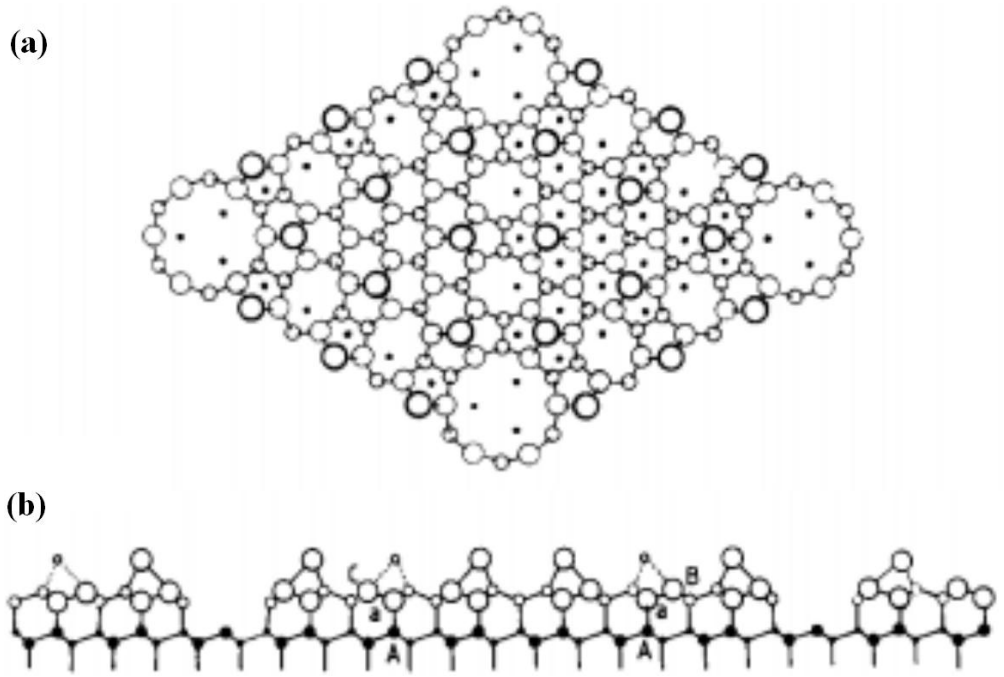

Fig. 2.1 Atomic structural model. DAS model of the Si(111)-7×7: (a) Top view and (b) Side view.

2.1.2 Preparation of reconstructed Si(111)-7×7 surface

The Si single crystal was cut along the direction perpendicular to [111], that is, the 1×1 structure of the (111) surface was obtained. Each of its surface atoms has a dangling bond, so the surface energy of this structure is very high and very unstable. Once exposed to the atmosphere, a thicker oxide layer will form on the surface. In order to obtain a clean Si(111) surface, the vacuum of the preparation chamber is better than 10^{-7} Pa. Si(111)-7×7 reconstruction is the most stable of all surface structures [7, 8], which can be formed using a flash heating [9-11]. The sample is heated to about 600 °C and kept at this temperature for 12 hours, so that the sample can be fully degassed. Then, the sample is rapidly heated to about 1200 °C to remove the oxide layer as well as impurities on the surface. In this process, when the vacuum is reduced to 10^{-8} Pa, the DC current should be switched off quickly and repeatedly, so that the vacuum will not be reduced to 10^{-7} Pa by heating. So that, the sample is heated to 1200 °C by direct current, then the temperature is slowly lowered. Repeat this process for 3 to 4 times, 7×7 reconstruction can be obtained, which has good periodicity and stability. Therefore, this surface is suitable to be used as a substrate material for epitaxial growth, which has an important significance to the study on surface properties.

In 1982, Dr. Gerd Binning and Heinrich Rohrer et al. successfully developed the first novel surface analyzer, namely, scanning tunneling microscope (STM). The system provides an opportunity for observing the distribution state of individual atoms on the surface, and the physical and chemical properties related to surface electronic behavior. In 1983, Binning et al firstly obtained the morphology of Si(111)-7×7 surface in the ultra-vacuum environment by STM. Questions related to the capability of STM devices to resolve the atomic electronic structure have been discussed above. As the important substrate material, Si(111)-7×7 is a surface with well-established atomic and electronic structures. Epitaxial growth attaches a great deal of significance to the study of surface properties. The 7×7 reconstruction of the

Si(111) surface is one of the most intriguing problems in surface science. In recent years, a great number of impressive experiments and theoretical discussion are involved in this reconstructed structure. About its basic unit cell with 49 atoms, there were still many difficulties to derive a structural model unambiguously even from an abundant set of experiments. For a long time, almost every new model would inevitably conflict with other models proposed before. More and more models seem to confuse the problem rather than clarify the issue. In order to make significant progress, some basically new approach is required. The recently atomic-level technique introduced by scanning tunneling microscopy is the key breakthrough. Taking account of the different vectors observed in STM images, possible structure model is obtained. For a single large cell superlattice structure, it can be considered as composed of several structural components. It is noted that a DAS model was developed, which is abbreviated for dimer-adsorbing atom-adatom-stacking fault model. Comply with LEED, RHEED, ICISS [12-14], this model well explains the results of other experiments before.

A truncated 1×1 surface is stabilized by forming a reconstructed Si(111)-7×7 surface, which composed of two half unit cells with different local density of state as shown by Hammers et al. [15]. One has a stacking fault (F-half), while the other has no stacking fault (U-half), which are distinguishable by a filled-state STM image attained at negative bias potential, as shown in Fig. 2.2 (a) [16-18]. Focus on the adsorption sites, there are only four kinds of sites on the Si surface, forming the DAS model structure: Near or away from the central point of both U-half and F-half. In 2008, the calculated PES of the Ag atom on the Si(111)-7×7 surface is shown in Fig. 2.2 (b). Different energy distribution corresponds to different characteristics of position on the substrate. Therefore, in the next study, we divide the adsorption sites into the center sites and corner sites.

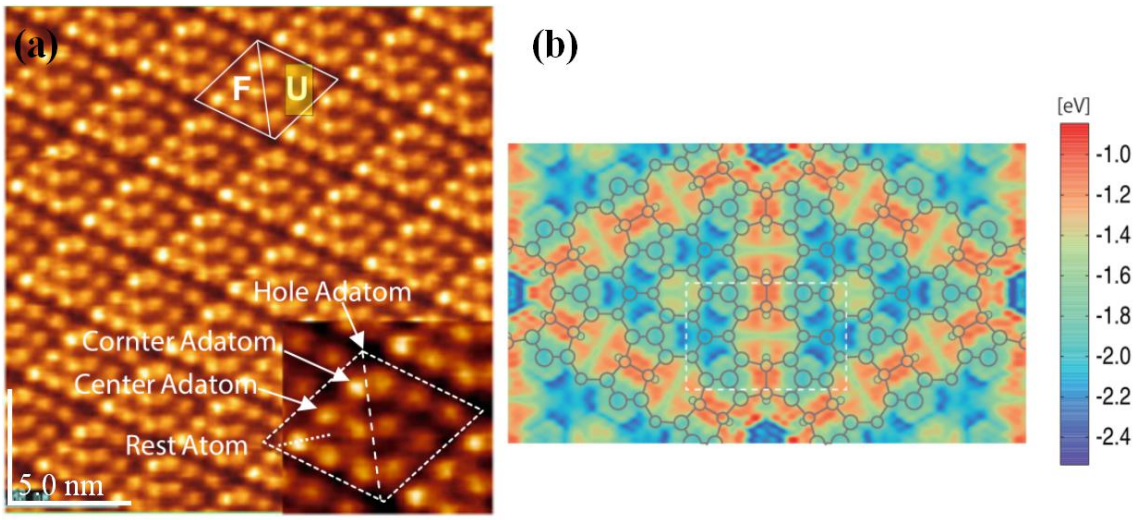

Fig. 2.2 (a) The STM image of Si(111)-7×7 reconstructed surface. Whether U structure or F structure, is composed of corner sites and center sites. (b) The calculated potential energy surface (PES) of an Ag adatom on the Si(111)-7×7 surface as well as the schematic top view of the surface structure.

2.1.3 Ladder region of Si(111) substrate

In recent years, research around the ladder region has increased the interest of researchers [19]. As the non-equilibrium effect of crystal substrate is eliminated, the surface will be deformed and turn the smooth surface into a ladder region with height difference [20, 21]. The adsorption of atoms on this region is different from the behaviors on the flat region, which is easy to form special nanostructures [22]. Based on low dimensional structure, the research of absorption point and nano-linear structure is becoming more and more important. However, it is still difficult to capture specific growth processes for atomic level research. An "amplifier" idea with catalytic effect arises at the historic moment. It is well known that thermal annealing of Si(111) substrate in ultrahigh vacuum conditions produces well-ordered singular atomic ladders separated by atomically smooth singular terraces. As an important micro phenomenon, the ladder region can not only change the anisotropy of the force field

of the surface, but also play an important role in the surface electron density. The formation of ladder region is the result of gradual stretching of boundary areas. The degree of tension can be reflected by the height difference, just as shown in Fig. 2.3 When the height difference was relatively small, a cliff area could be found which regarded as the initial stage. With the expansion of the ladder region, a stable ladder region was formed (Fig. 2.3 (b)).

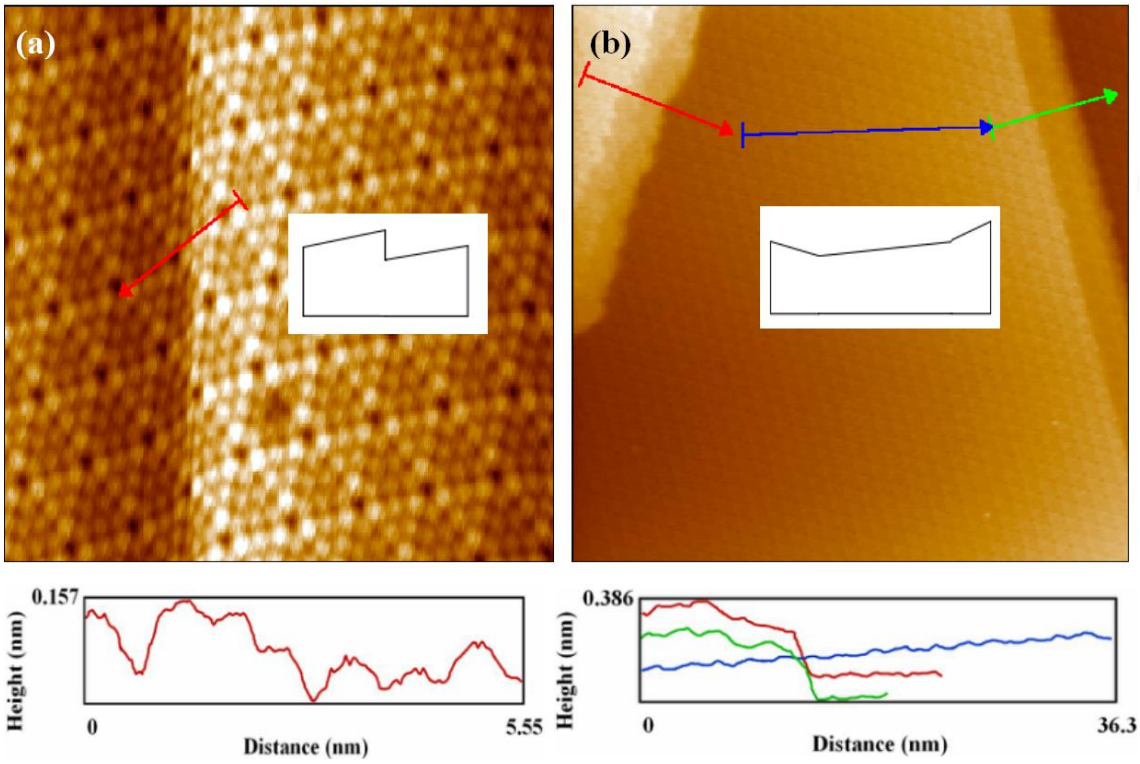

Fig. 2.3 STM images of the ladder region on Si(111)-7×7 reconstructed surface: (a) The height difference is less than about 0.1 nm, belonging to the initial stage of the ladder region, showing a cliff form. (b) The height difference is more than 0.25 nm, belonging to the stable period of the ladder region, showing a basin form.

2.2 Adsorption process analysis of the alcohols gas

2.2.1 Preparation of vacuum environment

Surface analysis of low-dimensional nano-structure is a research process at nanoscale. Therefore, even small particles (such as atoms, molecules, ions, etc.) will have a serious impact on the results, which need the support of ultra-high vacuum technology. Generally, any state below atmospheric pressure can be called vacuum. The gas molecules distribution of vacuum is much rarer than that of ordinary state. So that, the collision frequency between molecules is greatly reduced. Vacuum technology is the basis of establishing vacuum environment. The research of this subject also depends on it to explore the characteristics on the substrate.

The equipment that can obtain and maintain vacuum state is called vacuum pump [23-25]. (1) The mechanical pump: Usually mechanical pumps, which are divided into oil seal type and dry type. We use the former one in our laboratory. (2) The turbomolecular pump: Since turbomolecular pumps can not work directly at atmospheric pressure, usually combined with a mechanical pump. We used one in the preparation chamber. (3) The sputtering ion pump: One ion pump is used in our observation chamber as the secondary pump. It works in 10^{-4}~10^{-9} Pa environment, which can maintain the ultra-high vacuum of the system. This pump is very effective in pumping away reactive gases (such as O_2, N_2, etc.). However, for inert gases (He, Ne and Ar), only a very small part of them canbe extracted by ion pump. Besides, vacuum gauges are installed in all chambers to monitor the vacuum of the system in real time.

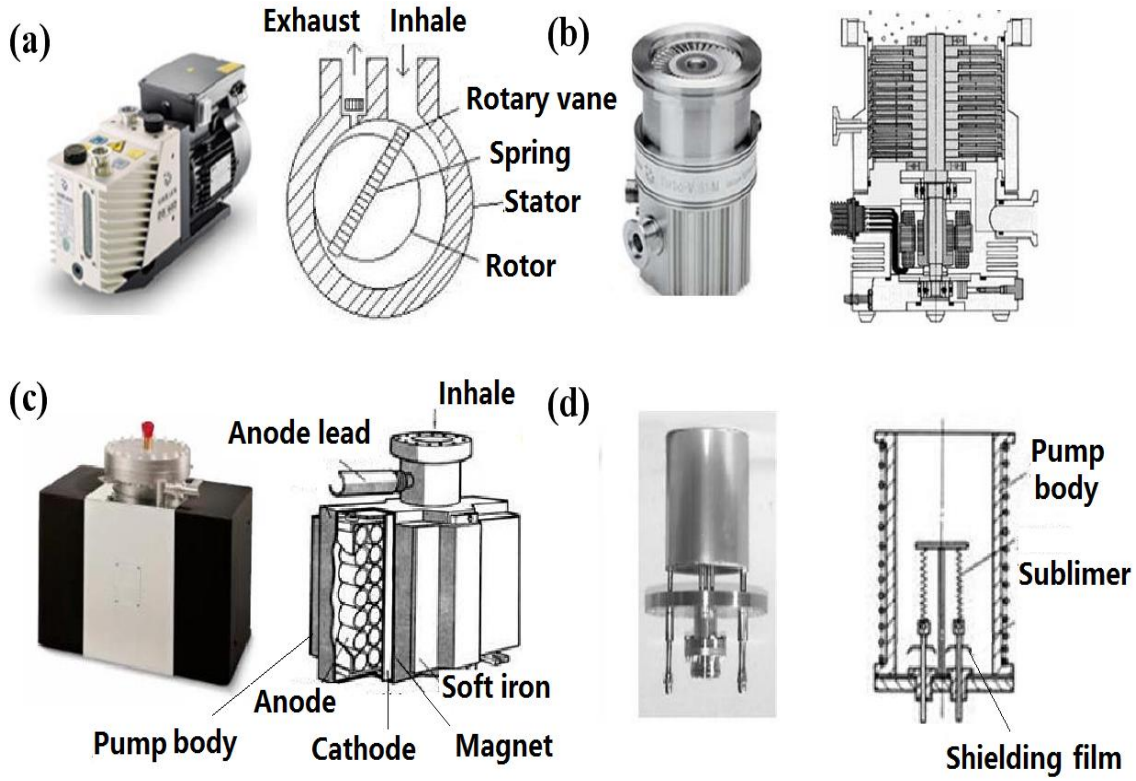

Fig. 2.4 Physical and structural images of: (a) mechanical pump; (b) molecular pump; (c) ion pump; (d) vacuum gauge.

2.2.2 Investigation on the experimental system in STM

Our experiments were adsorbed and observed by JSPM-4500S ultra-high vacuum scanning tunneling microscopy (STM) system (JEOL Ltd., Akishima-shi, Japan). Experiments were performed in the observation chamber with a base pressure of 1×10^{-8} Pa. And the vacuum degree is below the 4×10^{-8} Pa in the preparation chamber. At room temperature, the STM images were observed in a constant current mode. The single-crystal Si(111) substrate (n-type, ~0.1 Ω cm) was ultrasonically pre-cleaned in acetone, ethanol and deionized water. In order to obtain high quality STM images, it is very important to have a sharp and stable needle tip. At present, the most widely used tip materials are tungsten wire (W) and platinum iridium wire (Pt/Ir). We use the former one in our laboratory. There are many ways to make needle

tips, such as shearing, electrochemical corrosion, etc [26, 27]. W tips are usually prepared by electrochemical etching. The schematic diagram of the device for preparing W tip by electrochemical etching is shown in Fig. 2.6. The dielectric solution we used is NaOH solution. Besides, it should be noted that tungsten is easy to oxidize in the atmosphere. The oxide layer is also formed on the surface. Therefore, special treatment must be carried out before we send it into the observation chamber.

Fig. 2.5 JSPM-4500S ultra-high vacuum scanning tunneling microscopy (STM) system.

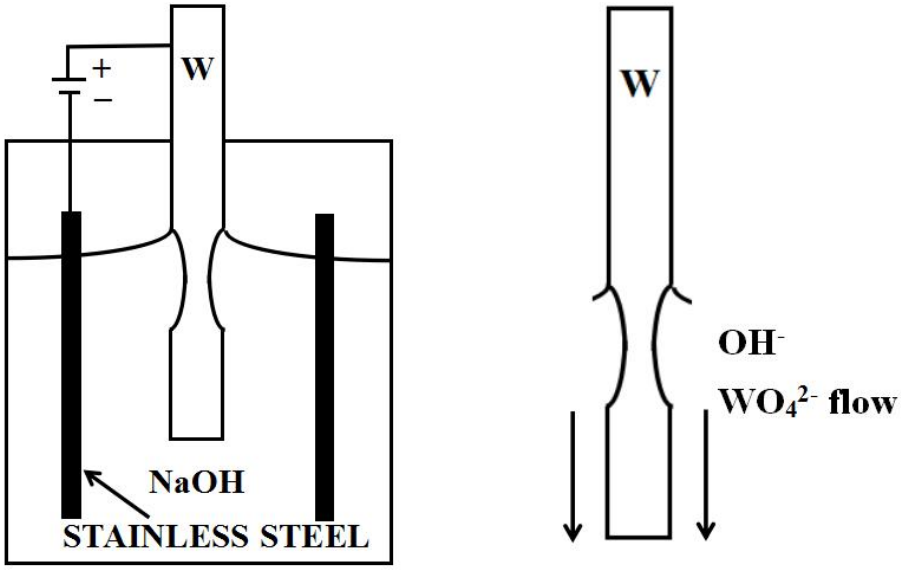

Fig. 2.6 Schematic diagram of the electrochemical corrosion and the part of W probe.

The preparation chamber of the STM system is equipped with three sample holders, which can be used to make three specimens at the same time and conditions. The specific experimental procedures are as follows: Specimens were degassed in the preparation chamber at about 450 °C. Then, the sample was repeatedly flashed at 1250 °C until a clean well-ordered Si(111)-7×7 reconstructed surface was obtained. After cooling, the sample was transferred to the observation chamber. Through the needle valve, one set of gas storage device is connected with this chamber, which is full on different gas. During the adsorption process of alcohol, the mass spectrometer was turned on to monitor the gaseous molecules composition in the observation chamber.

2.2.3 Analysis of atoms distribution based on LEED

Low-energy electron diffraction (LEED) is an experimental method to determine the surface structure of a single crystal [28-30]. When collimated low-energy electron beams (20-200 eV) are used to bombard the surface of the sample, the spot formed by

the diffracted electrons can be observed on the fluorescent screen. So, surface structures of the sample can be characterized. There are two important applications of low-energy electron diffraction:

(1) Qualitative analysis

Focusing on the analysis of diffraction pattern and spot location, the symmetry of surface structures can be obtained. If there are adsorbents on the surface, the unit lattice and relative size/direction of them can be determined by qualitative analysis.

(2) Quantitative analysis

It is mainly concerned with the relationship between the intensity of the diffracted electron beam and the energy of the incident electron beam. Further compare I-V curves with the theoretical prediction, the exact position information of surface atoms can be obtained.

The ultrahigh vacuum (UHV) system consists of a main chamber and a preparation chamber with a base pressure of 2×10^{-10} Torr. The observation chamber is equipped with a 4 grid-LEED/AES optics for sample surface characterization (model: BDL600IR) and a Gammadata Scienta SES-100 analyzer for sample surface composition. The preparation chamber is equipped with conventional UHV surface preparation and analysis tools. Si(111)-7×7 restructured surface and Si(111)-7×7-alcohol surface were be observed by LEED. In this process, the filament current was 2.8 A, the screen voltage was 4.0 kV, and the beam energy was 60 eV. The sample was moved into observation chamber for LEED measurement. Then the ethanol was introduced slowly into preparation chamber for 2 min at the pressure of 1×10^{-6} Torr. The Si(111)-7×7-alcohol surface was observed again by LEED.

Figure 2.7 shows LEED patterns of Si (111)-7×7 surface at the incident electron energy from 45-110 eV, from which Si (111)-7×7 restructured surface can be also observed. The diffusion patterns varied with the different incident electron energy. The positions of six first-order diffraction spots shift to the center. In order to identify these changes, the six first-order spots positions are marked in the images (✦). Figure 2.8 shows LEED patterns of Si(111)-7×7-alcohol surface at the incident electron

energy from 110 eV to180 eV.

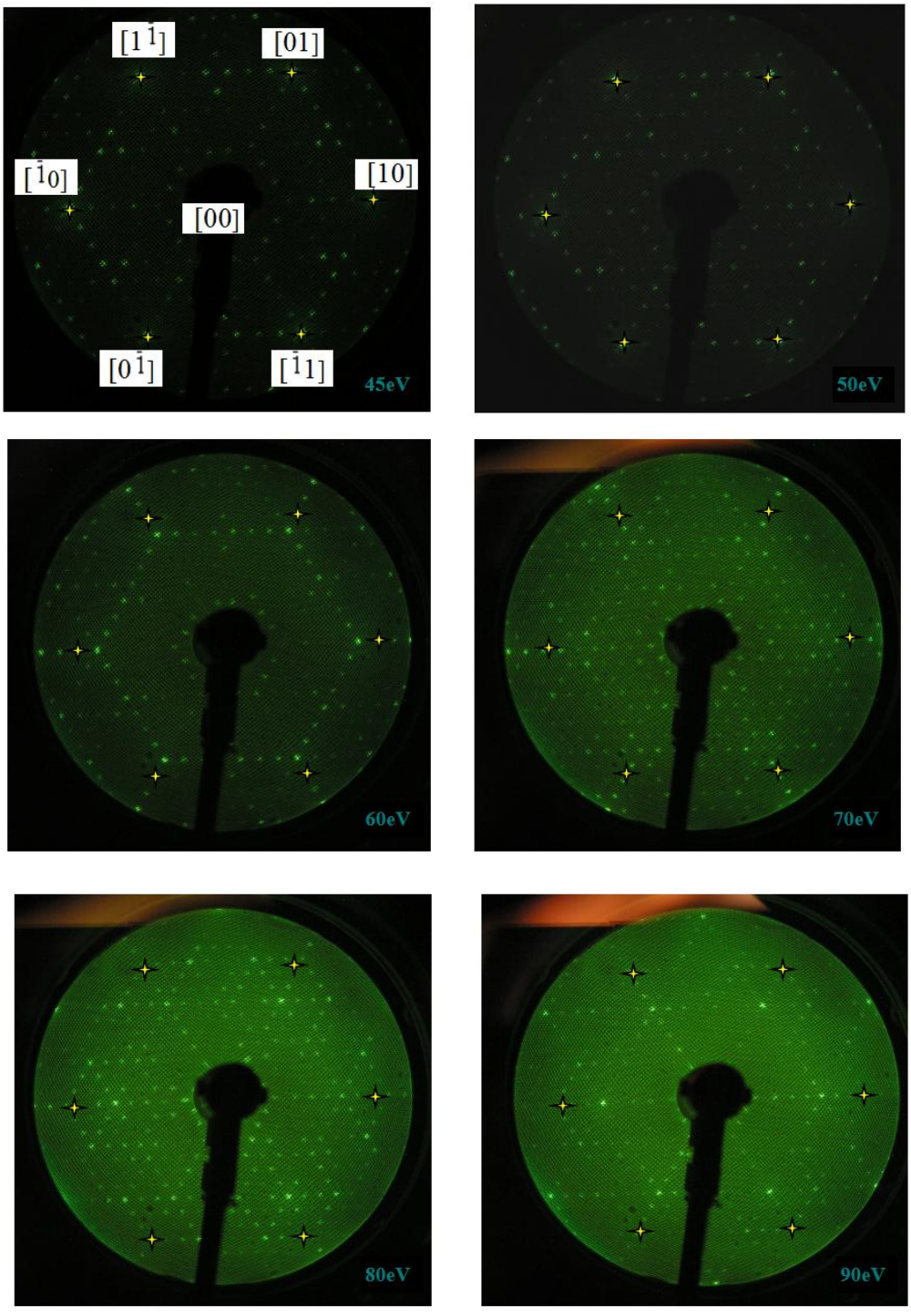

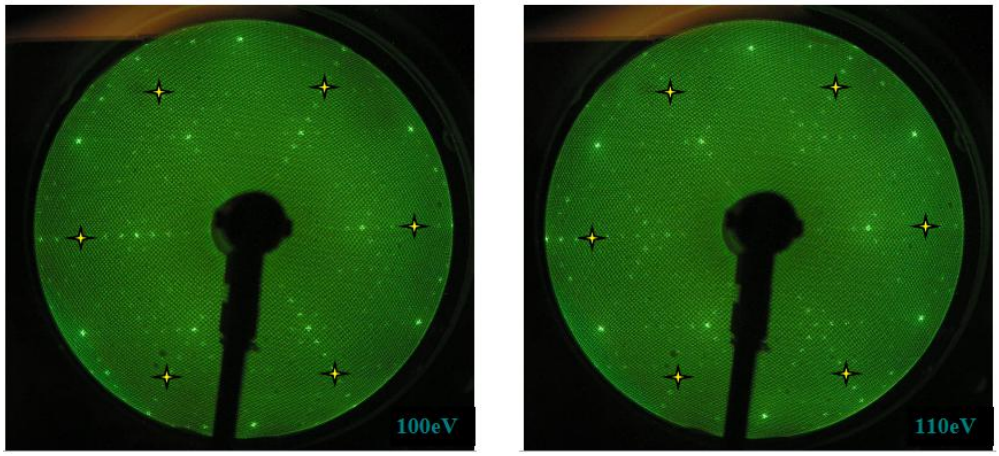

Fig. 2.7 LEED patterns of Si (111)- 7×7 surface (from 45 eV to 110 eV)

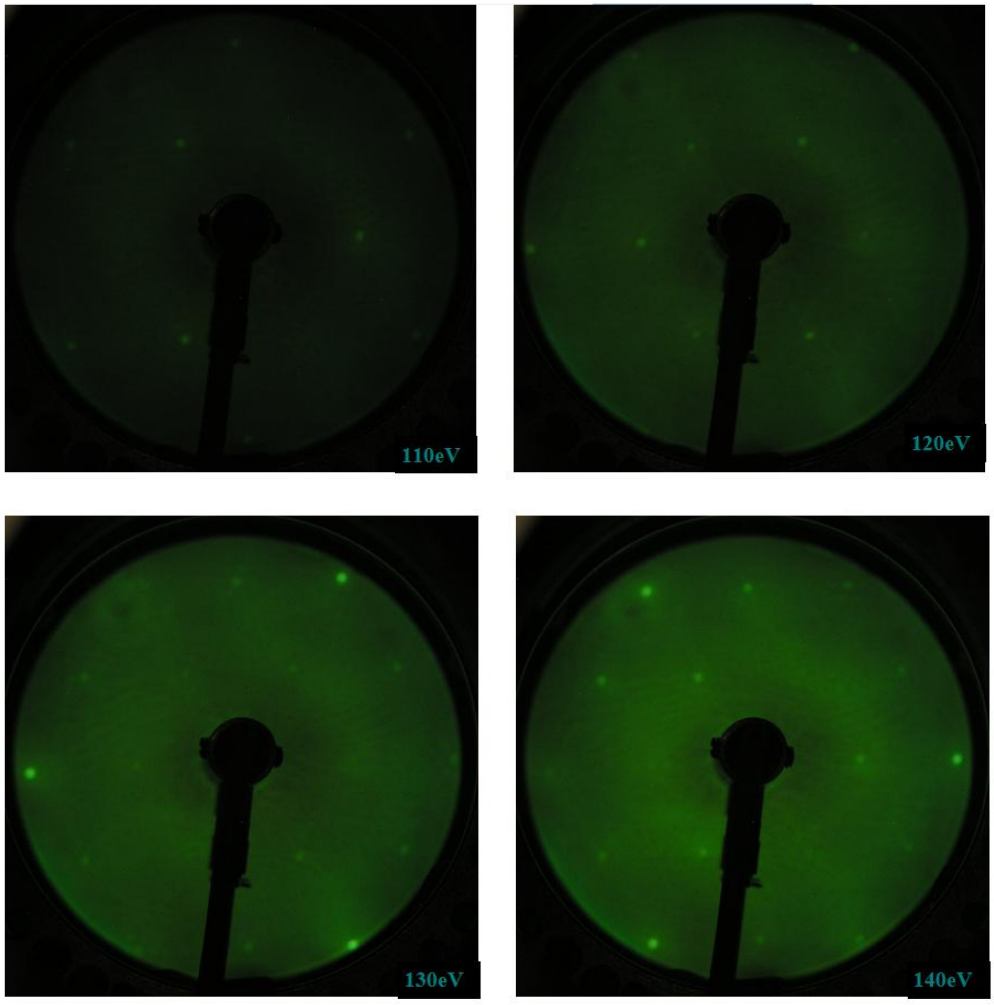

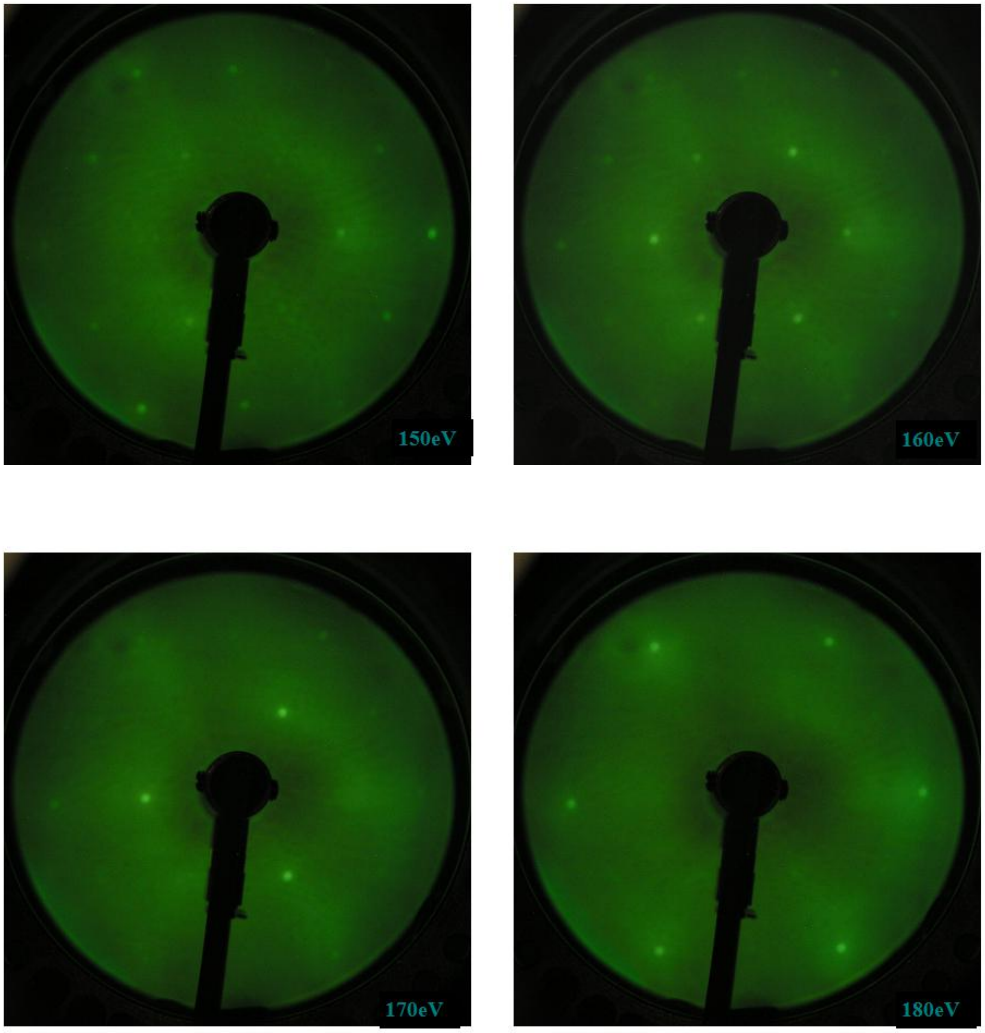

Fig. 2.8 LEED patterns of Si(111)-7×7-alcohol surface (from 110 eV to 180 eV)

2.3 Comparison of adsorption process of methanol, ethanol and propanol

2.3.1 Detect the dissociation process by mass spectrometer

The method of mass spectrometry was first identified by J.J. Thomson in 1913 and improved by F.W. and Aston. The modern mass spectrometer has been continuously improved [31]. Using the principle of electromagnetism, ion beams are

separated by charge to mass ratio. Mass spectrometry analysis is a kind of instrument for separating and detecting samples according to the principle that charged particles would deflect in the electromagnetic field. Ions of different masses have different offsets as they pass through the magnetic field. After that, they would focus on different locations, obtaining different mass spectra of isotopes. That is, the mass difference of matter atoms, molecules or molecular fragments. The mass spectrometer consists of ion source, mass analyzer and ion detector. Main experimental conditions of the instrument are designed in vacuum. To a large extent, the performance of ion source determines the ionization efficiency as well as its sensitivity. Among them, there are two main technical parameters. One is the range of mass-charge ratio (mass range) that can be measured, the other is the resolution. If the mass spectrometer can precisely distinguish between mass m and m+ Δ m, the resolution is defined as m/ Δ m. At present, the resolution of modern mass spectrometer ranges from 105 to 106, which can measure atomic mass accurately to 7 digits after decimal point. By dissociation, ions enter the ion detector in turn and ion signals can be amplifying collected. Through computer processing, the mass spectra can be draw. We find out the main ion peak (generally refers to the relative strength of the larger ion peak), and then to record the mass of these peaks (m/z) and their relative strength.

Three Si(111)-7×7 samples were successively sent into the observation chamber, which is filled with CH_3OH, C_2H_5OH and C_3H_7OH gas respectively. The tungsten tip was retracted away from the surface to reduce shadowing effect of the tip. At the same time, the mass spectrometer is turned on to monitor the gaseous ion composition in the observation chamber. The samples can be preheated by an external power source. Although much research has been devoted to pure Si surface, little attention paid to its intermediate layer [32, 33]. In the case of adsorption of CH_3OH, C_2H_5OH and C_3H_7OH, the precursor state is equally formed in the faulted and unfaulted halves at room temperature, STM images reflect the site-by-site dissociation probability of the alcohols. Firstly, accumulated by a large number of experiments, Fig. 1 shows the change in coverage rate when CH_3OH, C_2H_5OH and C_3H_7OH's concentration increase.

Alcohols' adsorption on the Si(111)-7 × 7 surface was proved to have a constant sticking probability until saturation. In the same conditions, CH_3OH is bound to have higher reaction efficiency. When its adsorption time reaches about 30 s, the coverage rate can maintain the stable 49% (nearly 1/2). In the case of adsorption of alcohol, the precursor state is equally formed in the faulted and unfaulted halves at room temperature. By analyzing surface images, the ratio of occupied Si adatoms to unoccupied Si adatoms becomes finally 1:1 in the saturated adsorption of methanol. The adsorption of CH_3OH, C_2H_5OH and C_3H_7OH on the Si(111)-7×7-alcohol surface is a good example. If a clean Si(111)-7×7-alcohol surface is exposed to CH_3OH or C_2H_5OH (R-OH), the molecules dissociate into Si-OR and Si-H on a pair of (Si adatom/Si rest atom) as described schematically in Fig. 2.9 (d).

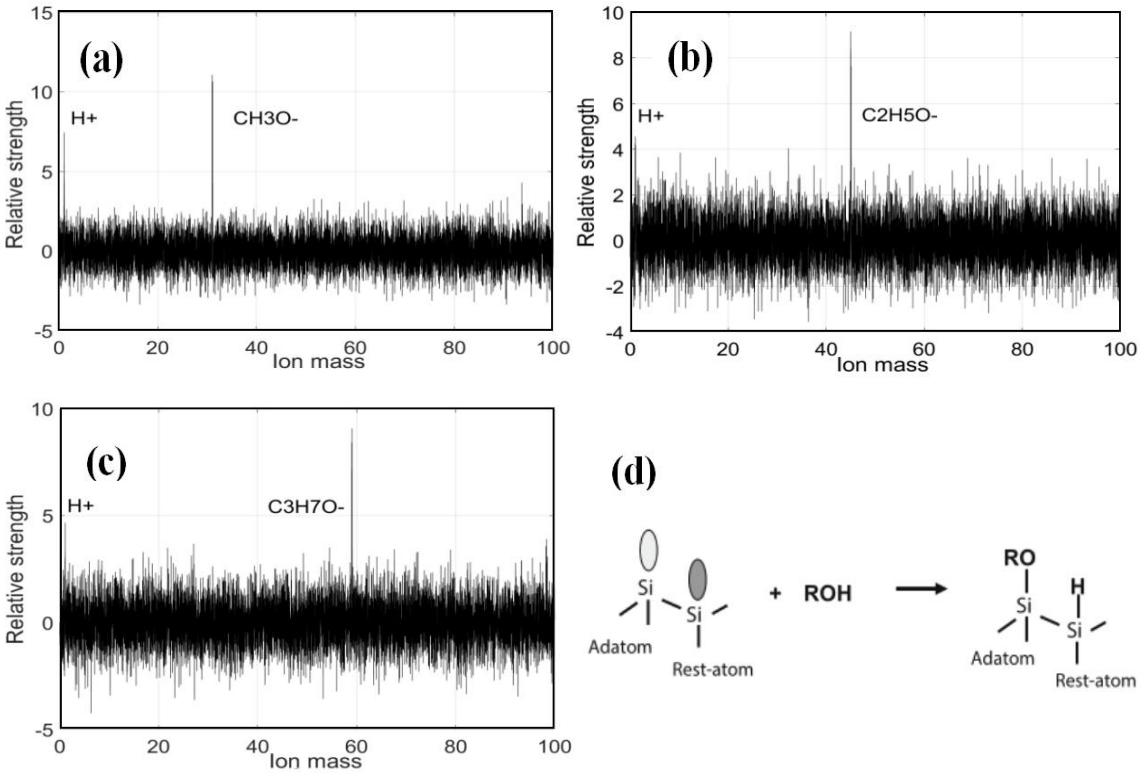

Fig. 2.9 Mass spectra images of (a) CH_3OH, (b) C_2H_5OH and (c) C_3H_7OH. (d) is schematic diagram of alcohols decomposition.

2.3.2 Study on the Adsorption mechanism of Alcohol

In Figure 2.10, according to the analytical method mentioned above, each triangle on Si(111)-7×7 surface is composed of six adsorption sites. In Figure 1 (a), according to the analytical method mentioned above, each triangle on Si(111)-7×7 surface is composed of six adsorption sites. Further, every six sites can also be divided into 3 center sites (red) and 3 corner sites (blue). Then, aim to analyze the specific dissociation process, based on the real-time monitoring data of mass spectrometer, the gas ion's composition in the cavity is simultaneously known (Fig. 2.8). There is a dissociation process in the adsorption stage of each alcohol gas:

$$CH_3OH = CH_3O^- + H^+ \qquad (1)$$
$$C_2H_5OH = C_2H_5O^- + H^+ \qquad (2)$$
$$C_3H_7OH = C_3H_7O^- + H^+ \qquad (3)$$

The STM image of adatoms and the tunneling spectroscopy at the rest atom position suggests that the CH_3OH molecule dissociates on an adatom and rest atom pair by forming Si-OCH_3 and Si-H, respectively. These facts indicate that the dissociation of the alcohols is accomplished via a precursor state in each half unit cell: that is, each half unit cell works independently as if it was a molecule. It is known that H_2O, NH_3 and CH_4 undergo dissociation on a pair site of Si-adatom and Si-rest atom, where the dangling bond on the Si-adatom is empty while that on the Si-rest atom is almost filled. Taking these facts into account, we infer that the key to the adsorption of alcohols is OH- rather than $(CH^+)_n$. Although there is no quantitative test, by observing the relative intensity data of ions in the cavity, we can find: The chemical reaction efficiency of H^+ and Si is much higher than that of $C_2H_5O^-$ or CH_3O^-. This important feature indicates that in the case of the top surface adsorption sites (namely, center sites and corner sites) are occupied, H+ can only be adsorbed on the lower rest positions. So that, the critical adsorption model of alcohol ion and hydrogen ion is proved (Fig. 2.10 (b)), which would help us to study the adsorption location in detail.

Then, we selected CH_3OH for further study. Every triangular half unit cell contains three Si-OCH_3 and three Si ad-atoms, which the former show as the bright dots and the latter is relatively dark in the STM image. The rest atoms on the lower layer of the substrate are further reduced at the height in the STM image and cannot be scanned. H atoms saturate the suspended key of rest atom, which also cannot be observed clearly. From the theoretical point of view, metal atom on the Si(111)-7×7 surface undergoes migration by hopping among Si-adatom and Si-rest atom. In this paper, we studied the deposition of metals on the Si(111)-7×7 surface saturated with CH_3OH, on which the whole Si-rest atoms are changed to Si-H so that the hoping migration of metal will be prohibited. More than this, CH_3OH coating can also effectively prevent the formation of FeSi, whose magnetic property is much lower than that of the pure Fe atom. In this paper, after understanding the specific adsorption mechanism of CH_3OH, we will use it to improve the success rate of Fe atomic linear structure.

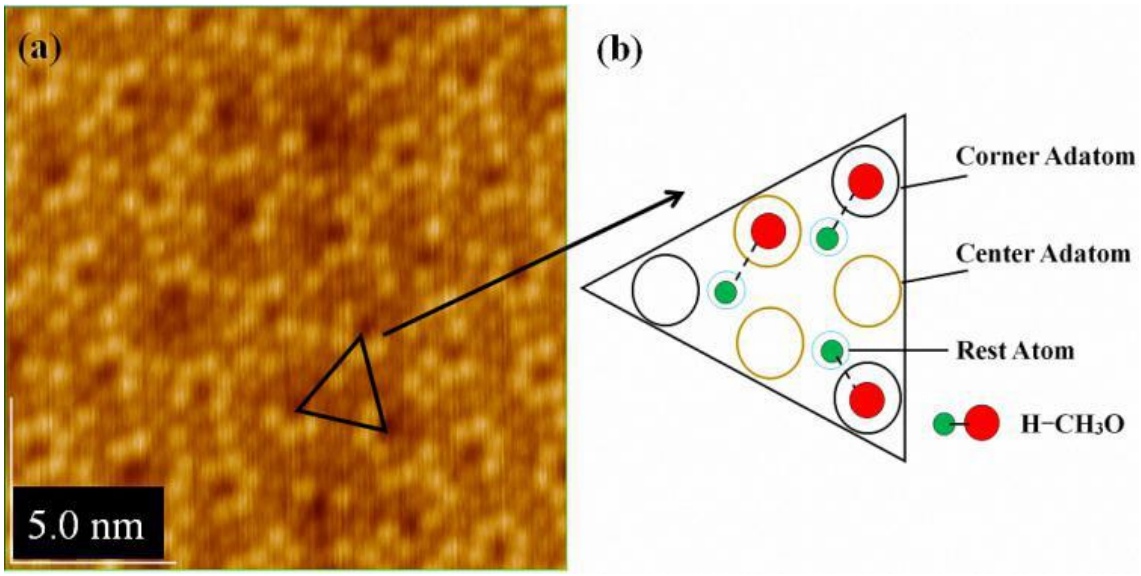

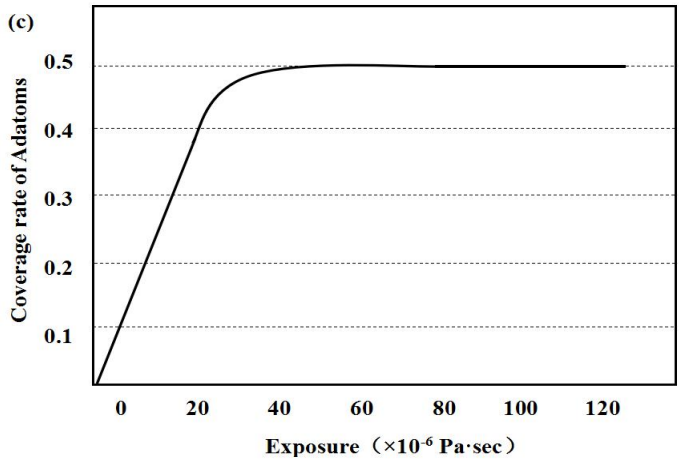

Fig. 2.10 (a) STM image of the Si(111)-7×7 surface with CH_3OH concentration is 10^{-6} Pa, and the gas adsorption time is 30 s; (b) The model of a half unit cell: three pairs of Si-OCH_3 and Si-H are formed at the adatom/rest sites; (c) Image of relationship between methanol adsorption time and its coverage.

2.3.3 Comparison the adsorption condition of different situation on Si(111)-7×7-alcohol surface

As describe below, the alcohol molecule (ROH) does not directly dissociate by collision at a pair of Si adatom/Si rest atom, but undergoes dissociation via a transformation state on either a center-Si-adatom or a corner-Si-adatom site. As shown in Fig. 2.10, bright points corresponding to methanol ion. H atoms adsorb on rest Si atoms without moving, which are consecutively increased in each half unit cell. Therefore, saturated adsorption is attained when a half of the adatoms are changed to Si-OCH_3 in every half unit cell. It is noted that the adsorption equally occurs on faulted and unfaulted halves with a constant sticking probability until the surface is saturated as shown in Figs 2.11 (a) and (b). This important feature indicates that the sticking probability, process of transformation, is little influenced by preadsorbed Si-OCH_3 and/or Si-H, although the dissociation probability (site selectivity) of the precursor depends on the local conformation of the sites. The sticking probability

obtained by the STM corresponds to the formation probability of the transformation state which goes to dissociation.

On the other hand, the STM image is formed in accordance with the site selectivity for the dissociation of the precursor. Therefore, the constant sticking probability does not mean the consecutive steps with an equal rate. As shown in Fig. 2.11 (b), the dissociation probability of a precursor state molecule is the same on the F-half compared to that on the U-half unit cell. It is worth noting that the adsorption (dissociation) probability of methanol (CH_3OH) is exactly equal to that of other alcohols (C_2H_5OH, C_3H_7OH) and their adsorption probability has a constant value up to the saturation. Moreover, the distribution of methanol is found identical on both regions of flat and ladder (Figs. 2.11 (c) and (d)). On the ladder region, methanol is evenly distributed. Whether in the FHUC/UHUC triangle or corner/center, methanol has no obvious adsorption bias, maintaining the probability of 1:1. Continue to increase the concentration, methanol does not grow in layers, nor does it form cluster. These facts all indicated that CH_3OH can be used as an ideal intermediate layer in the structural catalytic process.

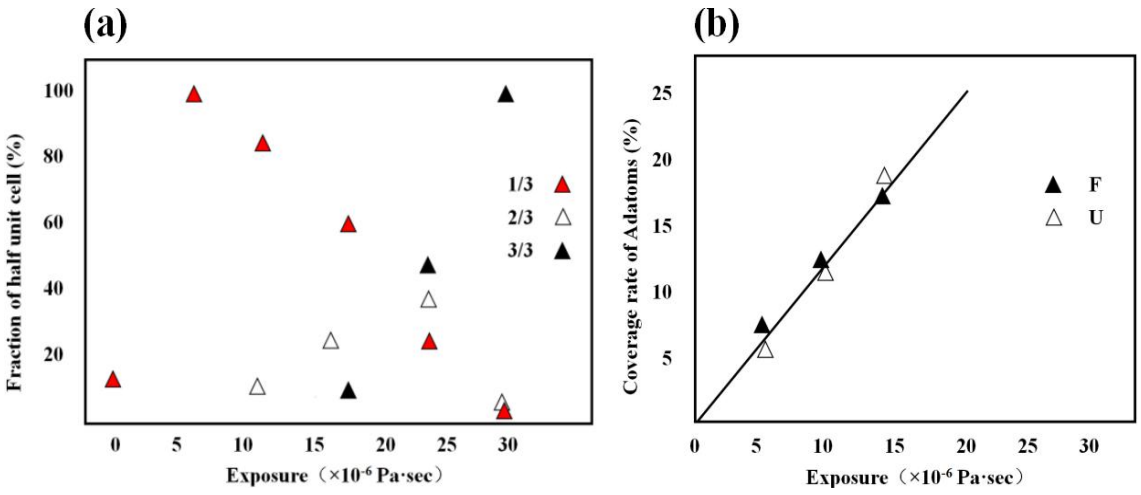

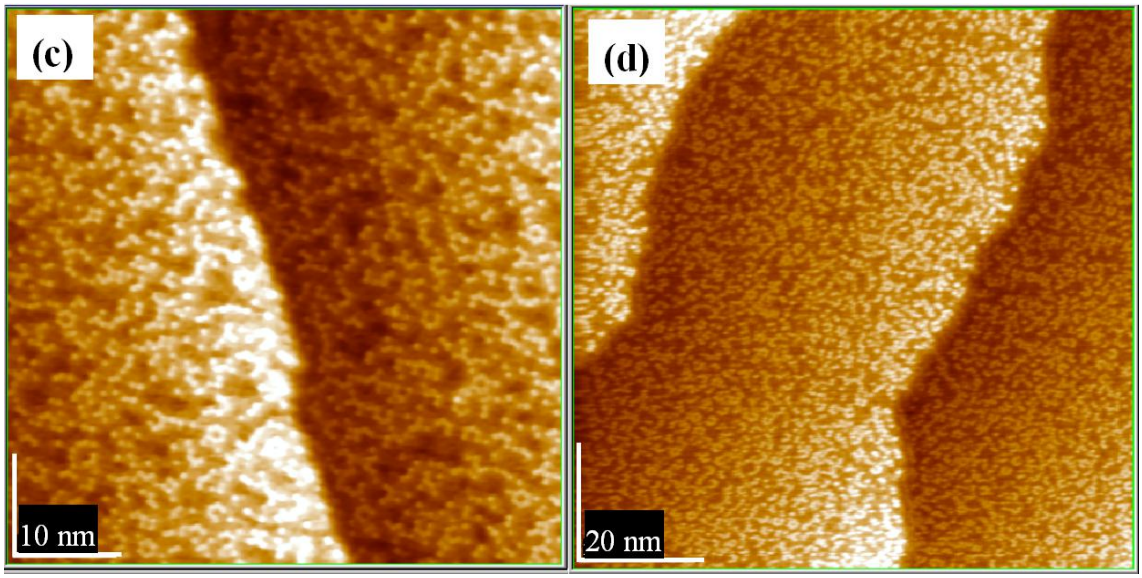

Fig. 2.11 (a) Consecutive change of the fraction of half unit cells with one, two, and three adsorption sites as increasing exposure. (b) Coverage of U/F cells increased with the exposure of CH_3OH. (c) and (d) are the origin/stable ladder region with CH_3OH concentration is 10^{-6} Pa, 45 s.

2.4 Classification of different metal clusters on silicon surface

As the important substrate material, the reconstructed Si(111)-7×7 is a surface with well established atomic and electronic structures. Epitaxial growth of it attaches much significance to potential applications on diverse areas, like smart materials industry. The recent progress in the multi-layer adsorption and its characterization, has increased the interest of researchers. Since 2004, the dynamics of metal atoms began to be concerned about. For example, a honeycomb layer composed of Sn_2/Zn_3 atoms was established as the increasing coverage. In contrast, some relatively stable atoms like Cu, Ag and Au have been systematically investigated and identified on the Si(111)-7×7 surface. As an important supplement, taking advantage of strong magnetism, Fe, Co and Mn also opened up a potential way for high-density magnetic storage market. Accumulating a large number of atomic adsorption cases (like Au, Sn

and Fe), some specific classifications could be verified and proposed (Fig. 2.12). Weak-compound is not easy to form a cluster structure, while strong-compound tends to hip or move because of its dynamic. Iron is classified as a quasi-strong compound since it can form stable clusters, but reacts with the substrate. A newly formed surface is stabilized by different atoms/molecules, forming different types of compounds. Moreover, the formation of each compound is always accompanied by a different degree of destruction on the surface. The characteristics of each reaction may be reflected by such a compound structure as the precursor state. As a quantitative concept, destruction could and should also be adjusted. In this paper, the introduction of the intermediate layer which could regulate the metallic compounds becomes the focus of our attention.

The formation of metal-cluster on the Si(111) substrate is a typical case, that is, if an elementary reaction involves a precursor state, the feature of chemical reaction is difficult to explain without the precursor state. Through the comparison of Au and Fe (Figs. 2.12 (a) and (b)): the former is easier to form linear structure, which belongs to weak-cluster; the latter takes advantage of its cluster structure, which can be defined as strong-cluster. From the viewpoint of application, the structure of linear clusters is an ideal state of atomic adsorption. Just like magnetic units, if arranged in a linear cluster structure, can be used as high-density storage device. We have enough reasons to believe that the perfect structure can be formed if the interaction adjusted in a reasonable range. As a theoretical prediction, the new concept of the quasi-strong cluster was proposed in Fig. 2.12 (c). It is hoped that the new type of cluster can not only have the advantage of linearity but also keeps the stability of the cluster. On this basis, the introduction of an intermediate layer has become the focus of our attention [34-37].

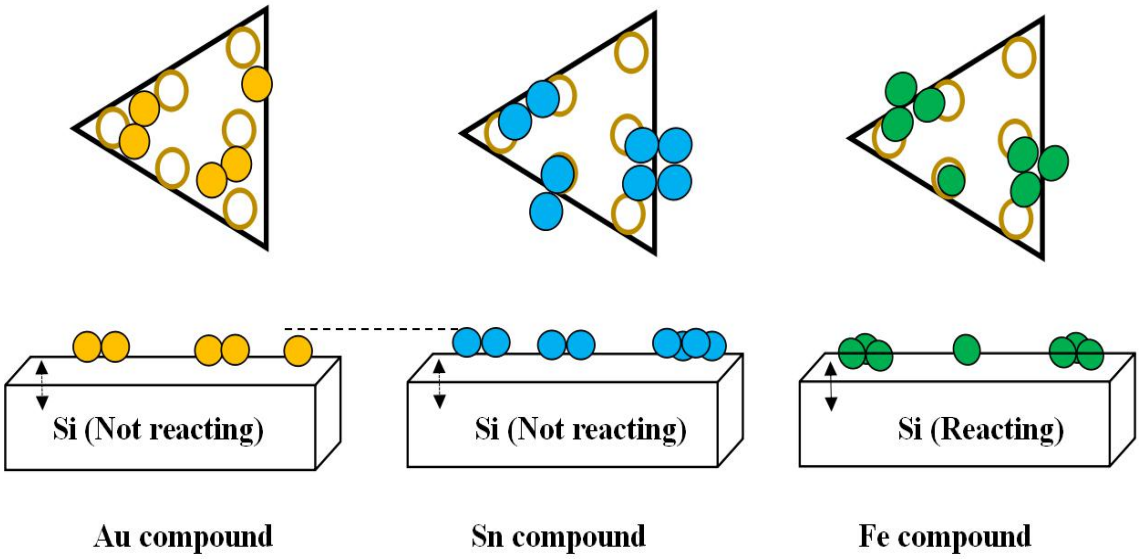

Fig. 2.12 Three typical compound models: the yellow one represents a weak-compound, which is enough stable to fix on the silicon surface; the blue one represents a strong-compound, which is easy to move and form cluster structure; the green represents a type of quasi-strong compound, which can not only form clusters, but also easy to fix on the surface.

2.5 Explore the dual characteristics of CH_3OH to the metallic atomic structures

2.5.1 The vertical (isolation) characteristic of methanol

Firstly, we were concerned with the Fe compound, which has a good prospect of application. However, it is very easy to react with Si, resulting in the low magnetic strength. As a progressive approach, in Fig. 4a: Fe atoms were steamed on Si (111)-7×7 reconstructed surface, which was saturated by CH_3OH molecules. Assisted by height measurement, two significant height values (high and medium high) can be found, which represent Fe layer and CH_3OH layer. In the point of vertical direction, CH_3OH showed its isolation characteristic as an intermediate layer. Just as shown in XPS verification (Fig. 2.13 (c)): The red line represents Fe deposited sample, the

green line represents the sample after O_2 introduction and the blue line represents the sample which was exposed in the air. The peaks of Fe $2p_{3/2}$ appeared at about 707 eV, which belong to the pure Fe atoms. And one conclusion could be deduced that the Fe compounds are stable in the above mentioned thin-air condition at room temperature. However, compared with Fig. 2.13, the original cluster structure of quasi-strong compounds was destroyed. How to regain and form more stable cluster structure by exploring methanol mechanism has become the focus of our work.

After verifying the isolation effect of CH_3OH to the quasi-strong compound, Sn attracted our attention since its characteristics of strong-compound. It is very significant to explore if the hopping migration is prohibited, the growth of Sn compound is controlled by the kinetics of precursor state atoms instead of the lattice energy relating to lattice matching or strain. After restricted by methanol, Sn compound (or cluster) can still expand from small size to large size. In the horizontal direction, whether CH_3OH still has the characteristics of isolation? Before this study, researchers usually judged Sn atoms' hoping migration by spacer scan, finding the different phenomenon. The specific structure of Sn compounds on Si-intermediate layer was not clear. Adjusting the concentration of both Sn and CH_3OH, some interesting results have been finally found. Just as the Fig. 2.14 (a) shown, Sn is obviously restricted by the CH_3OH. Enlarging the selected area, Sn compound is found to only expand in the direction of no-CH_3O^-. In addition to the height data, 3D surface display technology of the STM system was further used to observe the specific structure (Fig.2.14 (c)) [38, 39]. It proves that the isolation effect of methanol on Sn is greater than the boundary. After that, an external power supply was operated to simulate the current passing through the electronic component. According to the sample resistance (about 1 KΩ), surface temperature will rise rapidly when the external current passes. Just in the same steaming conditions, we found an opposite result in Fig. 2.14 (d). Sn compound seems no more restricted by the methanol, even started to expand in the direction of CH_3O^-. Observing the difference between Fig.2.14 (c) and (e): contrast to the sample before preheating, the integrity of CH_3O^- in the latter was destructed serious. As a phased conclusion, CH_3O^- can only play a

limited isolation role (mainly in the vertical direction). In the horizontal direction, we have enough reasons to believe that H^+ may play an important role in the adsorption process of these metallic compounds.

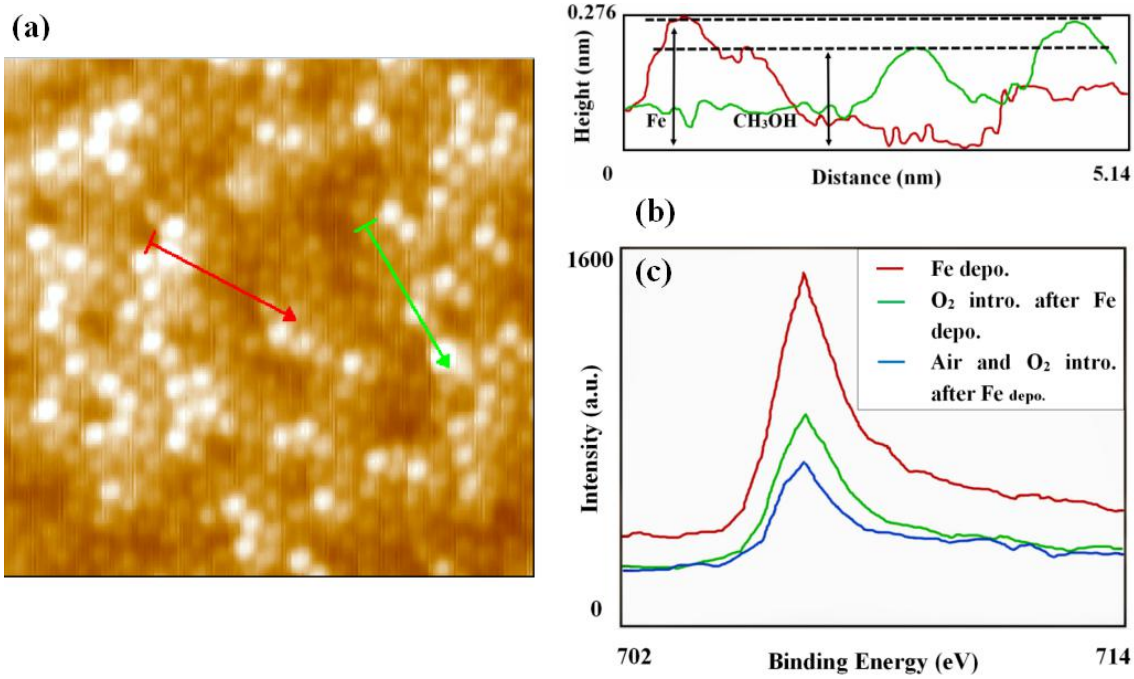

Fig. 2.13 (a) STM image of the Si(111)-7×7-CH_3OH surface steamed with Fe, 10^{-6} Pa, 20 s; (b) is the height measurement of (a); (c) XPS spectra of Fe and Si after Fe depo, O_2 intro and exposed in air.

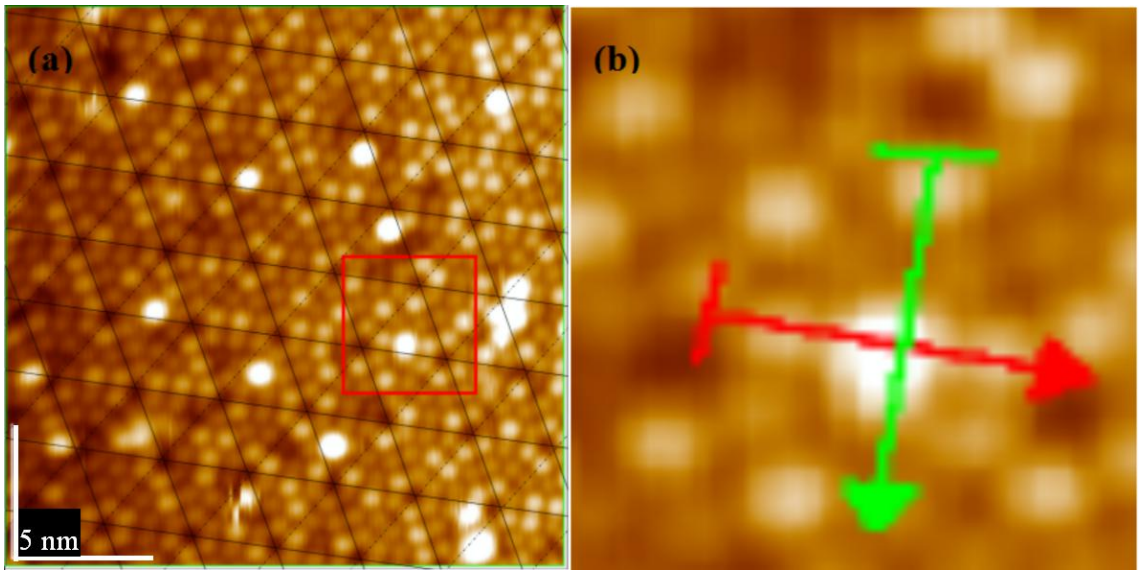

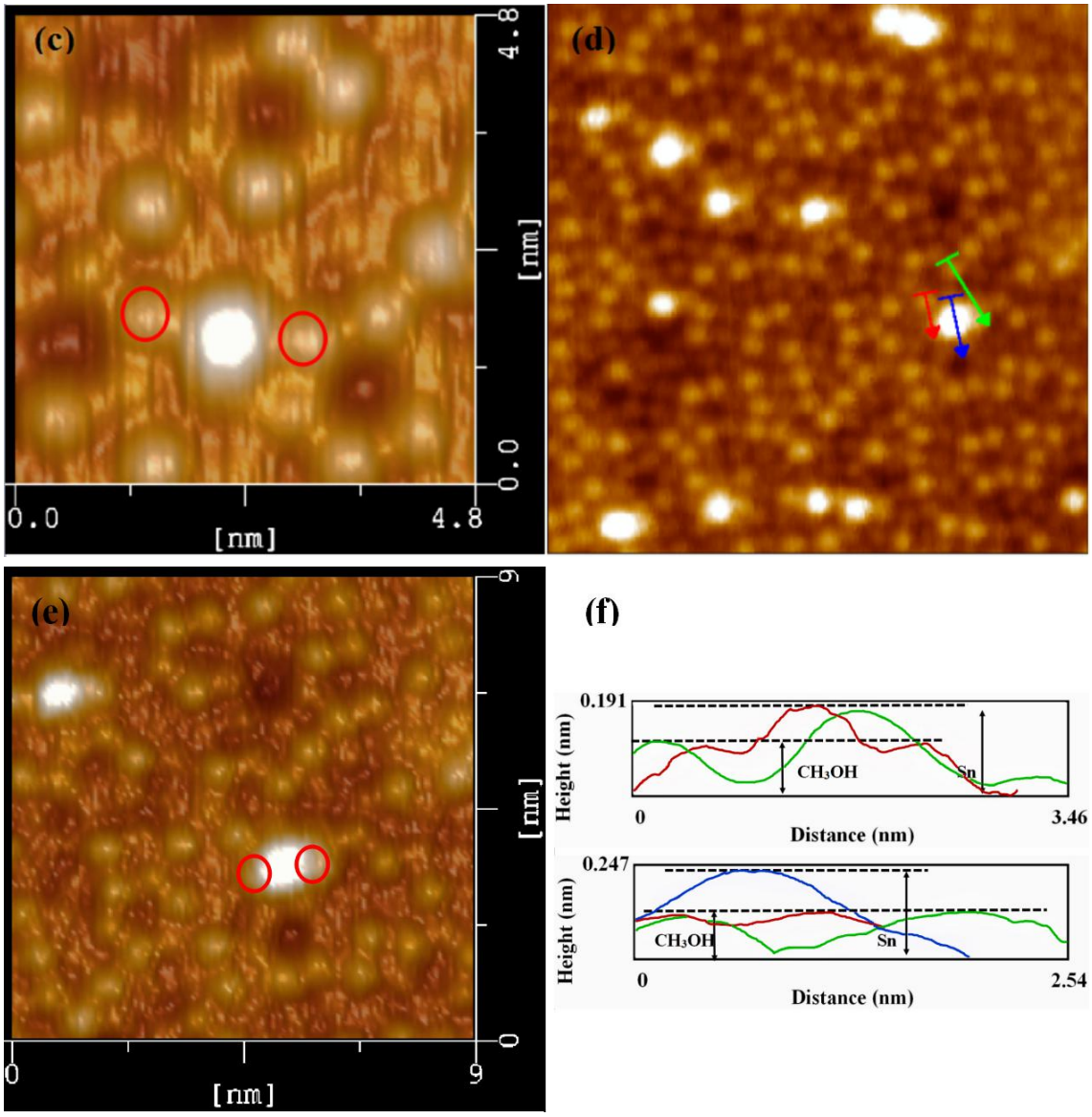

Fig. 2.14 STM images of: (a) the Si(111)-7×7-CH_3OH surface steamed with Sn atoms; (b) is the amplification image of the red box area in (a); (c) is the 3D model of (b), the red circle represents the CH_3O^-; (d) After heating the sample, 0.2 A, 3 s, the Si(111)-7×7-CH_3OH surface steamed with Sn atoms; (e) is the 3D amplification model of (d); (f) The height measurement of (b) and (d).

2.5.2 Evaluation on distribution behaviors after heating by current

As a result, a specific adsorption model of methanol is realized (Fig. 2.15 (a)), showing the adsorption location in detail. According to the sample resistance (about 1 KΩ), surface temperature will rise rapidly when the external current passes. Three Si(111)-7×7 samples were successively sent into the observation chamber, which was filled with CH_3OH gas. At the same time, the mass spectrometer was turned on to monitor the gaseous ion composition in the observation chamber. Si(111)-7×7-CH_3OH samples were heated in 0.2 A current with an external power source. Under the detection of an infrared radiation thermometer, the temperature of samples with heating time in 2, 3 and 4 s, were about 37, 55 and 76 °C, respectively.

Three Si-CH_3OH samples were heated over different extents of time. The charge transfer to the adatoms is influenced by the number of neighboring hydrogen-terminated rest atoms. The center adatom with two hydrogen-terminated rest atom gets most of the charge. By analyzing the change in apparent height of many adatoms one can conclude that the charge redistribution is very local. There is no evidence of a charge redistribution that extends to second-nearest-neighboring adatoms when a rest atom becomes hydrogen terminated. Just as figures 2.15 (b), (c) and (d) show, two types of adsorption sites were counted: The ratio of center/corner sites decreased with increasing heating time. Under the condition of transient heating above, it can be found that the thermal stability of CH_3O^- in a corner site is stronger than that in a center site. Repeated over another 3 samples, the same ratio change was found. Regularity is the basis of linearity. If the trend of this change is grasped effectively, then the linear structure later should be more obvious. Therefore, it is very significant to verify the change of Si(111)-7×7-CH_3OH before and after transient heating.

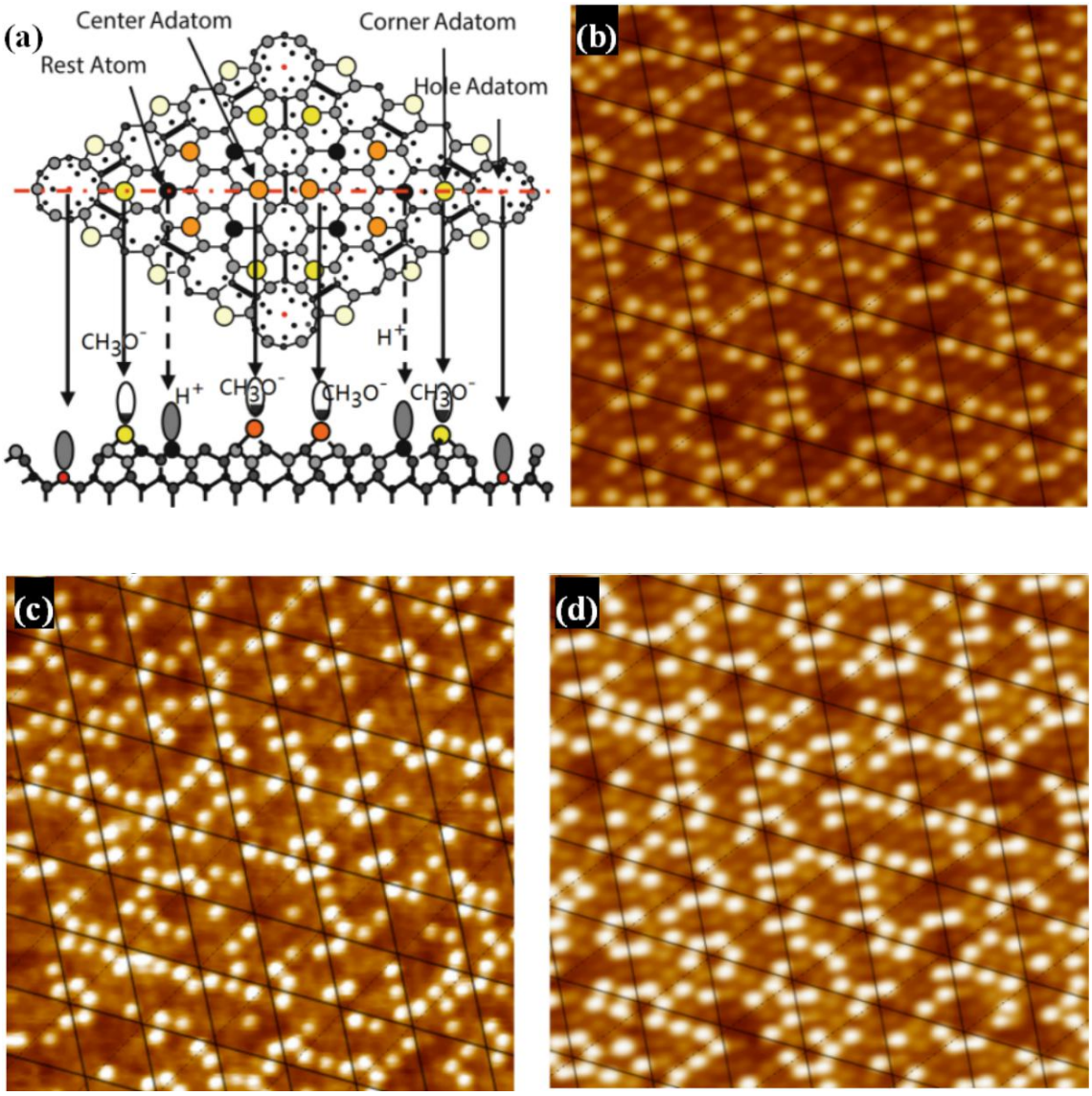

Fig. 2.15 (a) The adsorption positions of CH_3O^- and H^+. The bright spots (CH_3O^-) of three Si(111)-7×7-CH_3OH samples was counted; with the heating time is, (b) 2 s, center/corner= 86/140 = 0.614; (c) 3 s, center/corner = 77/144 = 0.535; (d) 4 s, center/corner = 65/133 = 0.489.

2.5.3 Explore the new rulers of metal-H^+ models

After verifying the isolation effect in the vertical direction, the characteristic on the horizontal direction is well worth looking forward to. The H atom saturates the suspended key at its location, the residual atoms on the lower layer of the surface are

further reduced at the height in the STM image and cannot be scanned. Atomic hydrogen adsorption on Si(111) or Ge(111) surface reveals many similarities, for example, other researchers observed the same mono- and dihydride phases in both cases [40, 41]. At higher temperature, monohydride phase (Si-H or Ge-H) occurs alone. While at room temperature, both mono and dihydride phases coexist on the two semiconducting surfaces. Recent advances in techniques of mass spectrometer suggested an interesting phenomenon after preheating the Si-CH_3OH sample. Compared with above, the strength of H^+ is obviously higher than that of CH_3O^- (Fig. 2. 16 (a)). Different bonds correspond to different critical temperature, it can be found that the thermal stability of CH_3O^- in corner/center sites is stronger than that of H^+. The results enlighten us that methanol can actually be divided into two parts, namely, the obvious CH_3O^- and the imperceptible H^+. Considering only the mass spectrometer data is not enough to convince, another weak-compound (Au) was selected for further study. Before using the methanol, Au atom is preferred to be adsorbed in the rest site at low concentrations. Just as shown in Fig. 2.16 (b), Au atoms are usually adsorbed in the corner or center sites of Si(111)-CH_3OH surface. When H^+ was disappearing since the preheating, the adsorption status of Au changed again (Fig.2.16 (c)). It can be found that Au atom in the corner/center site is higher than that of the rest site. As a result, the adsorption of metallic compounds has the possibilities to be regulated by controlling H^+.

On this basis, some models have been established for metal atoms and H^+. As can be seen from the change in Fig. 2.17, the purpose of this model was to reanalyze the situation of Sn compound above. One possible explanation is that H^+ occupied the rest sites preventing the extension of the Sn compound effectively. When the H^+ left the rest sites by preheating, Sn compound is able to expand in that direction. In the presence of hydrogen, the density of electronic states in this region was greatly decreased, the electronic charge also had a tendency to shift away. When the H^+ was disappeared, the charge was bound to return back, implying a moving trend. On this basis, we proposed the stable cluster structure in the case of Fe. Unlike the quasi-strong compound on intermediate layer before, a stable magnetic storage unit

can be realized (Fig. 2.17 (b)).

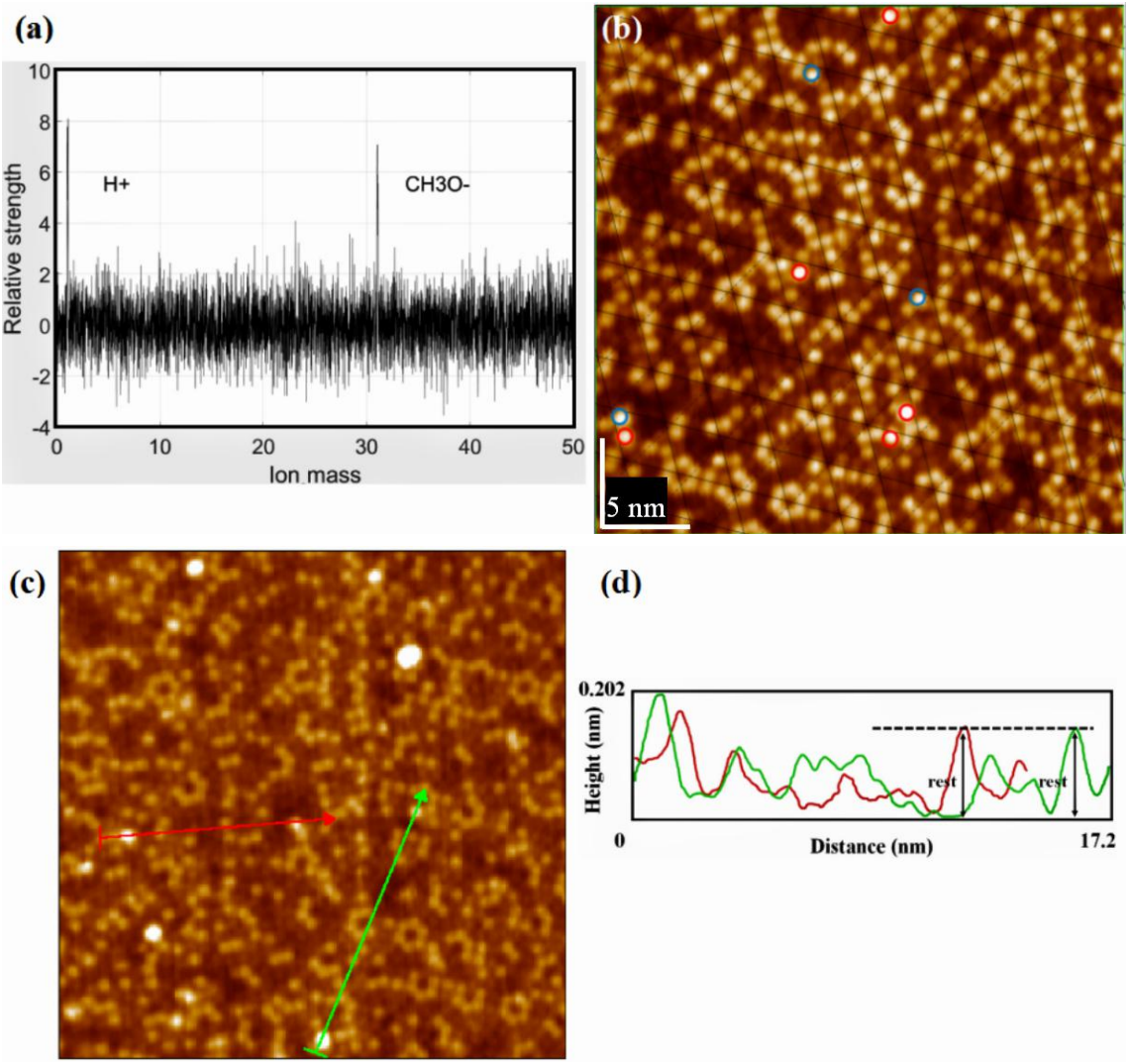

Fig. 2.16 (a) Mass spectra images of CH_3OH, after preheating; (b) STM image of the Si(111)-7×7-CH_3OH surface steamed with Au atoms, the red ones are center sites and the blue ones are corner sites; (c) After heating the sample, 0.2 A, 2 s, the Si(111)-7×7-CH_3OH surface steamed with Au atoms; (d) The height measurement of (c).

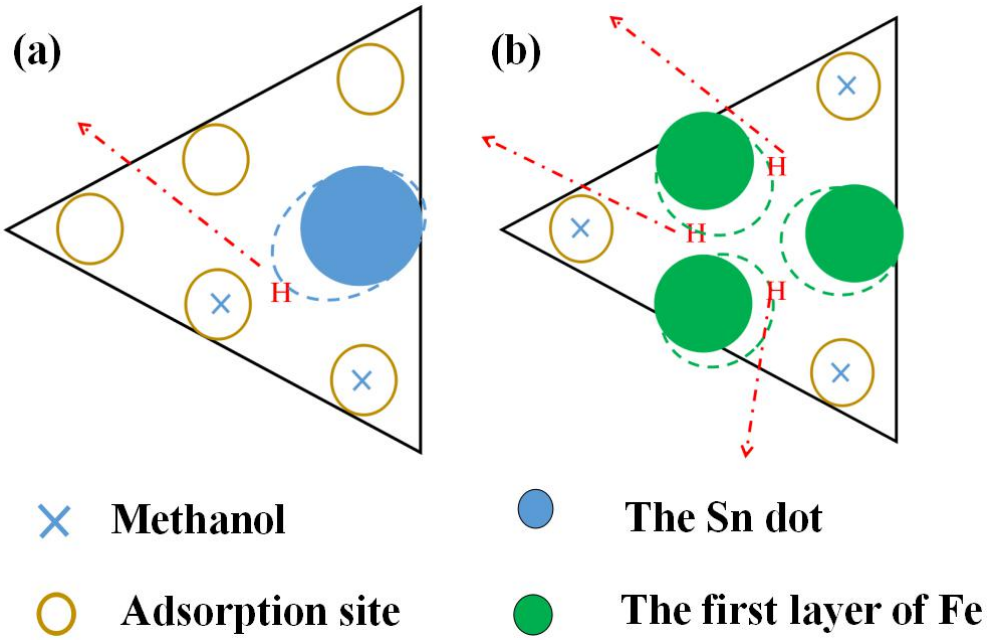

Fig. 2.17 Two typical metal-CH_3OH adsorption models: (a) the dashed line represents the situation after preheating. With the disappearance of H^+, Sn immediately expands to the H^+ position before vanishing; (b) the dashed line represents the situation after heating. With the disappearance of H^+, Fe atoms (in the same triangle) are more likely to gather together to form a stable cluster structure.

Concluding remarks

The preparation of high density storage must be based on a regular and stable substrate surface. In this paper, a regular 7×7 reconstructed structure is formed on Si (111) substrates by a series of cleaning, drying and annealing treatments. However, for some typical magnetic elements, such as Fe, it is very easy to react with Si surface, causing the original magnetic strength to be significantly reduced. According to the famous DAS adsorption model, the results can be described as follows:

1. By injecting various alcoholic gases into the observation chamber, it is found that they can be adsorbed stably on the silicon surface. Results of mass spectrometer comparison show that the key to their adsorption is H-O bond.

2. Characteristics of methanol were explored from vertical and horizontal directions respectively. In the vertical direction, the intermediate layer can affect the height and binding energy of the adsorbed atoms.

3 In the horizontal direction, the metal atoms hip can be effectively limited by methanol. The growth pattern of metal also changed from layer growth to island growth.

4 By heating si-ch3oh surface at low temperature, it can be found that the thermal stability of corner and center positions is different. By using it, there will be an important impact on the adsorption of metal atoms.

Reference

1 Takayanagi, K., Tanishiro, Y., Takahashi, M., & Takahashi, S. (1985). Structural analysis of Si(111)-7×7 by UHV‐transmission electron diffraction and microscopy. Journal of Vacuum Science & Technology A: Vacuum, Surfaces, and Films, 3(3), 1502-1506.

2 ZHANG, A. X., ZHOU, Q., & CHEN, L. (2005). Progress of silicone industry in China in 2004 [J]. Silicone Material, 3, 010.

3 Becker, R. S., Swartzentruber, B. S., Vickers, J. S., & Klitsner, T. (1989). Dimer–adatom–stacking-fault (DAS) and non-DAS (111) semiconductor surfaces: A comparison of Ge (111)-c (2× 8) to Si (111)-(2× 2),-(5× 5),-(7× 7), and-(9× 9) with scanning tunneling microscopy. Physical Review B, 39(3), 1633.

4 Qian, G. X., & Chadi, D. J. (1987). Si (111)-7×7 surface: Energy-minimization calculation for the dimer–adatom–stacking-fault model. Physical Review B, 35(3), 1288.

5 Tochihara, H., & Shimada, W. (1993). The initial process of molecular beam epitaxial growth of Si on Si (111) 7× 7: a model for the destruction of the 7×7 reconstruction. Surface science, 296(2), 186-198.

6 Takahashi, K., Nara, C., Yamagishi, T., & Onzawa, T. (1999). Calculation of surface energy and simulation of reconstruction for Si (111) 3×3, 5×5, 7×7, and 9×9 DAS structure. Applied surface science, 151(3-4), 299-301.

7 Ichimiya, A., & Mizuno, S. (1987). RHEED intensity analysis of Si (111) 7×7-H surface. Surface science, 191(1-2), L765-L771.

8 Giessibl, F. J. (2000). Atomic resolution on Si (111)-(7×7) by noncontact atomic force microscopy with a force sensor based on a quartz tuning fork. Applied Physics Letters, 76(11), 1470-1472.

9 Phaneuf RJ, Bartelt NC, Williams ED, Swiech W, Bauer E: Crossover from metastable to unstable facet growth on Si(111). Phys Rev Lett 1993, 71:2284

10 Olshanetsky BZ, Solovyov AE, Dolbak AE, Maslov AA: Structures of clean and nickel-containing high Miller index surfaces of silicon. Surf Sci 1994,306:327.

11.Tsai V, Wang XS, Williams ED, Schneir J, Dixson R: Conformal oxides on Si surfaces. Appl Phys Lett 1997, 71:1495.

12 Gotoh, Y., & Ino, S. (1978). Surface Structures of Ag on Si (111) Surface Investigated by RHEED. Japanese Journal of Applied Physics, 17(12), 2097.

13 Ino, S. (1980). An investigation of the Si (111) 7× 7 surface structure by RHEED. Japanese Journal of Applied Physics, 19(7), 1277.

14 Tanishiro, Y., Kaneko, K., Minoda, H., Yagi, K., Sueyoshi, T., Sato, T., & Iwatsuki, M. (1996). Dynamic observation of In adsorption on Si (111) surfaces by UHV high-temperature scanning tunneling microscopy. Surface science, 357, 407-413.

15 Cune, L. C., & Apostol, M. (2000). Ground-state energy and geometric magic numbers for homo-atomic metallic clusters. Physics Letters A, 273(1-2), 117-124.

16 Johnston, R. L. (2002). Atomic and molecular clusters. CRC Press.

17 Ariga, K., Ito, H., Hill, J. P., & Tsukube, H. (2012). Molecular recognition: from solution science to nano/materials technology. Chemical Society Reviews, 41(17), 5800-5835.

18 McHenry, M. E., & Laughlin, D. E. (2000). Nano-scale materials development for future magnetic applications. Acta materialia, 48(1), 223-238.

19 S. V. Sitnikov, A. V. Latyshev, S. S. Kosolobov, Advacancy-mediated atomic steps kinetics and two-dimensional negative island nucleation on ultra-flat Si (111) surface, J. CRYST. GROWTH. 457 (2017): 196-201.

20 J. Aulbach, S. C. Erwin, R. Claessen, Spin Chains and Electron Transfer at Stepped Silicon Surfaces, NANO. LETT. 16 (2016): 2698-2704.

21 K. Biedermann, S. Regensburger, T. Fauster, Spin-split silicon states at step edges of Si (553)-Au, PHYS. REV. B 85(2012): 245-413.

22 W. Ding, D. Ju, Y. Guo, K. Tanaka, F. Komori, Formation of linearly linked Fe clusters on si(111)-7×7-C2H5OH surface, NANOSCALE RES. LETT. 9 (2014): 377.

23 Shimizu, N., Kimura, T., Nakamura, T., & Umebu, I. (1990). An ultrahigh vacuum scanning tunneling microscope with a new inchworm mechanism. Journal of

Vacuum Science & Technology A: Vacuum, Surfaces, and Films, 8(1), 333-335.

24 Horch, S., Zeppenfeld, P., David, R., & Comsa, G. (1994). An ultrahigh vacuum scanning tunneling microscope for use at variable temperature from 10 to 400 K. Review of scientific instruments, 65(10), 3204-3210.

25 Meyer, G. (1996). A simple low‐temperature ultrahigh‐vacuum scanning tunneling microscope capable of atomic manipulation. Review of scientific instruments, 67(8), 2960-2965.

26 Ekvall, I., Wahlström, E., Claesson, D., Olin, H., & Olsson, E. (1999). Preparation and characterization of electrochemically etched W tips for STM. Measurement Science and Technology, 10(1), 11.

27 Pethica, J. B., & Oliver, W. C. (1987). Tip surface interactions in STM and AFM. Physica Scripta, 1987(T19A), 61.

28 Radican, K., Berdunov, N., Manai, G., & Shvets, I. V. (2007). Epitaxial molybdenum oxide grown on Mo (110): LEED, STM, and density functional theory calculations. Physical Review B, 75(15), 155434.

29 Sun, C. Q. (2001). O–Cu (001): I. Binding the signatures of LEED, STM and PES in a bond-forming way. Surface Review and Letters, 8(03n04), 367-402.

30 Lee, G., Kim, H., & Koo, J. Y. (2003). Atomic structure of the Ba-induced Si (111) 3×2 reconstruction studied by LEED, STM, and ab initio calculations. Physical Review B, 68(11), 115314.

31Jensen, K., Kim, K., & Zettl, A. (2008). An atomic-resolution nanomechanical mass sensor. Nature nanotechnology, 3(9), 533.

32 Alvarez, J.; De Parga, A.V.; Hinarejos, J.J.; De la Figuera, J.; Michel, E.G.; Ocal, C.; Miranda, R. Initial stages of the growth of Fe on Si (111) 7 × 7. Phys. Rev. B 1993, 47, 16048.

33 Mascaraque, A.; Avila, J.; Teodorescu, C.; Asensio, M.C.; Michel, E.G. Atomic structure of the reactive Fe/Si (111) 7× 7 interface. Phys. Rev. B. 1997, 55, R7315.

34 Tanaka, K.; Nomoto, Y.; Xie, Z.X. Dissociation mechanism of 2-propanol on a Si(111)-(7×7) surface studied by scanning tunneling microscopy. J. Chem. Phys.

2004, 120, 4486–4491.

35 Douglas, D. J., & French, J. B. (1981). Elemental analysis with a microwave-induced plasma/quadrupole mass spectrometer system. Analytical Chemistry, 53(1), 37-41.

36 Frey, N. A., Peng, S., Cheng, K., & Sun, S. (2009). Magnetic nanoparticles: synthesis, functionalization, and applications in bioimaging and magnetic energy storage. Chemical Society Reviews, 38(9), 2532-2542.

37 Geng, J. (2013). Three-dimensional display technologies. Advances in optics and photonics, 5(4), 456-535.

38 Sitti, M., Aruk, B., Shintani, H., & Hashimoto, H. (2003). Scaled teleoperation system for nano-scale interaction and manipulation. Advanced Robotics, 17(3), 275-291.

39 Kokott, S., Matthes, L., & Bechstedt, F. (2013). Silicene on hydrogen‐passivated Si (111) and Ge (111) substrates. physica status solidi (RRL)–Rapid Research Letters, 7(8), 538-541.

40 Alaoui, M., Ringeisen, F., Bolmont, D., & Koulmann, J. J. (1990). Photoemission study of low pressure hydrogen and disilane adsorption on Si (111) 7× 7 and Ge (111). Thin Solid Films, 184(1-2), 147-152.

41 Shane, S. F., Kolasinski, K. W., & Zare, R. N. (1992). Recombinative desorption of H2 on Si (100)‐(2× 1) and Si (111)‐(7× 7): Comparison of internal state distributions. The Journal of chemical physics, 97(2), 1520-1530.

Chapter 3 Growth of Fe clusters on the Si(111)-7×7 surface saturated with CH_3OH

3.1 Introduction

Based on the phenomenological theory of ferromagnetic material, the conception of magnetic domain was first proposed by P. E. Weiss in 1907 [1], and the structure of magnetic domain based on the interaction of the magneto-static energy was proposed by L. D. Landau and E. M. Lifshitz in 1935 [2]. Recently, it was found that the particles change to single-domain magnetic clusters by decreasing their size [3-5]. Accordingly, the preparation of single magnetic domain clusters is an interesting challenge to magnetic materials for high-density magnetic recording medium. At present, the reported critical sizes for single magnetic domains were 85 nm for Ni, 40 nm for Fe_3O_4, and 16 nm for α-Fe [3-5]. The metallic cluster with a size lower than the critical value displays super paramagnetism, which could not be applied for the magnetic storage medium. Aim to improve the density of magnetic storage without the restriction of super paramagnetism, it is necessary to prepare the single magnetic domain clusters with limited critical size. In this way, Fe single magnetic domain clusters have become the research focus, which could be analyzed for the spin in physics, controllable surface reaction in chemistry, Such as FeN/FeO_x with the critical size lower than 10 nm.

In the past few decades, using scanning tunneling microscopy (STM) and first-principles calculation, the adsorption sites of metal atoms on Si(111)-7×7 surface have been systematically investigated and identified [6,7]. However, since several specific models were not clear, the formation process could not be controlled accurately. Firstly, in the absence of an intermediate layer (like alcohol), Fe atom would inevitably react with Si, forming the Fe-Si compound [8,9]. In order to preserve the magnetic property of iron, this paper tended to focus on CH_3OH [10,11].

In this report, STM results showed that Fe clusters were deposited on Si(111)-7×7 restructured surface, which was saturated by methanol (Si(111)-7×7-alcohol). In the condition of low concentration, Fe atoms would be randomly deposited onto the surface of Si(111)-7×7-CH_3OH. With a longer deposition time, Fe clusters will arrange as a linear structure on the substrate. If the air was introduced onto the surface of sample, the line structure will be more obvious. We have observed the Si atom moving on the Si(111)-7×7-CH_3OH surface, and Fe cluster combining after air introduction. By the XPS test, it is known that Fe doesn't react with O_2 in the air, while Si reacts with O_2 and forms SiO_2.

3.2 The realization of the steaming process of the Fe atoms

3.2.1 Atomic layer deposition

Atomic layer deposition (ALD) is an attractive method to deposit thin films for advanced technological applications such as microelectronics and nanomaterial. In ALD, atomic layer structure has matured for 10 years, which was proved to be of technological importance. In our study, the influence of incident atomic energy on deposition reaction and the reliability of film deposition process control were studied. First of all, by adjusting different steaming temperature, initial incident energy of atoms can be controlled. Just as Fig. 3.1, the influence of incident atomic energy on the deposition process has also been studied. The results show that the incident energy is closely related to the movement of the deposited atoms on the surface of the substrate. There are usually two different deposition stages, namely, initial deposition and subsequent growth. The initial deposition stage has an important influence on the morphology of films (island growth or layered growth). The occurrence of shallow injection and deep injection will result in the displacement of atoms on the substrate during the deposition of thin films. Thus, the deposited films are confused and the quality of them is affected. As the energy of incident atoms increases further, the rebound of incident atoms will occur as shown in the figure.

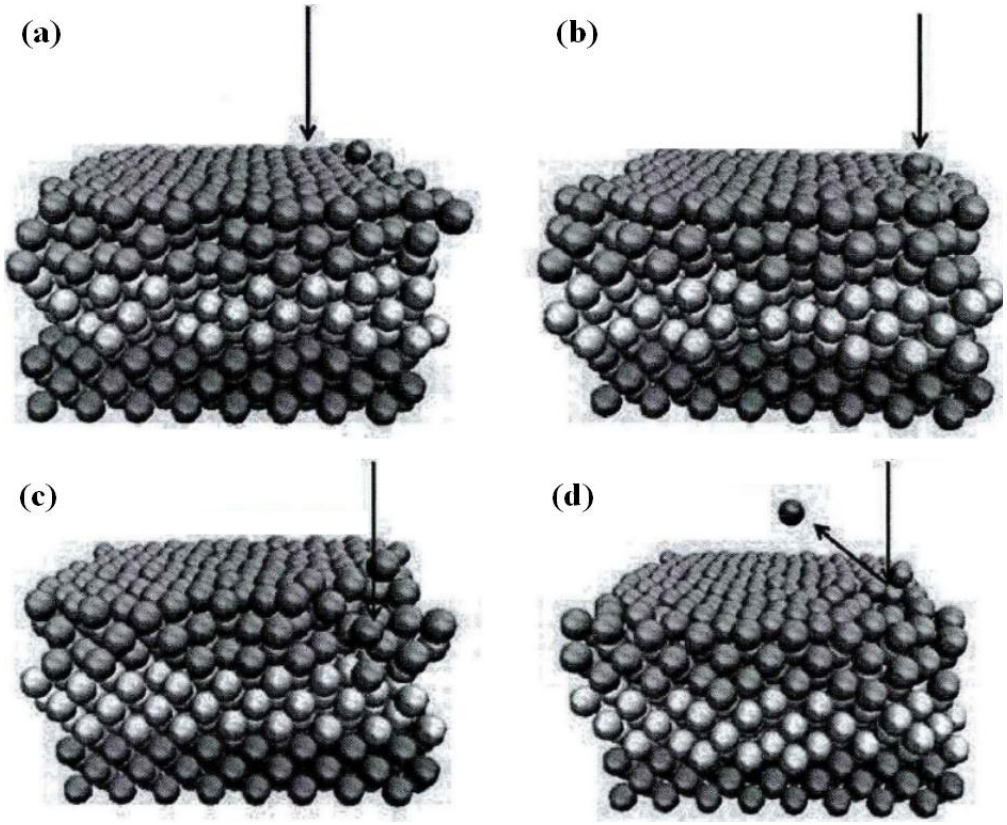

Fig. 3.1 Four types of atomic deposition: (a) Migration freeze; (b) Shallow injection; (c) Deep injection; (d) Rebound.

After the data of the mass spectrometer was collected, Si(111)-7×7-CH_3OH samples were moved to the preparation chamber. In the STM system, metal atoms can be deposited by controlling the evaporation time and pressure. Through the evaporation device, Fe atoms were evaporated by heating a W filament with iron wire (purity >99.995%). Different wire dimensions correspond to different rated operating temperatures. Aimed to improve the evaporation temperature in references (about 1000 °C) [12-14], a thinner Fe wire was selected to realize the higher temperature (about 1300 °C) and reduce the influence on the linear structure.

3.2.2 Realization of metal atom steaming process

At present, many vacuum deposition techniques can accurately control the deposition speed and time, which are often used for the growth of surface nanostructures. It is noted that low-dimensional nanomaterials are the basis of new generation of solid-state quantum devices. Controllable growth of high-quality and low-dimensional nanostructured materials and continuous progress in micro-fabrication technology may lead to a new revolution in micro-electronics as well as optoelectronics technology, which are of great significance. Therefore, the growth, characterization and device application of low-dimensional nanostructured materials have become a perfect research topic in the world. At present, many new methods have been developed to prepare regular nanostructures. For example, an ordered array of nanostructures can be fabricated by means of a multilayer stress film, which is perpendicular to the substrate surface. However, it is still quite difficult to control the density, uniformity and order of these metal dots accurately. An effective way to improve the regularity (linearity) is to optimize a substrate with periodic structure. Deposited atoms can aggregate to form nanoscale clusters at some specific positions of the periodic distribution on the substrate, and then form ordered two-dimensional arrays. Compared with the method of self-organized growth of nanostructures using periodic stress field, this method is more concise in experiment. Moreover, regular linear structures are easier to obtain. Here, Si(111)-7×7 was selected as substrate to prepare ordered two-dimensional superlattice structures on its surfaces.

In a ultra high vacuum system (lower than 10^{-6} Pa), the heating beam source makes the molecules or atoms with certain thermal energy sprayed to the substrate surface to be deposited. Including surface migration, decomposition, adsorption and deposition, cluster growth is achieved by the reaction of molecule/atom on the substrate surface. Besides, the angle and temperature of the substrate can be set artificially in advance, so it is easy to control and explore the effects of various

growth conditions on the film formation. In general, high-temperature steaming technology has the following characteristics:

(1) The source and substrate are heated and controlled separately, and the temperature of cluster growth is low. Thermal defects, impurities and diffusion of substrates can be reduced during the growth process.

(2) Low growth rate (about 0.1-1 nm/s). A baffle can be used to precisely control the direction and position of evaporation, which is also very important in atomic-level growth process.

(3) It is not carried out under the condition of thermal equilibrium, but a dynamic process. Therefore, materials which are difficult to grow under general thermal equilibrium conditions can be explored.

3.2.3 Investigation on scanning mode for metal deposition

The deposition and accumulation of multilayer iron clusters is an important research topic for the growth controlled by magnetic units. The morphology of nanostructures has been analyzed and studied by using the precise height analysis and large area scanning function of STM. The tip scanning component consists of three piezoelectric ceramics, (namely x, y and z), which are perpendicular to each other. Piezoelectric ceramics shrink or elongate under the action of voltage. When sawtooth wave and oblique wave voltage are applied in X and Y directions respectively, the tip of the needle is scanned on the XY plane. The tunnel current generated by bias voltage is compared with the reference value. The structure is fed back to piezoelectric ceramics in Z direction. If the tunnel current is greater than the reference value, the piezoelectric ceramics in the Z direction shrink, leaving the tip away from the sample. On the contrary, the piezoelectric ceramics in the Z direction are elongated so that the needle tip is close to the sample. Therefore, when the tip is scanned on the XY plane, the tunneling current as well as the relative position of piezoelectric ceramics in Z direction can be obtained, and the surface STM current and morphology can be obtained by drawing the two-dimensional image.

On sillicon surface, it is difficult to obtain atomic-level images because of the high roughness of substrates. It is found that the roughness of the substrate can be attributed to two situations. One is that the surface fluctuation is less than 0.5 nm in the range of tens of nanometers, while the other is that the roughness is more than 1 nm. STM scanning mode generally includes two modes: constant current mode and constant height mode. The constant current mode is to make the current constant by adjusting the tip of the needle with a feedback loop. This surface topography image is generated by recording the vertical position of the needle tip. Constant height mode is to keep the vertical position of the tip unchanged, that is, there is a very small structural feedback, or no feedback. As a function of lateral position, current was used to describe the surface image. This mode is only suitable for flat surfaces (atomic level). Conversely, the impact of needle tip is inevitable. It has the advantage that the scan frequency is very high (up to 10 KHz). In contrast, the frequency of scanning in a constant-current mode is about a few tens of seconds.

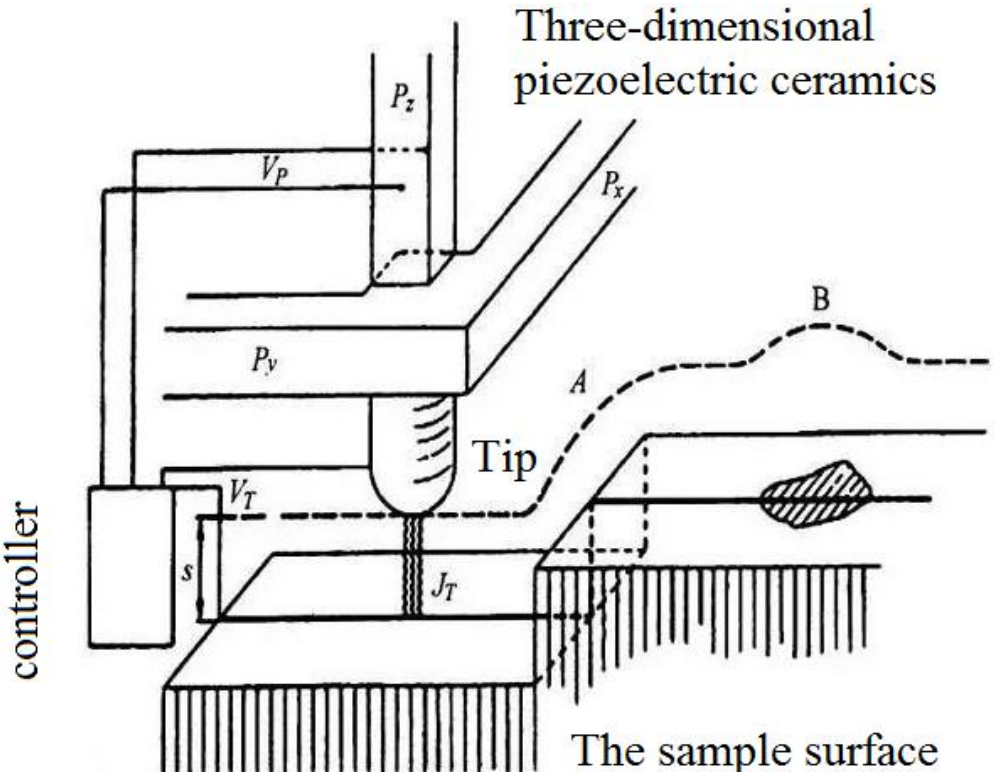

Fig. 3.2 The basic structure diagram of STM.

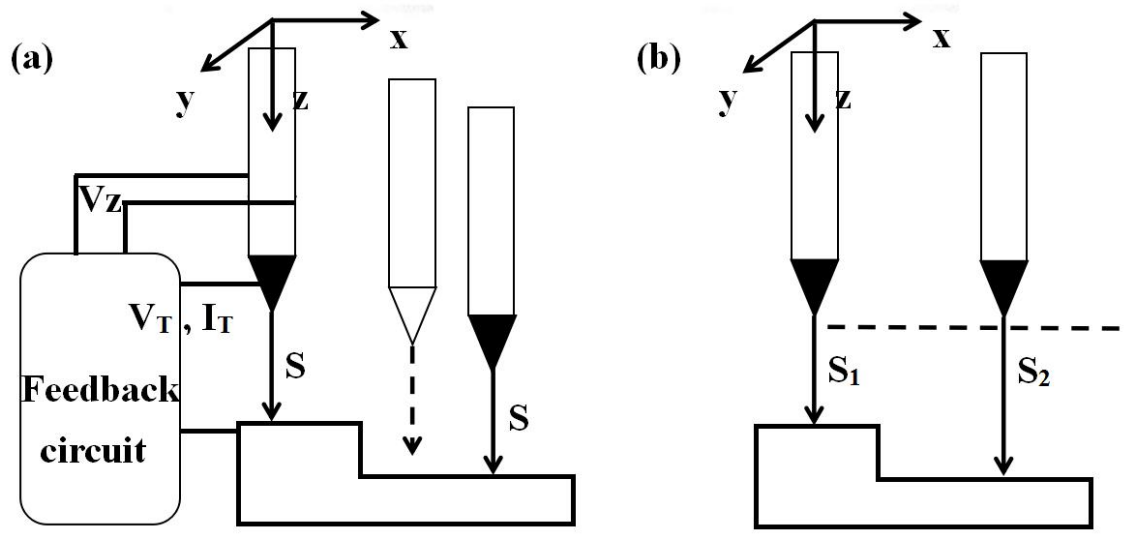

Fig. 3.3 (a) Constant current mode; (b) Constant altitude mode

3.3 The original discovery of linear Fe clusters structure on Si(111)-7×7

It is proved that methanol plays a "weakening" role in the catalytic process of metal adsorption. Also at the same concentration of Fig. 3 (b), the forming probability of Fe clusters was reduced on this intermediate layer. Fortunately, a linear structure was formed again (like Fig. 3.3 (c)) in the direction perpendicular to the boundary line. STM images of Fe clusters formed on Si(111)-7×7-alcohol surface are shown in Figure 3.2. In the condition of low concentration (0.01 ML), a few of Fe clusters are randomly formed on the Si(111)-7×7-alcohol surface, instead of dispersed single Fe atoms. The situation of these new Fe clusters was directly investigated in height measurement, there is no obvious height difference between the cluster and cluster. Just as shown in Fig.x, it can be recognized that a Fe cluster usually has 5-6 atoms, forming a pentagonal base pyramid structure [15, 16]. Although the formation of Fe clusters becomes more difficult, the linearity of them is enhanced. Continue to

increase concentration, several linear clusters were observed. When the Fe atom deposition was increased to 2 ML, some Fe clusters linked in straight chains as shown in Figure 3 (b). It is worthy of note that the straightly linked chain looks to grow to the lower or upper terrace on the Si(111)-7×7-alcohol surface by crossing the ladder region. When the Fe deposition was increased to 4 ML, almost Fe clusters were self-assembled by forming straightly linked chain structures.

It has been previously known that some irregular metal clusters are distributed on the surface of Si(111)-7×7 at low deposition rates. When the metal adsorption position is different, the shape of the cluster formed is also different. On this basis, we further control the extent of deposition to obtain uniform clusters of iron. It has been previously discussed that Fe atoms preferentially adsorb at the center sites of the Si (111)-7×7 surface. Therefore, we speculate that Fe atoms will first occupy three center sites, forming Fe_3 clusters. After that, Fe atom continues to adsorb around them, expanding the cluster structure. If deposition is further increased, Fe atoms will cover the entire Si(111)-7×7 surface. In order to explore the self-organized growth of Fe on Si(111)-7×7 surface, one of the most important parts of the formation process needs to be analyzed. That is, the diffusion process of adsorbed atoms on the substrate surface. Atoms on the substrates will not form ordered structures, without sufficient diffusion and migration. For example, if the diffusion and migration of the adsorbed atoms on the base surface are zero, they would stay at the initial adsorption sites. As a result, the morphology of the growth surface is very rough and amorphous epitaxial films are formed. Conversely, high mobility does not necessarily result in a flat growth surface. A large number of mechanisms remain to be further explored and analyzed.

3.4 Improvement of structural properties in iron cluster

3.4.1 Investigation on cluster property of metal dot

The cluster is a relatively stable microcosmic or submicroscopic group, which is

made up of a few atoms, or molecules, or ions, in the form of physics or chemistry reaction [17-19]. Its theoretical and applied properties vary with the number of atoms contained. Moreover, cluster is a concept of nanomaterials in atomic scale. The spatial scale of cluster is from several to several hundred aedes, which is too small to be described by inorganic molecules and too large to be described by small solid blocks. Generally, the physical and chemical properties of them are different from those of single atom molecules, solids and liquids, and can not be obtained by simple linear epitaxy or interpolation of their properties. Therefore, the cluster can be seen as a new level of physical structure between atoms, molecules and macros. It is a transitional state of various substances from atoms and molecules to bulk substances, representing the initial state of condensed matter. The main directions of cluster research are:

(1) The composition and electronic configuration, magic number, geometric structure and stability of clusters are studied.

(2) Study the nucleation and formation process and mechanism of clusters, and to study the preparation methods of clusters, especially to obtain uniform and controllable cluster beams.

(3) Study the optical, electrical, magnetic, mechanical and chemical properties of metal, semiconductor, non-metal and various compound clusters, their relationship with structure and size, and the key points of transition to bulk materials.

(4) Study the synthesis and properties of cluster materials.

(5) Explore new theories can not only explain the effects and phenomena of existing clusters, but also explain and predict the structure of clusters, simulate the dynamic properties of clusters and guide experiments.

(6) Develop new methods to modify and control the surface of clusters.

Metal nanoclusters have many excellent properties due to their size. In order to make nanoclusters play a role, we use many ways to functionalized them. Through the needle valve, one set of Ar gas storage device was connected with the preparation chamber. With or without introducing Ar, Fe atoms were evaporated by heating a W filament with an iron wire (purity > 99.995%). Different Si(111)-7×7-CH_3OH-Fe samples were sent into the observation chamber.

3.4.2 Observation on the effect of position adjustment of methanol adsorption

The structure of Si(111)-7×7-alcohol-Fe has attracted wide attention because of its linearity. As the degree of Fe atomic adsorption increased, some clusters linked in straight chains. It is noteworthy that the straightly linked chain looks to grow to the lower or upper terrace on the Si(111)-7×7-CH_3OH surface by crossing the step edges, but the low success rate and fuzzy formation process have always puzzled researchers. Here, we divide the Fe clusters position into 2 types. Attention was again focused on the corner site and center site in order to answer the question: Which one is more favorable for the formation of Fe cluster? Through observation, we find that when Fe clusters are randomly distributed, the methanol around them are also random. While, linear Fe clusters have more regular CH_3OH distribution. Further, the adsorption probability of Fe on center sites should be improved because of the more unoccupied sites. On the basis of Figure 3.6 (heating 3 s and 4 s), Fe atoms were deposited on these two Si(111)-7×7-CH_3OH samples. We have enough reasons to believe that if the CH_3OH adsorption regularly, can the perfect linearity found.

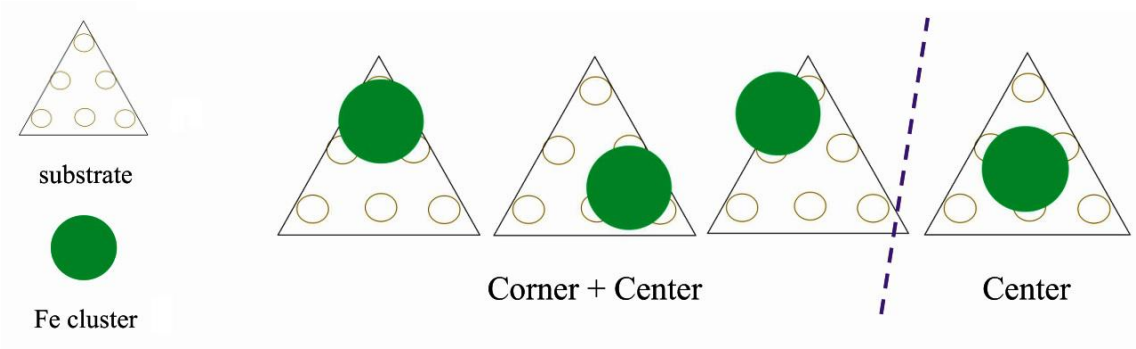

Fig.3.4 two types of Fe atoms adsorption sites

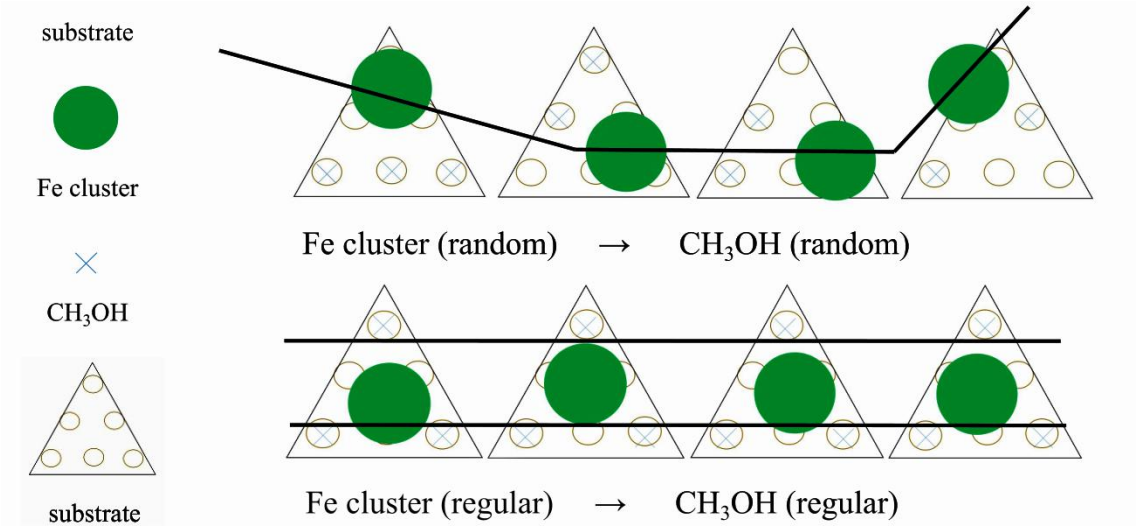

Fig. 3.5 The relationship between linearity and methanol adsorption position

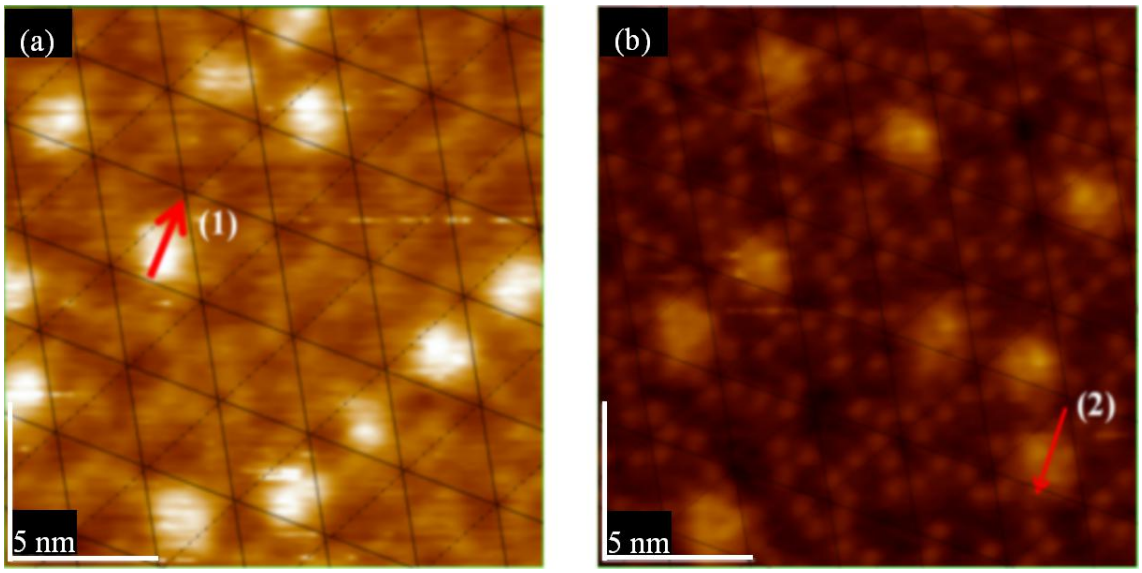

Fig. 3.6 STM images of the Si(111)-7×7-CH_3OH-Fe surface with the iron adsorption site ratio of, (a) center/corner = 44/48 = 0.916; (b) center/corner = 41/65 = 0.63;

3.4.3 The relationship of steaming temperature and crystal structure

Crystal structure (i.e. the microcosmic structure of a crystal) refers to the specific arrangement of atoms/ions/molecules in a crystal. The crystallization of a change in the arrangement of metal atoms. Crystal structure is one of the basic factors that determine the physical, chemical and mechanical properties of solid metals. Different structures lead to different properties of materials [20, 21]. There are mainly three metal lattices: face-centered cubic lattice, body-centered cubic lattice and dense hexagonal lattice. Crystals are homogeneous anisotropic objects. Crystals with good growth often exhibit some symmetry in appearance. Metal materials are not made up of only one large single crystal, but a amount of small crystals, namely polycrystals. If a large number of atoms are steamed on the base surface, there should be infinitely many different arrangements. While in the lowest energy state corresponding to the equilibrium state, atoms are likely to arrange regularly. One cluster is separated from the other in two-dimension plane, with the distances of 1-2 atoms.

So that, in addition to the promoting effect of CH_3OH, high evaporation temperature is another crucial determinant. Just as Figure 3.7 (a) shows, the structural model of Fe crystal changes with the increase of temperature. Different cluster structures have different stacking patterns, such as face centered cubic unit cell, body centered cubic unit cell, etc. Taking into account the Fe vapor pressure under 900 °C, it is difficult to believe that it is possible to evaporate Fe at such a low temperature. The result given in Figure 3.7 (b) validates this view: Fe atoms and Fe dots are simultaneously deposited on the surface of Si(111)-7×7-CH_3OH. Unlike the cluster, the dot does not have a regular adsorption structure. If only the atomic parts are observed, they are indeed somewhat similar to α-Fe model in Figure 3.7 (a). Compared to the equilateral triangle model of γ-Fe, these Fe atoms present an isosceles triangle arrangement like α-Fe model. A higher temperature was therefore selected to ensure that iron can be evaporated in the form of single atoms. When the

temperature is increased to 1200 °C, the arrangement of atoms changes to the γ-Fe pattern. One Fe atom (green one) continues to be adsorbed on the center of the first layer of Fe atoms (red ones), forming the second layer. Results given in different evaporation temperatures support our new model above, where the fuzzy formation process of Fe cluster can now be clear.

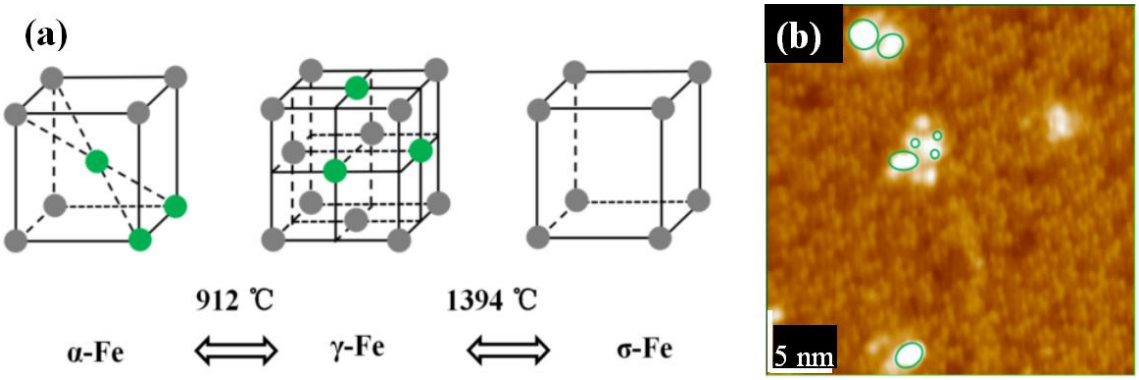

Fig. 3.7 (a) Temperature-Structure change diagrams of Fe cluster; (b) STM image of the Si(111)-7×7-CH_3OH-Fe surface, which the evaporation temperature is 900 °C.

3.5 The proposal of a double layers iron cluster model

The cluster is a stable state between atoms, molecules and massive materials. It does not have a strict conceptual boundary with the nanomaterials and particles, but is still different from the traditional research focus. The preparation of atomic level structure is one of the main ways for cluster applications, and it is also a major subject of cluster science which is of great interest to people. Undoubtedly, the size of cluster particles in atomic scale will be accompanied by strong quantum confinement effect, which will lead to many new phenomena and properties. The research of new cluster materials is still in its development stage, mainly focused on its physical properties. The unique phenomena of atomic clusters originate from their structural characteristics. Because of its small size, the proportion of atoms on the surface is

very high. While, the geometry, spin state and interatomic force of surface atoms are completely different from those of atoms in bulk phase. New properties of clusters are closely related to the surface interaction between internal units. For example, by adjusting the size of clusters, the material properties are greatly different. If a cluster contains only 10 iron atoms, it may be 1,000 times more efficient than a cluster of 17. The basic problem of cluster research is to find out how clusters evolved from atoms and molecules step by step. And with this evolution, how does the structure and properties of clusters change? Just like, when the size is large, it becomes a macroscopic solid. Thus, cluster science is also classified into an interdisciplinary category. The concepts and methods of atomic molecular physics, condensed matter physics, quantum chemistry, structural chemistry, atomic cluster chemistry, surface science and material science are interwoven, forming the central topic of current cluster research and developing into a new subject between atomic molecular physics and solid physics. Clusters widely exist in nature and human practice, involving many and many moving processes and phenomena of substances, such as catalysis, combustion, crystal growth, nucleation and solidification, phase transition, sol, film formation and sputtering, etc., forming an intersection of physics and chemistry, becoming a new growth point of materials science.

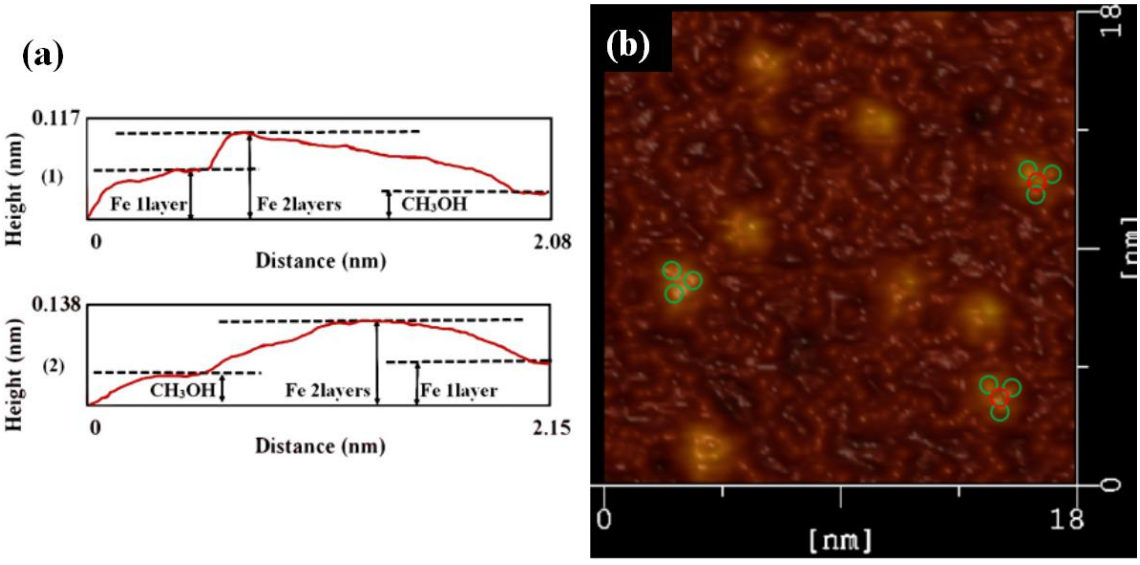

Fig. 3.8 (a) The height measurement image of the Si(111)-7×7-CH_3OH-Fe; (b) is the 3D model of Fe clusters.

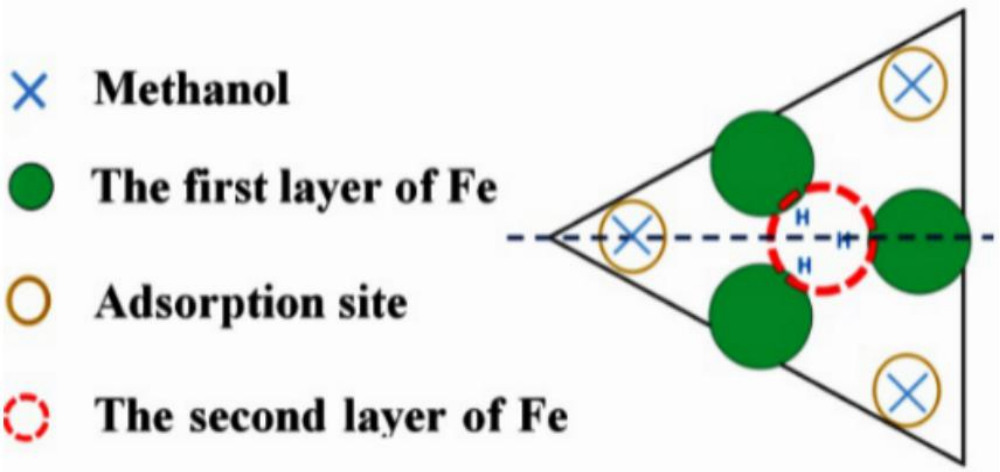

Fig. 3.9 Two-layer model of Fe cluster. The green circle represents an iron atom of the first layer, and the red circle represents an iron atom of the second layer.

Just as Figure 3.8 (a) shows, iron was more and more inclined to be adsorbed in the central area of each triangle. Fortunately, several linear structures were also observed on Si(111)-7×7-CH_3OH surface. Additionally, height measurements are presented. There are three height values (low, high and medium high) which clearly represent: CH_3OH on the corner sites, the second layer of Fe atoms, the first layer of Fe atoms. In addition to the height data, 3D surface display technology of the STM system was further used to observe the specific structure. In the ordinary scanning image, the adsorption situation was usually analyzed by the spot condition. However, 3D images transformed by the first-principles calculation can show the surface topography in a more visible pattern. Its calculation process is purely based on the positions of atoms, without any other empirical or semi-empirical parameters. If CH_3O^- on corner sites can be considered as an outer triangle, Fe atoms in the first layer are more like an inner triangle, just as Figures show. Moreover, Fe atoms in the second layer are mostly on the center of both the outer triangle and the inner triangle.

3.6 Study on linearity of ultrathin films

3.6.1 Concept of Stacking model

If in a periodical change of crystal structure or chemical composition in the atomic position, can produce a structure for a long period of time. Moreover, the original cell becomes a structural unit of structure for a long period of time. The changes are as follows: the ordered distribution of atoms in doped elements or solid melts, the orderly stacking of densely packed layers, and the long-term distribution of crystal defects. In the long period structure of iron clusters, but also related to two aspects of stacking orderly and chemical orderly.

Crystals themselves can also be thought of as being composed of many identical layers of atoms stacked one by one in a certain way. For some crystals with complex microstructure, the description of the microstructure of crystals by the atomic layer and its stacking method can often reveal the geometric features of the spatial arrangement of atoms more clearly, making the crystal with complex microstructure become clear at a glance. Different surfaces often correspond to different stacking modes, as shown in the figure 3.10.

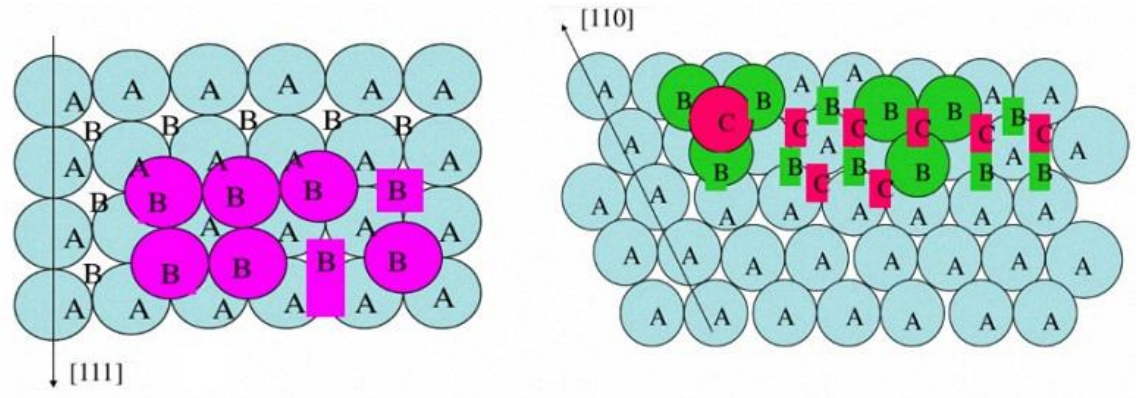

Fig.3.10 The stacking models on (110) and (111) plane.

3.6.2 Explore linear Fe clusters on Si(111)

The magnetic linear structure refers to the magnetic nanomaterials with width ranging from several nanometers to tens of nanometers, whose length is about hundreds of nanometers. The anisotropy of magnetic shape and the anisotropy of crystal structure also exist in the magnetic linear structure. The factors affecting the crystal structure include composition, deposition conditions and heat treatment [22-24]. For magnetic materials such as Fe and Ni with cubic structure, the shape anisotropy is much larger than the magneto-crystalline anisotropy constant, so the main factor determining their magnetic properties is shape anisotropy. For the one-dimensional magnetic linear structure, the demagnetization energy in the vertical and parallel directions of nanowire axes differs significantly due to its unique one-dimensional linear structure. The demagnetization energy reaches its maximum in the direction perpendicular to the nanowire axis. On the contrary, in the direction parallel to the nanowire axis, the demagnetization energy is the smallest. Therefore, the easy magnetization direction of the magnetic linear structure is parallel to the nanoaxis, and the difficult magnetization direction is perpendicular to the nanoaxis.

In order to explore the formation process, the surface reaction has been explained by assuming an appropriate activation complex reflecting the potential energy surface. This idea was proposed by the deposition of metal on clean Si(111)-7×7 surface and Si(111)-7×7-alcohol surface, but hasn't been confirmed yet. The potential barrier theory was used to explain the reaction rate, while the specific reaction characteristics could not be predicted from it. Based on the cluster model above, this paper further explored the linear structure from the point of macro view. In the direction of Reference (111), the atomic stacking model of face centered cubic unit cell (Figure 3.10) should be referenced. In atomic stacking theory, as the concentration of iron increases, stable clusters are always presented in the form of intervals. The more regularity, the higher forming probability of linear cluster structure. Just as Figure shows, on the one hand, the interval between units (clusters) can avoid some of the

mutual interference problems associated with the small size effect and the surface effect [25, 26]. On the other hand, the regularity of each stable cluster further implied the chemical stability of the whole linear structure. During repeated experiments, more and more linear structures (like Figure 3.11) were realized. Obviously, there is a continuity between the previous theoretical predictions and experimental data [26]. The stability of Fe linear structure was preliminarily investigated in height measurements. In a linear Fe cluster structure, it seems that the interaction between each unit could not affect the stability of our cluster model. A single Fe cluster was also compared with the cluster in the linear structure, no obvious height difference was found.

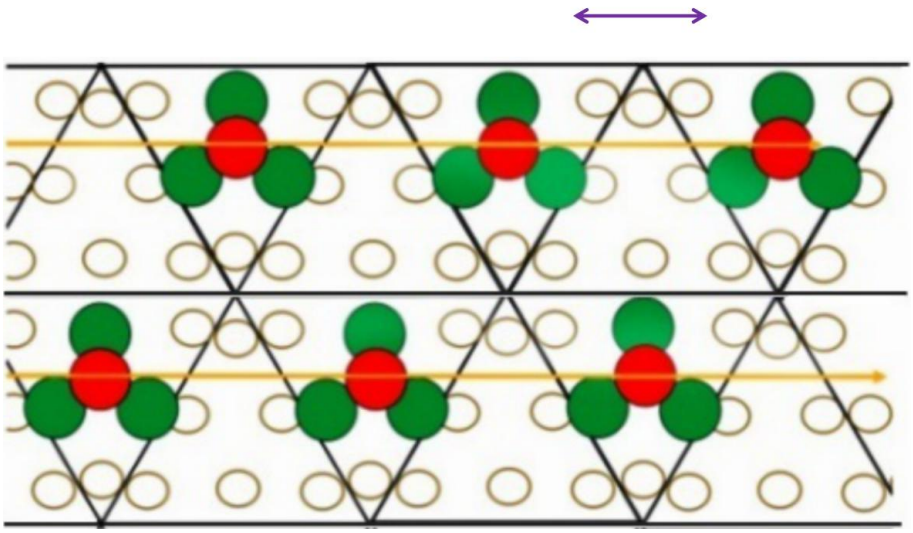

Fig. 3.11 The stacking model on the Si(111)-7×7 surface, in which, the yellow represents the substrate atoms, the green represents stacking atoms in the first stage, the red represents stacking atoms in the second stage.

3.7 Stability verification for large-scale application

3.7.1 The investigation and comparison of structure dimensions

Nanometer effect means that nanomaterials have strange or abnormal physical

and chemical properties that traditional materials do not have. For example, copper, which is supposed to conduct electricity, does not conduct electricity until it reaches a nanoscale limit. The original insulation of silicon dioxide, crystals, etc., begins to conduct electricity at a nanoscale boundary. This is due to the characteristics of nanomaterials such as small particle size, large specific surface area, high surface energy and large proportion of surface atoms. That is, three unique effects including surface effect, small size effect and macro quantum tunneling effect.

(1) surface effect

The surface area of a spherical particle is directly proportional to the square of the diameter, and its volume is directly proportional to the cube of the diameter [27, 28]. Therefore, the ratio (surface area / volume) of the two is inversely proportional to the diameter. With the decrease of particle diameter, the specific surface area will increase significantly, indicating that the percentage of surface atoms will increase significantly. When the diameter is larger than 0.1 micron, the surface effect of particles can be neglected; when the size is smaller than 0.1 micron, the percentage of surface atoms increases sharply. For example, when the particle size is 10 nm, the number of surface atoms is 20% of the total number of grain atoms. When the particle size was 1nm, the percentage increased to 99%.

(2) small size effect

With the quantitative change of particle size, the qualitative change of particle properties will be induced under certain conditions [29, 30]. The change of macroscopic physical properties caused by smaller particle size is called small size effect. For ultrafine particles, the size decreases and the specific surface area increases significantly, resulting in a series of novel properties. For example, the melting point of nanoparticles is significantly lower than that of large bulk materials, and the melting point of gold particles at 2 nm is 600 K. With the increase of particle size, the melting point rises rapidly, and the bulk gold is 1337 K. Similarly, the magnetic properties of small-sized nanoparticles are significantly different from those of bulk materials [31].

(3) tunnel effect

A thin insulating layer between two metal conductors forms an electronic tunnel junction. Experiments have shown that electrons can pass through a tunnel junction, called a tunneling effect. Electrons are both particle and wave, so there is tunnel effect. It has been found that some macroscopic physical quantities, such as the magnetization of micro-particles and magnetic flux in quantum coherent devices, also show tunneling effect, which is called macroscopic quantum tunneling effect. Quantum size effect and macroscopic quantum tunneling effect are the basis of future micro-electronics/optoelectronic devices, which will also lay the foundation for further miniaturization of existing micro-electronics devices. When microelectronic devices are further miniaturized, the above quantum effects must be taken into account. For example, in the manufacture of semiconductor integrated circuits, when the circuit size is close to the electronic wavelength, the electrons overflow the device through the tunnel effect, which makes the device unable to work properly [32, 33].

The regularity of each stable cluster further implied the chemical stability of the whole linear structure. During repeated experiments, more and more linear structures (like Figure 3.12) were realized. Obviously, there is a continuity between the previous theoretical predictions and experimental data. The stability of Fe linear structure was then preliminarily investigated in height measurements. In a linear Fe cluster structure, it seems that the interaction between each unit could not affect the stability of our cluster model [34, 35]. A single Fe cluster was also compared with the cluster in the linear structure, no obvious height difference was found.

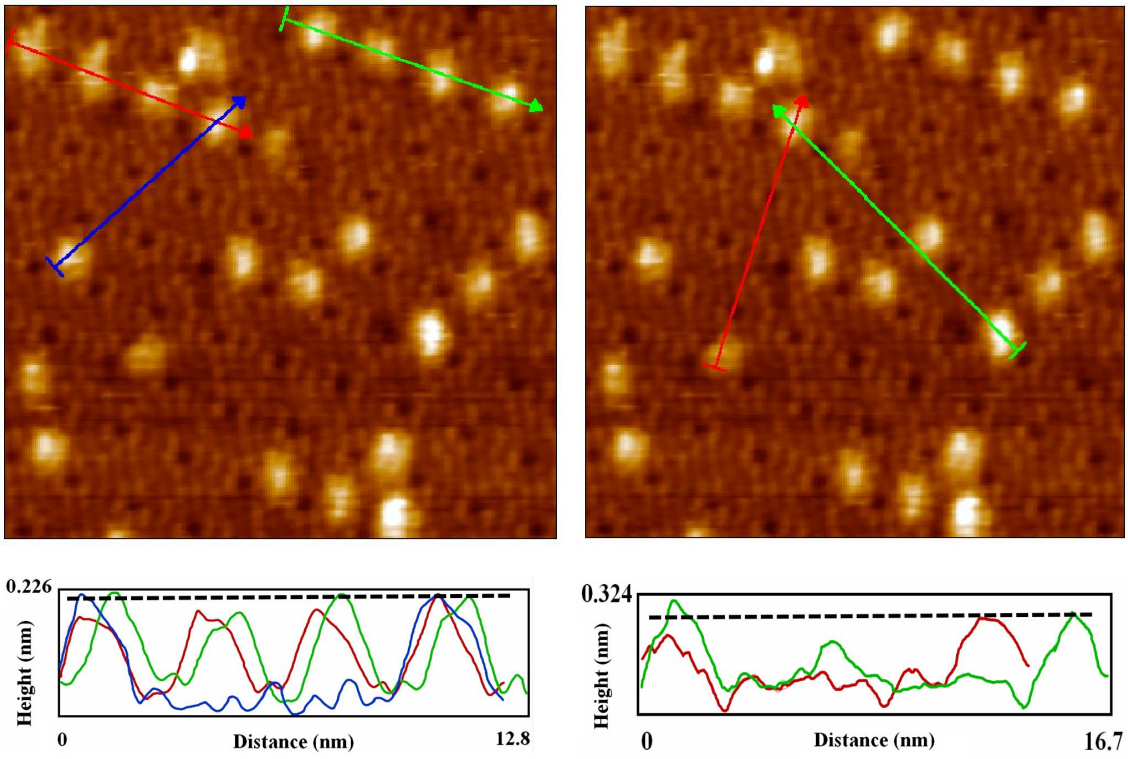

Fig. 3.12 STM images of the Si(111)-7×7-CH_3OH surface steamed with linear Fe clusters, and its height measurement. Adsorption sites are also identified in figure.

3.7.2 Analysis of element distribution based on XPS

X-ray photoelectron spectroscopy (XPS) uses X-ray to irradiate the sample and excite the inner electrons or valence electrons of atoms or molecules [36, 37]. XPS has became a typical surface analysis method. Although X-ray can penetrate the sample very deep, only a thin layer of photoelectrons emitted (near the surface of the sample) can escape. When a photon hits the surface of a sample, it can be absorbed by electrons in an element's atomic orbital. The electron is then released from the nucleus with some kinetic energy, becoming a free photoelectron. While, the atom itself becomes an excited state ion. Just refer to Einstein's law of photoelectric emission:

$$E_k = h\nu - E_B \qquad (1)$$

In the formula, E_k is the photoelectron kinetic energy emitted, hv is the energy of

photons from X-ray sources, and E_B is the binding energy on specific atomic orbitals (different atomic orbitals have different binding energy).

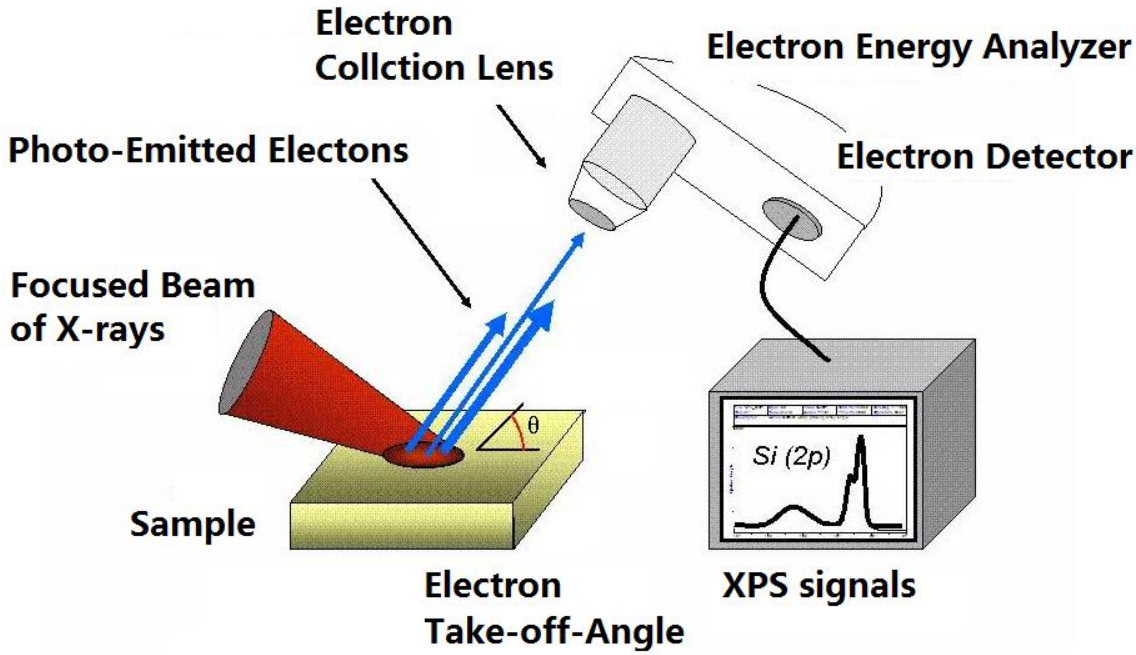

Fig. 3.13 XPS test schematic diagram.

Generally, the information of element composition, chemical state and molecular structure on the surface of samples can be obtained from the peak position and shape of XPS spectra. Photoelectron spectroscopy can be made to obtain the composition of the analyte. While, the surface element content or concentration can be obtained from peak strength. XPS can be used for qualitative analysis and semi-quantitative analysis.

(1) Qualitative analysis of elements. All elements except H and He can be identified according to the location of the characteristic lines appearing in the energy spectrum.

(2) Quantitative analysis of elements. The atomic content or relative concentration is determined by the intensity of the photoelectron spectrum line (the area of the photoelectron peak) in the energy spectrum.

(3) Solid surface analysis, including surface chemical composition or element composition, atomic valence, surface energy distribution [38-40]. The electron cloud distribution and energy level structure of surface electrons are also determined.

(4) Explore the structure of compound. The chemical shift of the inner electron binding energy can be measured accurately, and the information of chemical bond and charge distribution can be provided.

The electrons excited by photons are called photoelectrons, which can measure the energy of photoelectrons. Taking the kinetic energy of photoelectron as the abscissa and the relative intensity (pulse/s) as the ordinate. For a sample with unknown chemical composition, full spectrum scanning should be performed to determine the chemical composition of the surface. The scanning range of full spectrum energy is generally 0-1200 eV, because the strongest peaks of almost all elements are in this range. Not only the characteristic energy values of the photoelectron, but also Auger lines of the constituent elements are unique. The existence of a specific element can be identified by comparing it with the XPS standard spectrum manual and database. If chemical displacement is measured, or some data processing, such as peak fitting, deconvolution, depth analysis, etc., narrow scanning is necessary to obtain accurate peak position and good peak shape. The scanning width should be sufficient to complete both sides of the peak, usually between 10 eV and 30 eV. In order to obtain better signal-to-noise ratio, data can be collected by computer and scanned many times. The intensity of the photoelectron is related not only to the concentration of the atom, but also to the mean free path of the photoelectron, the surface finish of the sample, the chemical state of the element, the intensity of the X-ray source, and the state of the instrument. Therefore, instead of the absolute strength, XPS technology can only give the relative intensity of each element.

3.7.3 Results of STM-XPS in thin-air condition

Because of the volatility, the thermal stability of CH_3OH was studied above. Furthermore, the chemical stability of linear structure should also be detected since

the oxidizability of iron. The spectra of XPS were shown in Figure 3.14. The red line represents the Fe deposited sample, providing the existence of a pure Fe cluster. The peaks of Fe $2p_{3/2}$ and Si $_{2p}$ appeared at about 707 eV and 99 eV, which belonged to the Fe-Fe and Si-Si bond respectively. Further, the green line represents the sample after O_2 introduction and the blue line represents the sample which was exposed in thin air. Based on the XPS results, one conclusion could be deduced that the pure Fe clusters are stable in the above mentioned thin-air condition at room temperature. It can be also proved that the oxygen reacts with Si, instead of Fe. Originally, even if a sample has a perfect regular CH_3OH layer, the Fe cluster positions would be random, and there might not be cluster chains. However, the driving force making linear structures in Figures above should be the magnetic force of pure Fe clusters. Without improving the formation process, the magnetic strength of the sample is very weak and no linear structure can be formed. Accordingly, when linear structures appeared on the surface of our Si(111)-7×7-CH_3OH-Fe, magnetic strength increased obviously. Therefore, if the iron cluster in the linear structure can be regarded as a relatively independent magnetic unit, it will undoubtedly greatly enhance the existing storage density. From the current situation [41-43], new models and methods proposed in this paper have certain advantages in the exploration of a high-density magnetic memory device.

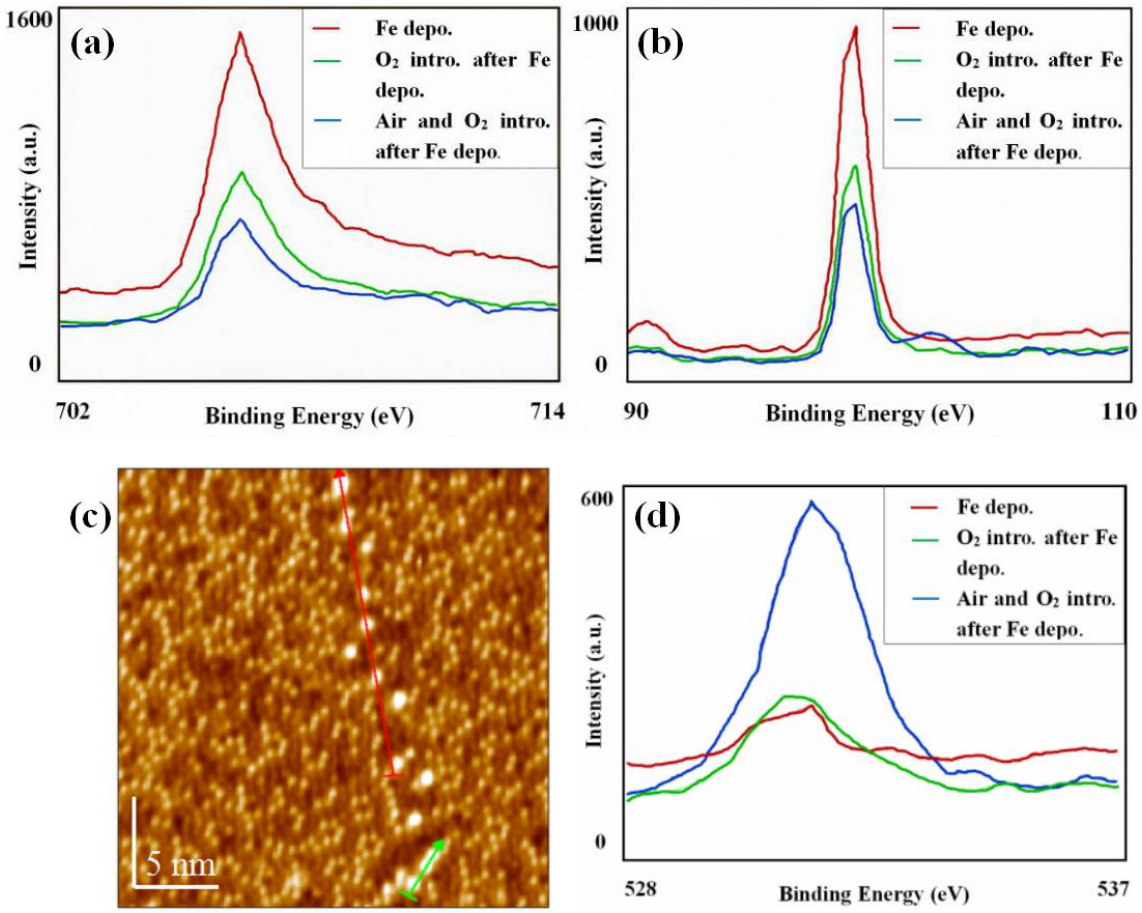

Fig. 3.14 High-resolution XPS spectra of (a) Fe $2p_{3/2}$, (b) Si $_{2p}$ and (d) O_{1s} before and after introduction of O_2 (10^{-4} Pa, 10 min) and thin air (10^{-1} Pa, 2 min). (c) is the STM image of sample, which is exposed in air for 2 h.

Concluding remarks

In this chapter, we steamed the iron atoms on the surface of the Si-CH_3OH. On the one hand, excellent size implies the possibility of high density storage. However, on the other hand, there are still two drawbacks that deserve our attention: (a) the formation mechanism is not clear. It seems that they can only appear in the ladder region. (b) The growth pattern is still layered-island rather than island. After continuous exploration and adjustment, the results can be described as follows:

1. By injecting argon, the thickness of iron layer is effectively adjusted, and the formation process of iron clusters is clear.

2 From the perspective of the middle layer, iron atoms can effectively cooperate with the temperature regulation of methanol. So that, the adsorption position is also regularized

3. From the viewpoint of iron cluster itself, the steaming temperature is further adjusted. The law of cluster structure changing with temperature is also clear.

4. The linear cluster structure conforms to the atomic stacking rule on 111 plane and has good stability.

Finally, the isolation effect of methanol and the stability of linear clusters are well verified by XPS experiments.

Reference

1 Weiss P: Hypothesis of the molecular field and ferromagnetic properties.J Phys 1907, 4:661.

2. Landau LD, Lifshitz E: On the theory of the dispersion of magnetic permeability in ferromagnetic bodies. Phys Z Sovietunion 1935, 8:153.

3 Mills DL, Bland JAC: Nanomagnetism: Ultrathin Films, Multilayers and Nanostructures. Amsterdam: Elsevier BV; 2006.

4 Cullity BD, Graham CD: Introduction to Magnetic Materials. Hoboken: Wiley;2009.

5 Hubert A, Schäfer R: Magnetic Domains: The Analysis of Magnetic Microstructures. Berlin: Springer; 2009.

6 Zhang, C.; Chen, G.; Wang, K.; Yang, H.; Su, T.; Chan, C.T. Experimental and theoretical investigation of single Cu, Ag, and Au atoms adsorbed on Si (111)−(7×7). Phys. Rev. Lett. 2005, 94, 176104.

7 Tanaka, K.I.; Xie, Z.X.; Egawa, T. Aramata, M. Dynamics of Sn and Zn atoms on a Si(111)-7×7 surface. J. Mol. Catal. A-Chem. 2003, 199, 19–26.

8 Alvarez, J.; De Parga, A.V.; Hinarejos, J.J.; De la Figuera, J.; Michel, E.G.; Ocal, C.; Miranda, R. Initial stages of the growth of Fe on Si (111) 7 × 7. Phys. Rev. B 1993, 47, 16048.

9 Mascaraque, A.; Avila, J.; Teodorescu, C.; Asensio, M.C.; Michel, E.G. Atomic structure of the reactive Fe/Si (111) 7× 7 interface. Phys. Rev. B. 1997, 55, R7315.

10 Xie, Z.X.; Uematsu, Y.; Lu, X.; Tanaka, K.I. Dissociation mechanism of methanol on a Si(111)−(7 × 7) surface studied by scanning tunneling microscopy. Phys. Rev. B 2002, 66, 125306.

11 Vlaic, S.; Gragnaniello, L.; Rusponi, S.; Cavallin, A.; Donati, F.; Dubout, Q.; Brune, H. Interlayer exchange coupling in ordered Fe nanocluster arrays grown on Al2O3/Ni3Al (111). Phys. Rev. B 2014, 89, 245402.

12 Ding, W.; Ju, D.; Guo, Y.; Tanaka, K.; Komori, F. Formation of linearly linked Fe clusters on si(111)-7 × 7-C2H5OH surface. Nanoscale Res. Lett. 2014, 9, 377.

13 Byun, J.H.; Ahn, J.R.; Choi, W.H.; Kang, P.G.; Yeom, H.W. Photoemission and STM study of an In nanocluster array on the Si (111)−7× 7 surface. Phys. Rev. B 2008, 78, 205314.

14 Tanaka, K.I.; Jiang, X.; Shimojo, M. Growth of nano-crystalline metal dots on the Si(111)-7×7 surface saturated with C2H5OH. Surf. Sci. 2007, 601, 5093–5097.

15 Heer WA, Paolo M, Chatelain A: Coulomb excitation of the collective septuplet at 2.6 MeV in Bi209. Phys Rev Lett 1990, 23:488.

16 Guevara J, Llois AM, Wei Ssmann M: Model potential based on tight-binding total-energy calculations for transition-metal systems. Phys Rev B 1995, 52:11509.

17 Hasegawa, Y., Kamiya, I., Hashizume, T., Sakurai, T., Tochihara, H., Kubota, M., & Murata, Y. (1990). Cluster formation of Li on the Si (111) 7× 7 surface. Journal of Vacuum Science & Technology A: Vacuum, Surfaces, and Films, 8(1), 238-240.

18 Zilani, M. A. K., Sun, Y. Y., Xu, H., Liu, L., Feng, Y. P., Wang, X. S., & Wee, A. T. S. (2005). Reactive Co magic cluster formation on Si (111)?(7× 7). Physical Review B, 72(19), 193402.

19 Azatyan, S. G., Iwami, M., & Lifshits, V. G. (2005). Mn clusters on Si (1 1 1) surface: STM investigation. Surface science, 589(1-3), 106-113.

20 Park, T. J., Papaefthymiou, G. C., Viescas, A. J., Moodenbaugh, A. R., & Wong, S. S. (2007). Size-dependent magnetic properties of single-crystalline multiferroic BiFeO3 nanoparticles.?Nano letters,?7(3), 766-772.

21 Harder, J.M.; Bacon, D.J. Point-defect and stacking-fault properties in body-centred-cubic metals with n-body interatomic potentials. Philos. Mag. A 1986, 54, 651–661.

22 Yang, X. H., Wang, Y. F., Liu, A. P., Xin, H. Z., & Liu, J. C. (2005). Studies on magnetic nanomaterials by atomic force microscopy with high resolution. Modern Physics Letters B, 19(09n10), 469-472.

23 Evans, R. F., Fan, W. J., Chureemart, P., Ostler, T. A., Ellis, M. O., & Chantrell, R. W. (2014). Atomistic spin model simulations of magnetic nanomaterials. Journal of Physics: Condensed Matter, 26(10), 103202.

24 Corr, S. A., Byrne, S. J., Tekoriute, R., Meledandri, C. J., Brougham, D. F., Lynch, M., ... & Gun'ko, Y. K. (2008). Linear assemblies of magnetic nanoparticles as MRI contrast agents. Journal of the American Chemical Society, 130(13), 4214-4215.

25 Roduner, E. Size matters: Why nanomaterials are different. Chem. Soc. Rev. 2006, 35, 583–592.

26 He, J.; Lilley, C.M. Surface effect on the elastic behavior of static bending nanowires. Nano Lett. 2008, 8, 1798–1802.

27 B?dker, F., M?rup, S., & Linderoth, S. (1994). Surface effects in metallic iron nanoparticles. Physical Review Letters, 72(2), 282.

28 Binder, K., & Hohenberg, P. C. (1974). Surface effects on magnetic phase transitions. Physical Review B, 9(5), 2194.

29 Ma, D. D. D., Lee, C. S., Au, F. C. K., Tong, S. Y., & Lee, S. T. (2003). Small-diameter silicon nanowire surfaces. Science, 299(5614), 1874-1877.

30 Chen, C., Kitakami, O., & Shimada, Y. (1998). Particle size effects and surface anisotropy in Fe-based granular films. Journal of applied physics, 84(4), 2184-2188.

31 Sljivancanin, Z.; Pasquarello, A. Supported Fe nanoclusters: Evolution of magnetic properties with cluster size. Phys. Rev. Lett. 2003, 90, 247202.

32 Ruder, W.C.; Hsu, C.P.D.; Edelman, B.D., Jr.; Schwartz, R.; LeDuc, P.R. Biological colloid engineering: Self-assembly of dipolar ferromagnetic chains in a functionalized biogenic ferrofluid. Appl. Phys. Lett. 2012, 101, 063701.

33 Varadan, V. K., Chen, L., & Xie, J. (2008). Nanomedicine: design and applications of magnetic nanomaterials, nanosensors and nanosystems. John Wiley & Sons.

34 Hupalo, M., & Tringides, M. C. (2002). Correlation between height selection and electronic structure of the uniform height Pb/Si (111) islands. Physical Review B, 65(11), 115406.

35 Hupalo, M., Yeh, V., Berbil-Bautista, L., Kremmer, S., Abram, E., & Tringides, M. C. (2001). Uniform-height island growth of Pb on Si (111)− P b (3× 3) at low temperatures. Physical Review B, 64(15), 155307.

36 Martinez, H., Tison, Y., Baraille, I., Loudet, M., & Gonbeau, D. (2002). Experimental (XPS/STM) and theoretical (FLAPW) studies of model systems M1/4TiS2 (M= Fe, Co, Ni): influence of the inserted metal. Journal of electron spectroscopy and related phenomena, 125(3), 181-196.

37 Machet, A., Galtayries, A., Zanna, S., Klein, L., Maurice, V., Jolivet, P., ... & Marcus, P. X. P. S. (2004). XPS and STM study of the growth and structure of passive films in high temperature water on a nickel-base alloy. Electrochimica Acta, 49(22-23), 3957-3964.

38 Seah, M. P. (1980). The quantitative analysis of surfaces by XPS: a review. Surface and Interface Analysis, 2(6), 222-239.

39 Czanderna, A. W. (Ed.). (2012). Methods of surface analysis (Vol. 1). Elsevier.

40 Tougaard, S. (1996). Quantitative XPS: non-destructive analysis of surface nano-structures. Applied surface science, 100, 1-10.

41 Cowburn, R. P. (2002). Magnetic nanodots for device applications. Journal of magnetism and magnetic materials, 242, 505-511.

42 Yang, Y. C., Pan, F., Liu, Q., Liu, M., & Zeng, F. (2009). Fully room-temperature-fabricated nonvolatile resistive memory for ultrafast and high-density memory application. Nano letters, 9(4), 1636-1643.

43 Heinrich, B., & Bland, J. A. C. (Eds.). (2006). Ultrathin magnetic structures II: Measurement techniques and novel magnetic properties (Vol. 2). Springer Science & Business Media.

Chapter 4 Formation process and mechanism of iron-nitride compounds on Si(111)-7×7-CH_3OH surface

4.1 Introduction

The new generation of magnetic recording materials are required to have the characteristics of high permeability, low coercivity and high resistivity at high frequency, high oxidation resistance, and very high saturation magnetization.Because of the good application prospects of materials, they have been extensively studied by scientific researchers. It was found that the composition and magnetic properties of the products were directly affected by the experimental conditions in the preparation of iron-nitrogen compounds. Therefore, in order to obtain samples with good magnetic properties, it is necessary to study the effects of various parameters in the experiment on the products. In this paper, magnetic atomic linear structure was composed of stable clusters and in-situ observed by the scanning tunneling microscopy (STM) system. Originally, Fe atoms were deposited on Si(111)-7×7 restructured surface, which had been covered by CH_3OH molecules. While, as magnetic storage units, they still have much room for improvement. So that, nitriding experiments were implemented and adjusted on the existing Fe clusters. A newly formed surface is stabilized by a quasi-potential made by breaking, and adsorbed atoms or molecules can be stabilized by forming “quasi-compounds”. Then, aim to greatly enhance the magnetic properties of the memory units [1, 2], nitriding experiments were implemented on the existing Fe compounds.

With the in-situ observation of STM, a series of Fe_3N structures make up the newly emerged iron-nitride compounds, showing good linear characteristics. By adjusting the concentration, this study further explored its formation process and compounds models. When the deposition of Fe atoms was increased to a certain extent, about 7 nm Fe clusters were formed and underwent one-dimensional

self-assembly crossing the surface of substrate. After initial nitridation, the linear width increases to more than 10 nm while the magnetic strength does not increase significantly. Aim to improve its application of magnetic memory material, both formation process and models, has been explored in this paper. Two typical Fe_3N_x cluster models were put forward in this study, which were established with height measurement and 3D surface display technology. Different steaming temperatures predicted different iron-nitride structures. By adjusting the steaming temperature, the improved iron-nitride clusters tend to be more "sharp". On the other hand, if the thickness of Fe layer is further reduced (from the film thickness to the atomic level), the new nitriding mechanism is worth exploring and analyzing. By introducing argon, a single layer of iron cluster can be formed. Although the crystal structure of iron cluster was not as obvious as before, the linear structure of iron-nitride was improved significantly. By comparing the XPS and magnetization measurements of different thickness samples, a transformation model of NH_3 was proposed. After confirming the better nitriding efficiency adjusted by thickness, the stability of the new FeN nano-structures was further investigated. The results proved that our linear iron-nitride clusters can still maintain good stability with the increase of magnetic strength. Even in the condition of thin air introduction, FeN clusters showed a good performance, which suggested the possibility of magnetic memory application in the future.

4.2 Atomic-level material and its catalytic theory

4.2.1 The theory of quasi-compound

How can we consider the surface of solid materials? As shown by the model below, one-dimension-lowered materials are created by the breaking of solid materials. For example, two-dimensional graphene, model (Fig. 4.1), gives a one-dimensional material along the edges, and the chemical properties of the edge should be different

from those of graphene itself [3]. That is, one-dimension-lowered materials are new materials, and the properties are quite different those of from our known materials. Chemical reaction of these new materials may provide new compounds named "quasi-compounds". One cannot make a free two-dimensional potential space in three-dimensional space, but one can prepare a quasi "two-dimensional potential space" by breaking solid materials, where "quasi-compounds" are stabilized. Therefore, catalysis is a chemical process restricted to the quasi-low-dimensional potential, where not only the transport of intermediates but also their rotational motion is restricted. A quasi-compound has its own stoichiometry and characteristic conformation, but it cannot be taken out from the surface, because it can exist only in a specific two-dimensional potential space given by the surface.

For this reason, "quasi-compounds" are different from the so-called ordinary clusters and instead are new materials, and their contribution is indispensable in some catalysis. Homo-atomic molecules such as H_2, O_2, and N_2 give one kind of adsorbed species, but hetero-atomic molecules such as CH_3OH, NH_3, and H_2O provide two or more forms of adsorbed species. Adsorption of iron on the Si(111)-7×7-CH_3OH surface is a prominent example, where the quasi-compounds are formed without react with substrate. This result suggests that the Fe atom seems stable at room temperature, but forming linear structure. Not only for themselves, the special dynamic characteristic of quasi-compounds will have an interesting effect on the subsequent adsorption gas.

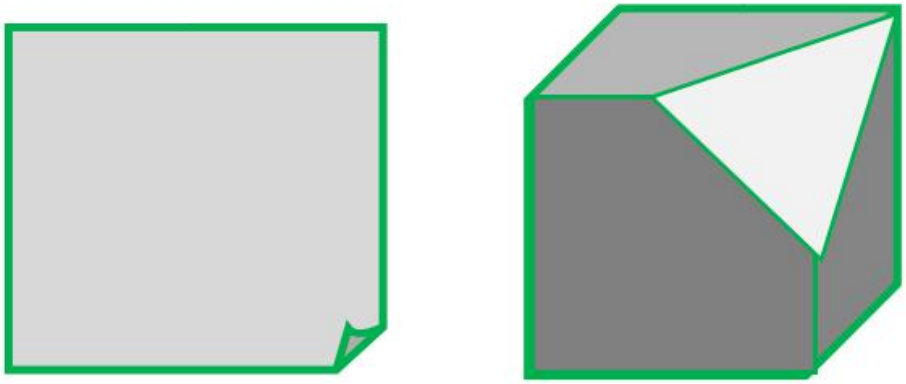

Fig. 4.1 Diagram of three-dimensional clusters in two-dimensional thin films.

4.2.2 The theory of transformation state

The transformation theory is based on statistical thermodynamics and quantum mechanics. It mainly studies the transformation state from reactant to product in chemical reaction. It is also known as "Activated Complex Theory", "Absolute Rate Theory" and "Absolute Reaction Rate Theory". The basic idea is that the potential energy of system is a function of atoms position. The change of potential energy surface can reflect a process of rearrangement of interatomic valence bonds. It can be said that there is a generalized transition theory, which connects the reactants and product structures through a minimum energy path. Although the transformation state theory provides a basis for exploring the chemical reaction process, it also has some defects. For example, it is not suitable for high temperature reaction. How to search the transformation state structure is difficult to obtain experimentally. The effective method is to predict and describe the transformation state by computational chemistry.

In order to avoid the chemical reaction between deposited Fe and Si substrate, the surface was passivated by the adsorption of methanol in the observation chamber according to the procedures above. As shown in Fig. 4.2 (a), the sticking probability for adsorption of CH_3OH on Si would be stable after the exposure of about 10^{-6} Pa, 30 s. By calculating surface images, the methanol ion is saturated at the adatom coverage of 1/2. Every triangular half unit cell contains three Si-OCH_3 and three Si ad-atoms, which the former show as bright dots and the latter are relatively dark in the STM image. H atom saturates the rest site, which cannot be observed clearly. With the help of mass spectrometer, the dissociation process can be proved, so as to establish its adsorption model. The specific process is shown in Fig. 4.2 (b), suggesting the existence of a transformation state between methanol molecule and methanol ion/hydrogen ion. At the moment of bond breaking, the exact location of methanol is worth exploring and analyzing. If we regard the whole adsorption process as a kind of "destruction" to the surface, two possibilities should be speculated (possibilities (1)

and (2)). In general, greater destruction implies the deeper penetration. The interesting phenomenon in methanol/ethanol/propanol adsorption confirmed that the key to adsorption is Si-H, not Si-O. That is, the formation of Si-H bond is earlier than that of Si-O bond. Combined with the bigger attractiveness of electron-rich Si rest-atom, there is enough reason to infer that the possibility (2) is much more likely than (1). The clarity of this transformation state not only explains the specific mechanism of methanol adsorption, but also provides an important reference to the later adjustment of the nitriding process.

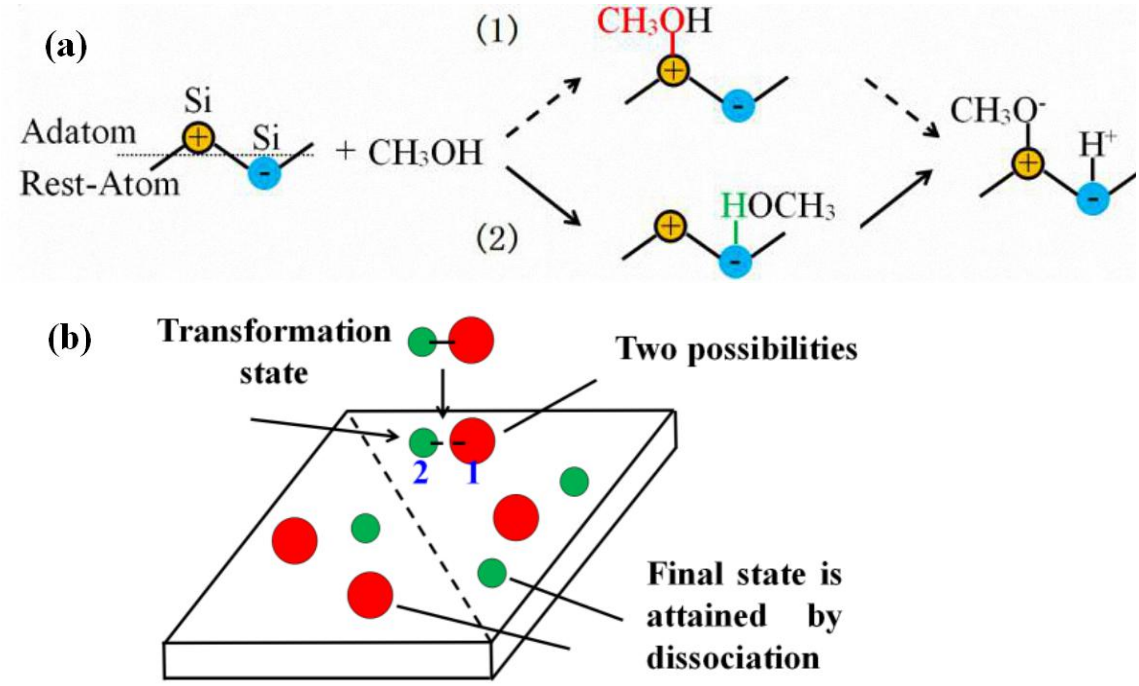

Fig. 4.2 (a) The model of a Si(111)-7×7 surface saturated with CH_3OH. It is inferred that there are two possibilities in the dissociation process. The possibility (2) was proved as the transformation state of CH_3OH adsorption. (b) The model of adsorption process including a transformation state.

4.3. Structural analysis of iron-nitride

4.3.1 High resolution observation at high concentration

From the perspective of pseudomorphic film, the lattice constant is the same as that of the substrate because of the strong interfacial interaction [4]. The famous small size effects and surface effects have puzzled researchers for a long time, storage density is critical for storage capacity improvement [5]. On the basis of a significant reduction in the distance between each memory cell, considering the characteristics of magnetic storage, the strong interaction between cluster and cluster will cause bad consequences if it is too large [6, 7]. In the precursor state, the rudiment of a linear structure is gradually formed along with the relatively weak interaction. Some previous linear structures are very attractive, although the success rate is not yet ideal. In general, the arrangement of the iron-nitride compounds is quite messy and does not maintain the linearity of the iron compounds. While the theoretical adsorption site can be reconciled with the experimentally observed bright STM spot, the calculation could not fully reproduce the stability of different adsorption sites. So that, how to improve the success rate and stability of linear iron-nitride compounds become the focus of our work in these years. In this paper, the adsorption mechanism in second breaking stage was studied in detail. Originally, the potential barrier of the microcosmic idea was used to explain the reaction rate, but the characteristics of chemical reaction cannot be predicted exactly. In order to find out the causes of these messy of Fe_3N in another way, the steaming temperature was taken into consideration as shown in Figure 4.3. Different compound structure has different stacking pattern, such as face centered mode, body centered mode and so on. After the accumulation of a large number of experimental data, the phenomena before and after nitriding were compared. It can be found that when the linear of iron-nitride compounds is perfect, the iron in the region is mainly γ-Fe. In contrast, when the linearity is disorganized, α-Fe is the dominant factor (as shown in Fig.4.3 (e)).

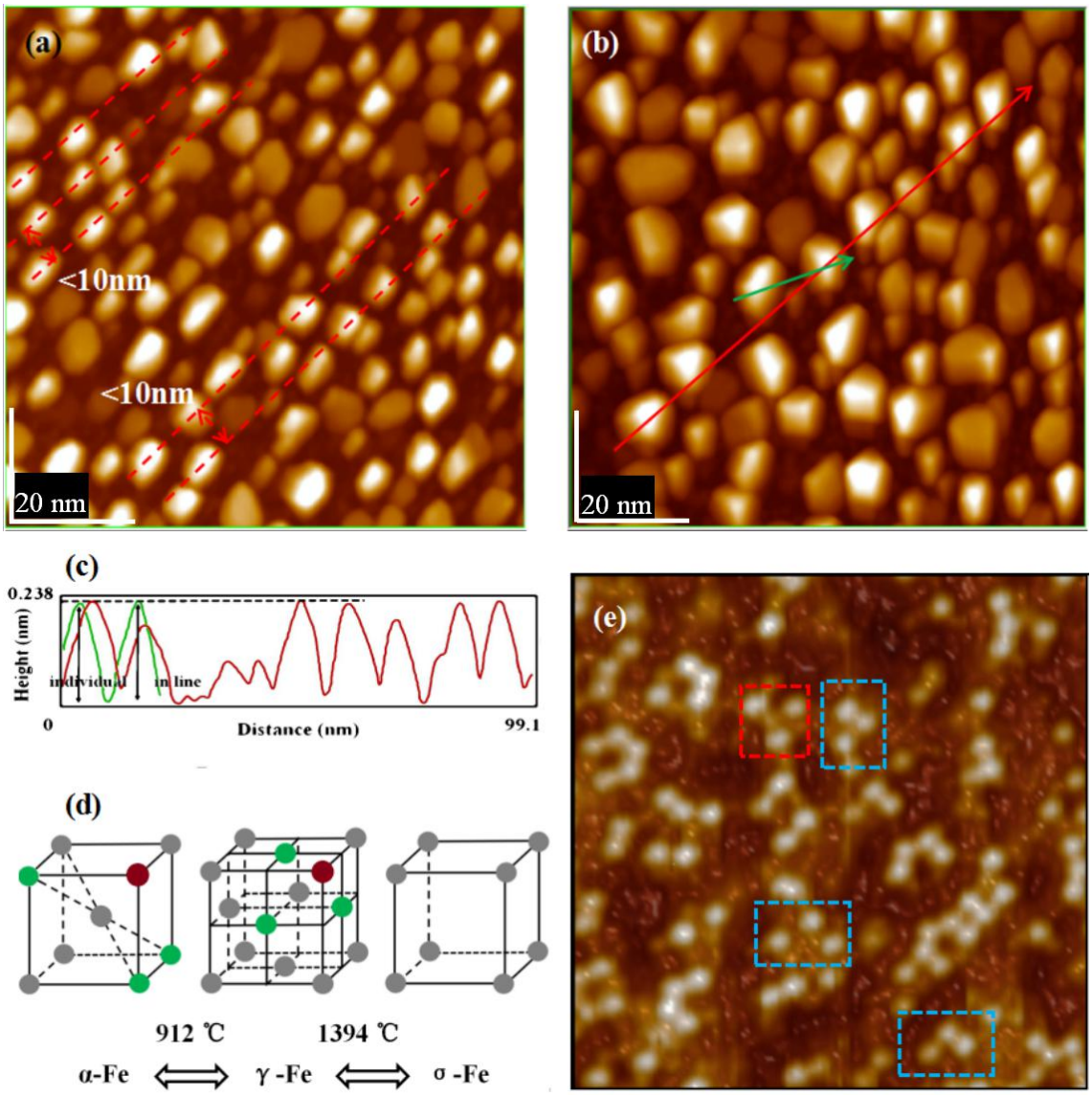

Fig. 4.3 (a) STM images of the Si(111)-7×7-CH_3OH-Fe surface with adsorption of NH_3, 10^{-6} Pa, 30 s: (a) Perfect situation with good linearity; (b) General situation with disorganized linear structure. (c) is the height measurement of (b). (d) Stacking model of Fe clusters in different temperature; About (d), the equilateral triangle model is marked with red square and the right-angled triangle is marked with blue square.

4.3.2 High resolution observation at low concentration

Adjusting(decreasing) the concentration of various materials, figures 4.4 (a) and (b) show the typical STM image of Si(111)-7×7-CH_3OH-Fe with low concentration of ammonia, where the inset was the high magnification with 17×17 nm^2. Through repeated scans, the specific structure of the iron-nitride compound was found on Si(111)-7×7-reconstructed surface. From the point of structural model, it is obvious that the height of N atom and Fe atoms are different. Measuring the height change in this new model, there are three height values, including: low, high, medium high, which represent: Methanol ion, Fe atom and N atom. Based on the theories above, this interesting phenomenon can be explained as follows: Before the formation of the Fe-N bond, the ammonia reacted with Si surface and the N-H bond was broken. As the degree of nitridation continues to increase slightly, the iron-nitride compounds appeared in a certain scale. Repeated height measurements (Fig. 4.4 (c)), the depression at the crest proved the previous structure model again: N atom is on the center of three Fe atoms. On this basis, the precursor state of metal compounds maybe clear now. With the increasing number of Fe_3N compounds have been found, the two typical structural models are proved: One is an equilateral triangle, grown by the γ-Fe mentioned above; the other is a right-angled triangle, corresponding to the α-Fe structure from Fig. 4.4 (d) and (e). Considering only the physical model and its height measurements may be not convincing enough, the 3D imaging technology of STM system was used to analyze the influence of N atom on its three iron atoms. Under the condition of lower concentration and higher resolution, the phenomenon of nitriding before and after nitriding is compared again, and the subtle structural changes are analyzed. In the case of an equilateral triangle, the three iron atoms expand, with the distance between atoms and atoms increasing. It is also very important that the opposite result was found in right-angled triangles: The three iron atoms tend to move closer, and the distance between Fe atom and Fe atom decreases. Under the respective effects of the two kinds of influence, the positive triangle of iron-nitride is consistent

with the linearity of the original iron cluster, and the right angle triangle always presents a deviation angle.

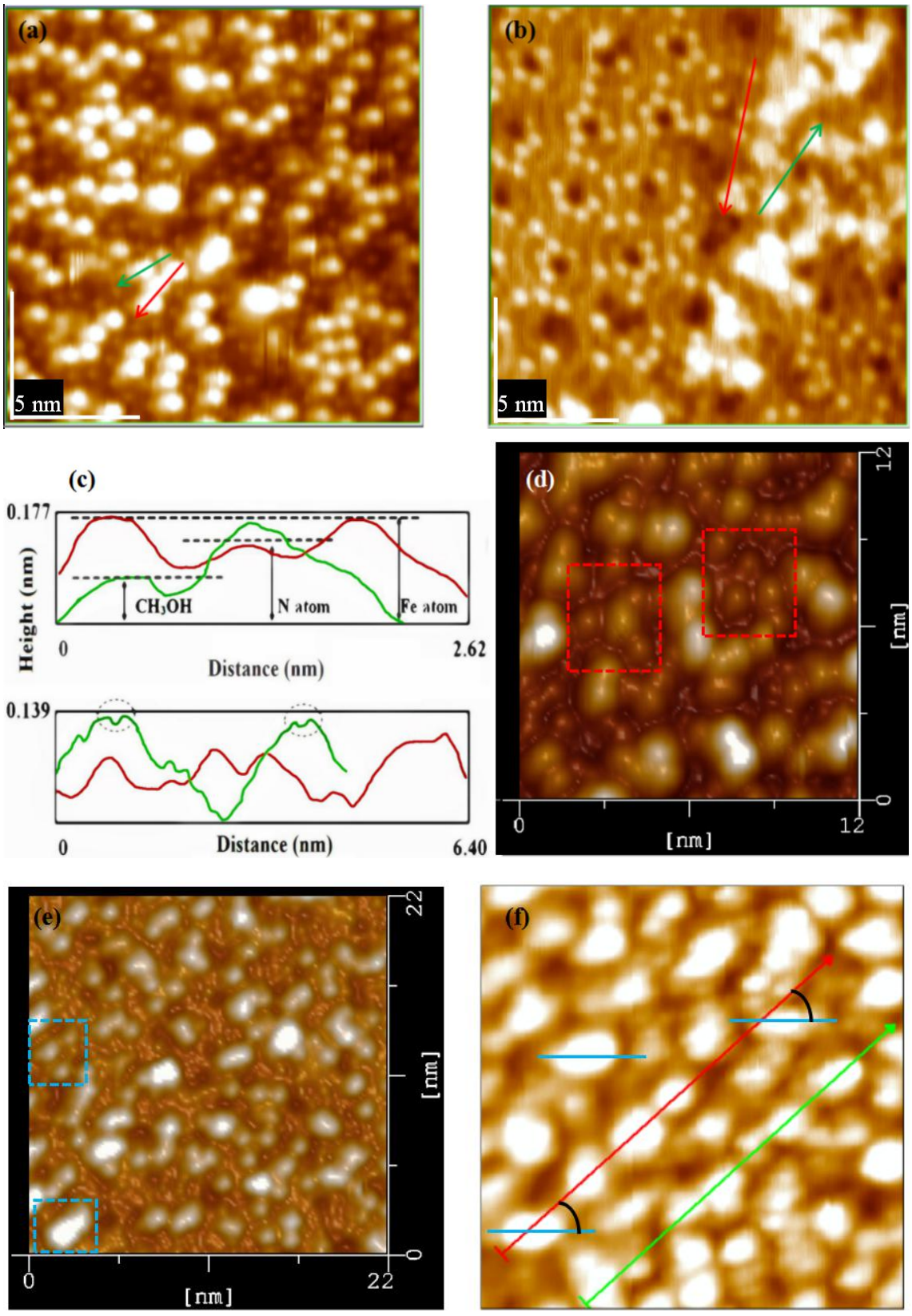

Fig. 4.4 Successive STM images of the Si(111)-7×7-CH_3OH-Fe surface with adsorption of NH3, which was deposited with a different time: (a) 10^{-6} Pa, 15 s; (b) 10^{-6} Pa, 20 s; (f) 10^{-6} Pa, 25 s. (c) is the height measurement of (a) and (b). (d) The influence of N in the equilateral triangle model; (e) The influence of N in the right-angled triangle model. The equilateral triangle model is marked with red square and the right-angled triangle is marked with blue square.

4.3.3 Compare and analysis two FeN structures at different stages

Crystallizing semiconductor nanowires and thin films at room temperatures by using catalytic behavior of metals has become an increasingly active field of research. Accordingly, thin film materials are also given higher expectations, such as the thinner thickness of atomic linear structure, the higher density of storage units, etc. In recent years, metal clusters and metallic compound grow on the surface of silicon which are promising for low cost high density devices. As shown by the Si-alcohol model of this reconstructed Si(111)-7×7, one-dimension-lowered materials are usually created by the breaking of adsorption materials. The weak interaction between the new metal compounds and substrate can be explained as different recombination probabilities in different positions. Fe atoms were deposited on Si(111)-7×7 restructured surface, which had been covered by CH_3OH molecules. A newly formed surface is stabilized by a quasi-potential made by breaking, and adsorbed atoms or molecules can be stabilized by forming “quasi-compounds”. Then, aim to greatly enhance the magnetic properties of the memory units, nitriding experiments were implemented on the existing Fe compounds. With the in-situ observation of STM, a series of Fe_3N structures make up the newly emerged iron-nitride compounds, showing good linear characteristics. By adjusting the concentration, this study further

explored its formation process and compounds models.

With the increasing of ammonia concentration, the new linear iron-nitride compounds can also be formed. Among them, two typical models of iron-nitride are proved, the weak interaction of N atom on the iron atoms in each model is also investigated. When the number of iron atoms is fixed, N^{3-} will effectively play its weak role, which is directly represented by the change of cluster’ s shape. For the same nitriding time, iron clusters can still be found on the surface with the main structure of the regular triangular, which hardly been found on the sharp triangle case. As a result, the regular triangular linear structure is characterized by strong stability, but poor linearity and magnetic intensity. The sharp triangle structure has better linearity, and the magnetic intensity has been improved. At the beginning, we have found that N ions will affect the position of Fe atoms, but very weak. With the increase of ammonia concentration, the cluster height scanned increases. It is noted that the more iron atoms in the iron-nitride cluster, the stronger the magnetism. Metal nitride has robust bonding between metal and nitrogen atoms. However, with the increase of nitriding time, the proportion of N element in the cluster structure increases, and the magnetism decreases. Specifically, the x value in the Fe_3N_x structure is increasing. The structure of Fe_4N will be gradually converted to Fe_2N, and the magnetism will be weakened. As a result, when the nitriding degree is appropriate, the linearity is obvious. Once the nitriding time is excessive, the cluster height increases and the linearity is destroyed again. It is not absolute that the thinner the Fe layer, the higher the nitriding efficiency. There should be a parabolic critical value between 2.5 ML and 3 ML. Linear Fe clusters were still found in 2 ML samples, and too thin Fe structure could not be nitrided. Although considering the relationship between instrument sensitivity and sample thickness, the magnetic strength of 2 ML sample should be much smaller than that of 3 ML sample.

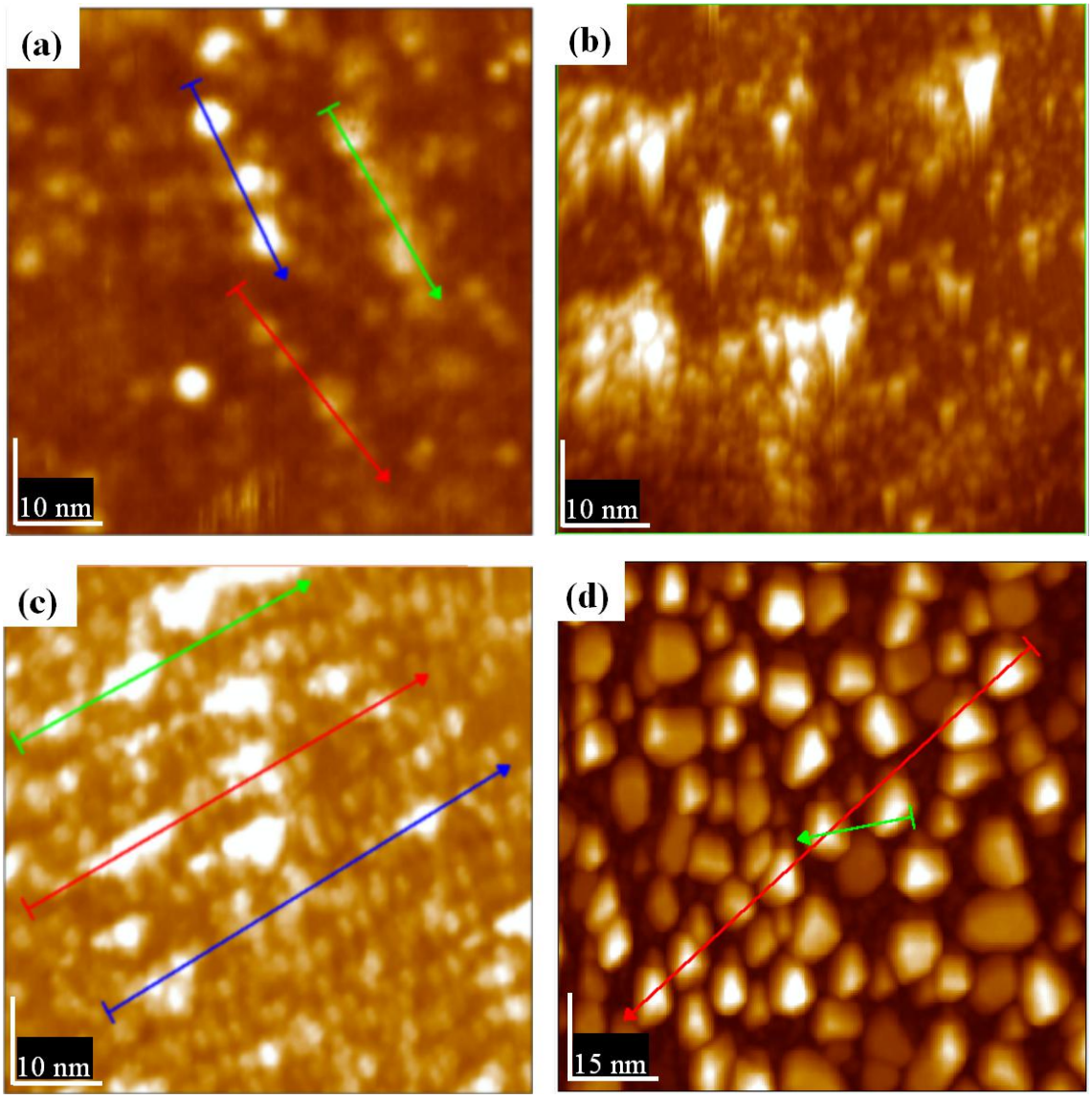

Fig. 4.5 STM images of Si(111)-CH_3OH-FeN based on two types of Fe cluster: (a) is mainly regular triangle structure, (b) is mainly sharp triangular structure. (c) and (d) are the results of nitriding at low and high concentrations, respectively.

4.4 Introduction of magnetic measurement

Magnetic measurement refers to the measurement of magnetic field and magnetic material, through magnetic measurement to measure other physical quantities. Basic measurement parameters including magnetic flux Φ, magnetic

induction intensity B, magnetic field intensity H, magnetization M, etc. Hysteresis loop is an important characteristic of magnetic materials, which reflects the magnetization characteristics of iron-nitride structure. The residual magnetism of hysteresis loop reflects how much magnetism intensity the sample retains after magnetization. The coercive force indicates the ability of the magnetic material to remain magnetism intensity after magnetization. Materials with low coercivity are easy to magnetize and demagnetize, which belong to "soft" magnetic materials. While, the material with high coercivity reflects "hard" magnetism. The direction of each magnetic domain remains unified direction after the external magnetic field is removed.

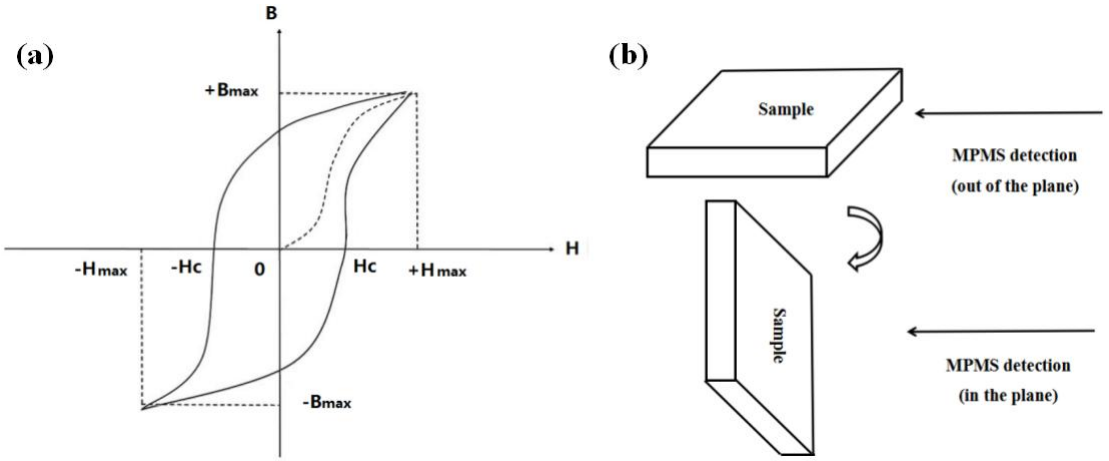

Fig. 4.6 (a) Schematic diagram of magnetization curve; (b) MPMS magnetic detection in horizontal (out of the plane) and vertical directions (in the plane).

Tab.4.1 Accuracy of magnetic field setting.

	High field accuracy	Low field accuracy
MPMS XL-5	1.0 Oe @5T	0.1 Oe @5000 Oe
MPMS XL-7	2.0 Oe @7T	0.2 Oe @6000 Oe

With the progress of science and technology, precision magnetometer is also in constant development. Among Quantum Design, MPMS (Magnetic property Measurement System) is a system for measuring materials with high accuracy in a

wide range of temperature and magnetic fields. Using superconducting quantum interference devices (SQUID), MPMS has the sensitivity to measure the magnetization intensity (dc) in $10e^{-8}$ emu. Specifically, it is a base system, assembled of various components. The basic system mainly includes superconducting SQUID detection part, software operation part, temperature control part, magnetic field control part, sample operation part and gas control part. During the measurement, the sample moves along the axis of the superconducting detection coil, which can generate induced current in the detection coil. Since the detection coil, the connection and the SQUID input signal line form a superconducting closed loop. Any flux change in the detection coil will cause the corresponding change of the current in the closed loop. Through SQUID conversion, we can get the voltage signal which corresponds strictly to the magnetic moment of the sample. Since SQUID is very sensitive to the fluctuation of magnetic field, it needs very high stability to work normally. Further, good magnetic shielding is necessary.

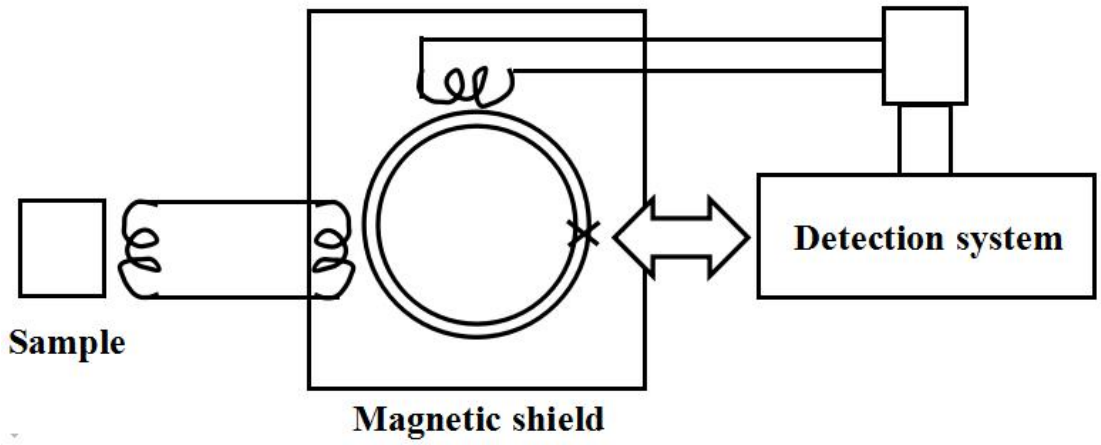

Fig. 4.7 SQUID-MPMS XL-7 Magnetic measuring system and its structural sketch.

4.5 The original discovery of linear FeN clusters structure on Si(111)-7×7

4.5.1 Experiment on the adsorption of NH_3

Nitriding usually refers to a chemical heat treatment process in which nitrogen atoms infiltrate into the surface of the workpiece under a certain temperature and environment. The gas nitriding system was published in 1923. NH_3 gas was directly transported into the chamber at 500-550 °C, decomposed into (N) gas and (H) gas in atomic state after 20-100 h. The dissociation rate of NH_3 varies depending on the flow rate and temperature. The dissociation rate decreases with the increase of flow rate and increases with the increase of temperature. NH_3 gas was decomposed at 570 °C as follows:

$$NH_3 \rightarrow [Fe]\ N + 3/2\ H_2 \qquad (1)$$

The decomposed N diffuses into the surface of iron to form iron-nitride structure. The disadvantage is that the hardening layer is thin and the nitriding treatment time is long.

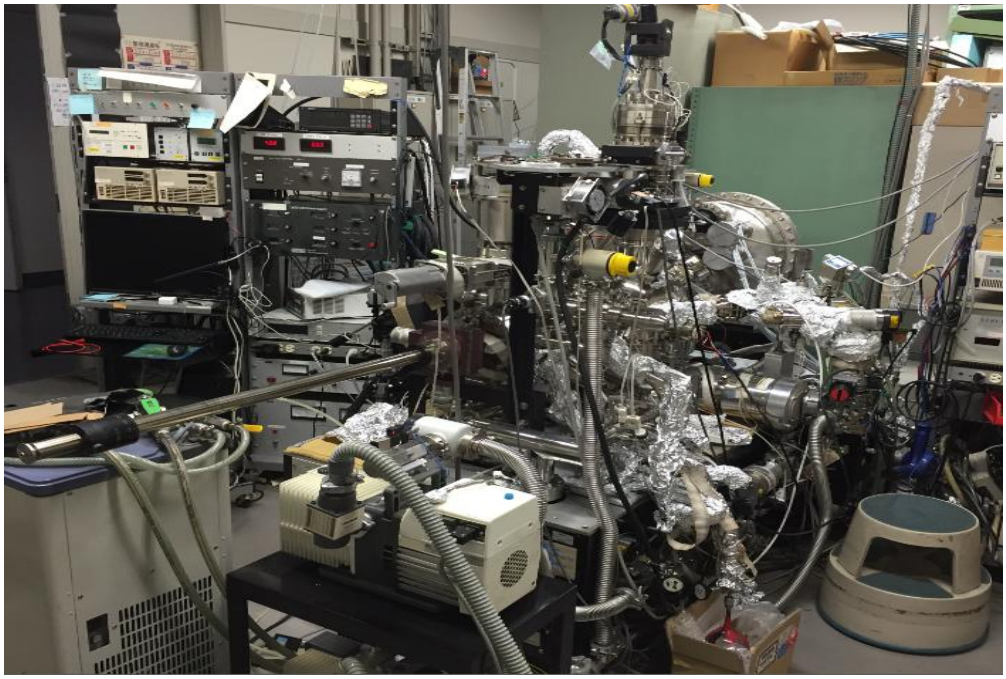

Fig. 4.8 Schematic diagram STM-XPS measurement.

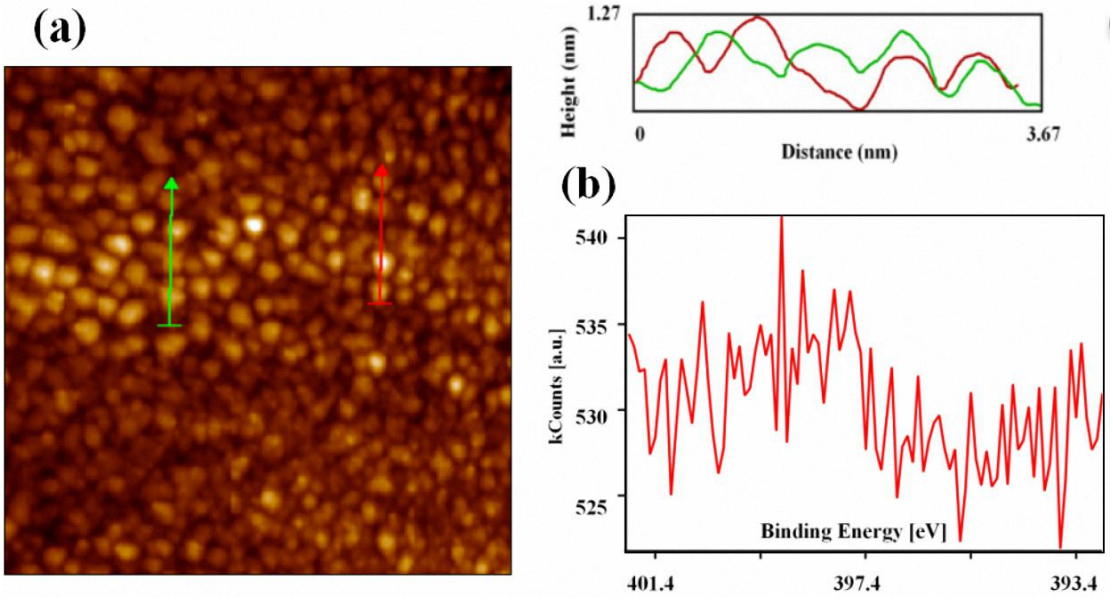

Fig. 4.9 (a) is the STM image of preliminary iron-nitride compounds and (b) is the XPS result of (a).

Since the injection of air can not affect the stability of Fe cluster, N_2 seems not

the best choice for nitriding. Inspired by the alcohol experiments above, this study prefer NH_3 to other gas (like N_2, NO and NO_2) [8-10]. About the observation chamber, a set of gas storage device is connected with it through a needle valve. During the adsorption procedure of CH_3OH or NH_3, the STM tip was retracted far away from the surface to reduce the adsorption shielding by the tip. At the same time, the mass spectrometer is turned on to monitor the gaseous ion composition in the observation chamber.

In the steaming condition of 10^{-6} Pa×30 s, the width of linear Fe clusters was measured about x nm. After that, ammonia was selected as a kind of nitriding gas. Like methanol, NH_3 undergoes dissociation on a group sites of Fe-adatom and Si-rest atom, where the stabilized structure of clue iron are broken again. In the vertical direction (Fig. 4.9 (a)), the distance between the magnetic units on the two linear structures is controlled within 10 nm. The measured height was 1.15 nm, which indicates multi-layer atomic stack. Like other metal atoms (like Au, Sn and Zn...) deposited on the present surface of Si(111)-7×7-CH_3OH, the obvious linear structure has not been found again. The interesting phenomenon was assumed to be the result of ferromagnetic effect. As an important intuitive parameter, linearity is not only a necessary condition for future applications, but also implies the magnetic strength of iron-nitride clusters as memory units. While the ferromagnetic property of Fe clusters was destroyed, the magnetic intensity of iron-nitride had not been enhanced as expected. Moreover, in the absence of enough N atoms on the surface, it is difficult to find an obvious nitrogen peak in XPS (Fig. 4.9 (b)).

4.5.2 The evaluation of magnetic intensity

Previously, magnetic materials and semiconductor materials developed independently. With the innovation of nanotechnology and semiconductor technology, magnetic metals (Fe, Co, Ni, Cr, Mn) and semiconductor materials (Si, Ga, As, Ge) have attracted more and more attention. As the main material of semiconductor, Si has

attracted much attention. The research on the structure and magnetism of magnetic metals grown on Si, tunneling junctions of magnetic metals/Si, magnetic metal compounds, etc., are of great significance for the integration between nano-scale devices and micro-semiconductor devices. First of all, it is an urgent problem to prepare thin magnetic memory at room temperature, especially memory cells that can be integrated with the mainstream Si technology. The second problem is the origin of magnetism in thin magnetic semiconductors. For ferromagnetic metal compounds, when Fe forms small clusters, it will affect the magnetic properties of nanostructures themselves. How to eliminate the adverse influence of clusters is an important problem. In addition, metal atoms are likely to form solid materials on semiconductor substrates, thus affecting the subsequent catalytic and dissociation effects.

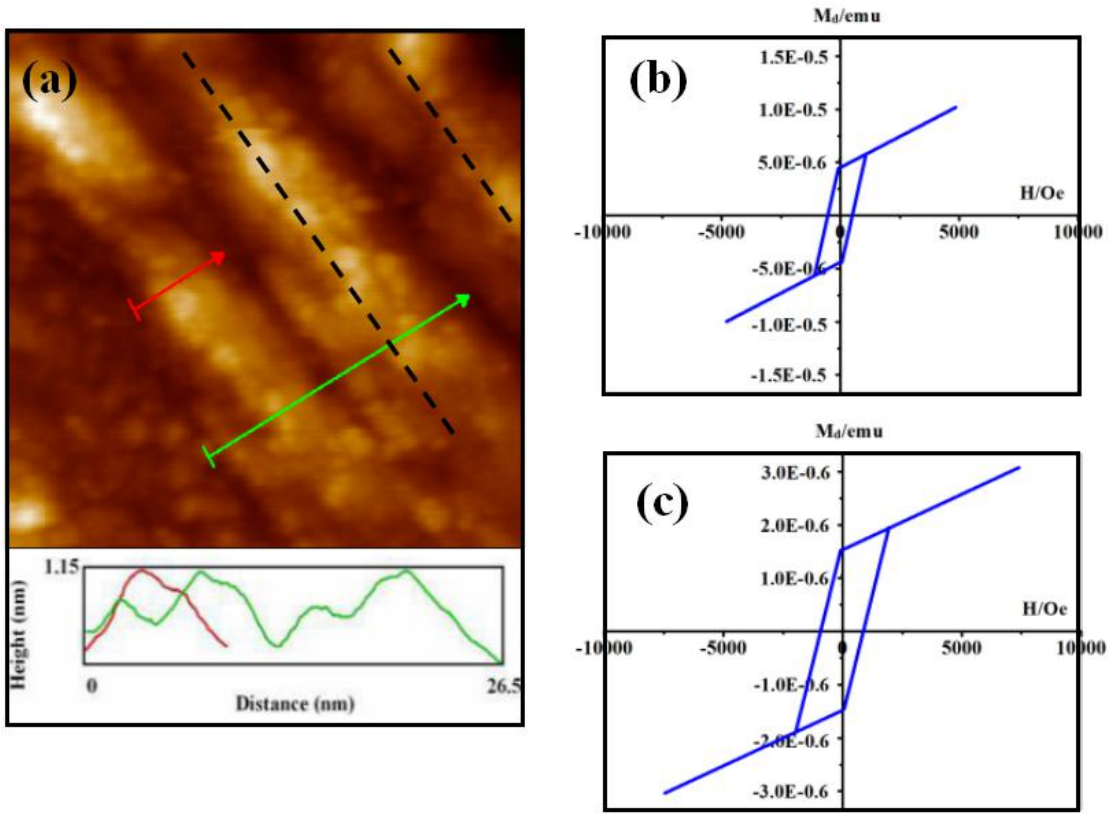

Fig. 4.10 (a) STM image of the Si(111)-7×7-CH_3OH surface steamed with linear Fe clusters, and its height measurement. (b) and (c) are the magnetic test results of Fig. 4.10 (a) and Fig. 4.9 (a).

With the help of MPMS-7T, the magnetization was measured as shown in the Fig. 4.10. Although not strong, the ferromagnetism does exist with the easy magnetization axis in the horizontal direction of the substrate. After that, ammonia was selected as a kind of nitriding gas. Like methanol, NH_3 undergoes dissociation on group sites of top Fe atoms. If Fe layer is regarded as a catalyst, the stable cluster structure should not promote the dissociation process effectively. Just as the magnetic result shown, the strength is even weaker than that of the pure iron sample. Moreover, it can be seen from the XPS data that the concentration of N ion on the sample surface is obviously insufficient. Low nitriding efficiency suggests low dissociation efficiency, the transformation state was concerned again as the key parameter.

4.5.3 The comparison experiment on the N^+ ion bombardment

The nitrogen atoms that penetrate the surface of samples during ionic nitriding are unlike those produced by the decomposition of ordinary ammonia gas. First, the electric field accelerates the collisions between the nitrogen molecules or atoms, forming ions. The highly active nitrogen atoms are formed by adsorption and enrichment on the surface of samples. Considering the complexity of multi-layer adsorption, N^+ can directly sent into the observation chamber by ion bombardment (0.5 k eV) at room temperature (RT). Monoatomic films with a hexagonal atomic structure were formed near the ladder region as well as the monoatomic Fe_2N film. Ion nitriding [11, 12], as a new nitriding method rising in the 1970s, is characterized by:

(1) The nitriding speed is faster. Compare with the gas nitriding, the period can be shortened to 1/3-2/3 of it.

(2) The temperature range is relatively wide. A layer of nitrided layer can be obtained even below 350 °C.

(3) The brittleness of nitriding layer is small. In addition, the deformation caused

by nitriding layer is small, which is especially suitable for precision parts with complex shapes.

(4) Partial nitridation is easy to realize. Using mechanical shielding or iron plate, the non-nitriding part is easy to protect. The structure of the compound layer, the thickness of the permeation layer and the microstructure can be controlled.

(5) Ion bombardment can also purify the sample surface and remove passivation film automatically. Stainless steel and heat-resistant steel can be nitrided directly without removing passivation film beforehand.

As a result, its application has been improved greatly. On the one hand, energy and ammonia consumption can be saved. Electric energy consumption is 1/2-1/5 of ordinary gas nitriding. And ammonia consumption is 1/5-1/20 of gas nitriding. On the other hand, ion nitriding treatment is carried out under relatively high pressure. Pollution-free, almost no harmful substances are produced. It can be applied to all kinds of materials, including stainless steel, heat-resistant steel with high nitriding temperature, tool steel and precision parts with low nitriding temperature. As for our subject, relatively low temperature condition is quite difficult for gas nitriding.

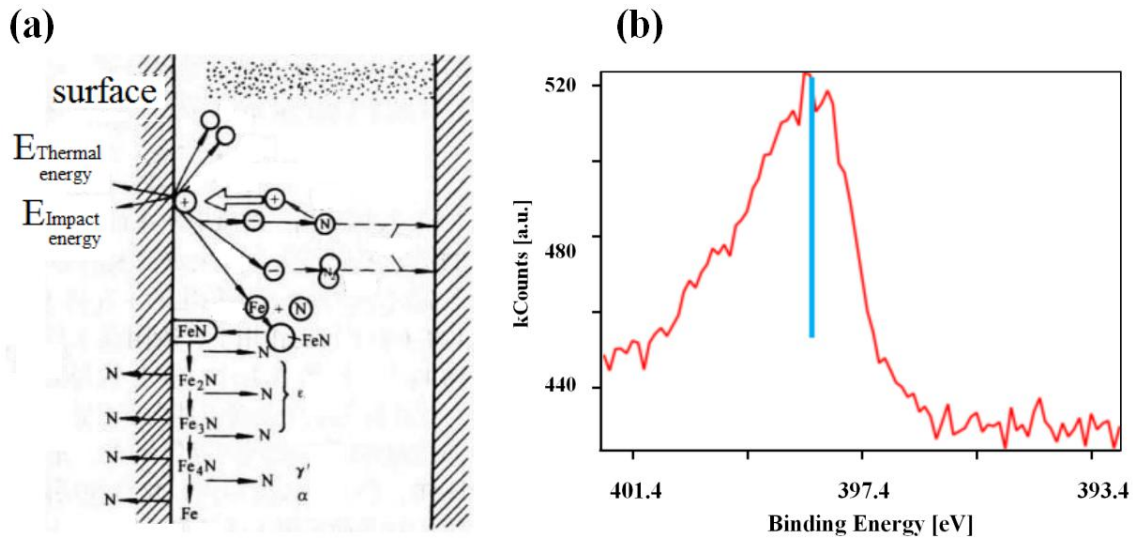

Fig. 4.11 (a) The principle diagram of the ion nitriding and its XPS result (b).

4.6 Thickness-dependent mechanism and magnetic properties of iron-nitride

4.6.1 Improvement of steaming technology on thickness

Compared with bulk metals, nanoclusters have very different magnetic properties. From the size (or thickness) of the nanoclusters, the magnetic properties of the small size areas vary greatly. As the thickness increases, the variation of magnetic elements gradually decreases and finally converges to the value of the block metal. Generally speaking, nanoclusters have completely different physical and chemical properties compared with bulk materials and atoms. Moreover, its performance varies significantly with the size/thickness of clusters. At present, nanoclusters have attracted wide attention in various fields as materials with new functions. If the thickness of nanoclusters can be controlled, it is possible to find new functional groups of material.

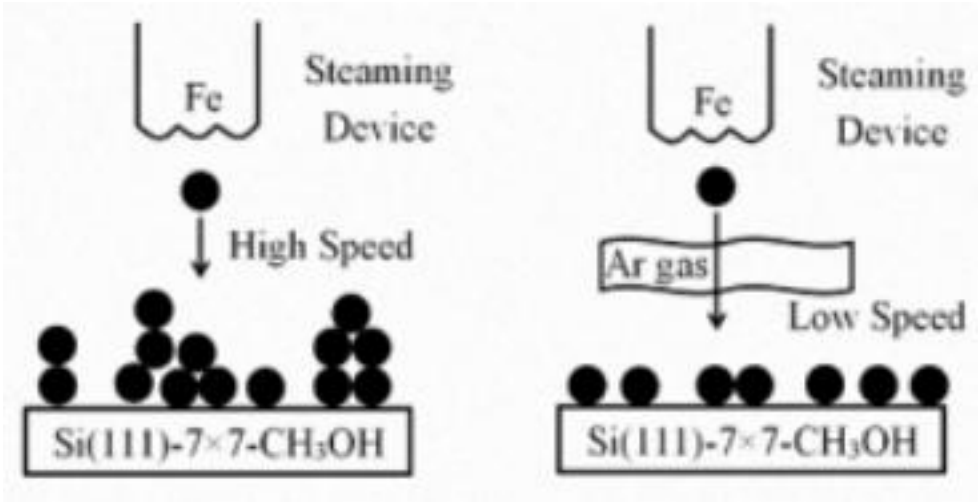

Fig. 4.12 The steaming process without and with Ar gas introduction.

Low nitriding efficiency suggested low dissociation efficiency, only by improving the dissociation efficiency of ammonia can the formation probability of iron-nitride be increased. By analyzing the whole adsorption process of NH_3, the

thickness of Fe layer was concerned as the key parameter. The more layers of iron cluster, the more its behave like a thin film or a block. The first and second layers of Fe atoms in contact with Si(111)-7×7-CH_3OH are supposed to have properties different from those of higher layers. Accordingly, we called these two special layers as quasi-layer. Previously, we used methanol as an intermediate layer between silicon and iron. Now, Fe layer itself becomes a "barrier" between ammonia and quasi-layer. In this way, we tried to reduce the thickness of the Fe layer. As shown in Fig. 4.12, iron atoms were mainly stacked on Si(111) surface in the form of multi-layer. In the process from the wire to the sample, Fe atoms were steamed with introducing argon gas.

4.6.2 Thinner outcome of iron-nitride

The structural parameters of magnetic multilayers include: (1) the thickness of nitrided layer, which is usually a few nanometers to several nanometers from zero; (2) the thickness of iron layer; (3) the thickness of intermediate layer. The factors affecting the microstructure of multilayers generally include the influence of substrate and growth conditions. The thinner the iron layer is, the more different it is from the bulk compounds. This also requires the deposition rate. Excessive deposition rate will inevitably affect the formation quality of nitrided layer. Fig. 4.13 (a) showed a thinner deposition outcome, whose height and distribution were changed greatly. After that, the sample was nitrated again under the same conditions of Fig. 4.9 (a). As can be seen from the new results (Figs. 4.13 (b) and (c)), the linearity as well as the magnetic intensity has been significantly improved. With the increase of magnetic intensity, the corresponding linearity becomes more obvious. Higher nitriding efficiency directly leads to the obvious nitriding peak in Fig. 4.13 (d). The XPS result was clearly in favor of the existence of FeN_x with a N_{1s} binding energy (398.6 eV) and agrees fairly well with the N_{1s} values of surface iron-nitride, which occur in the 396.2-398.3 eV range. Moreover, its Fe $2p_{3/2}$ value also has a obvious change. Unlike 706.5 eV of Fe-Fe bond, the new peak found in 709 eV should be the new Fe-N bond [13-16]. As

a result, the nitriding effect of ammonia on iron clusters was verified.

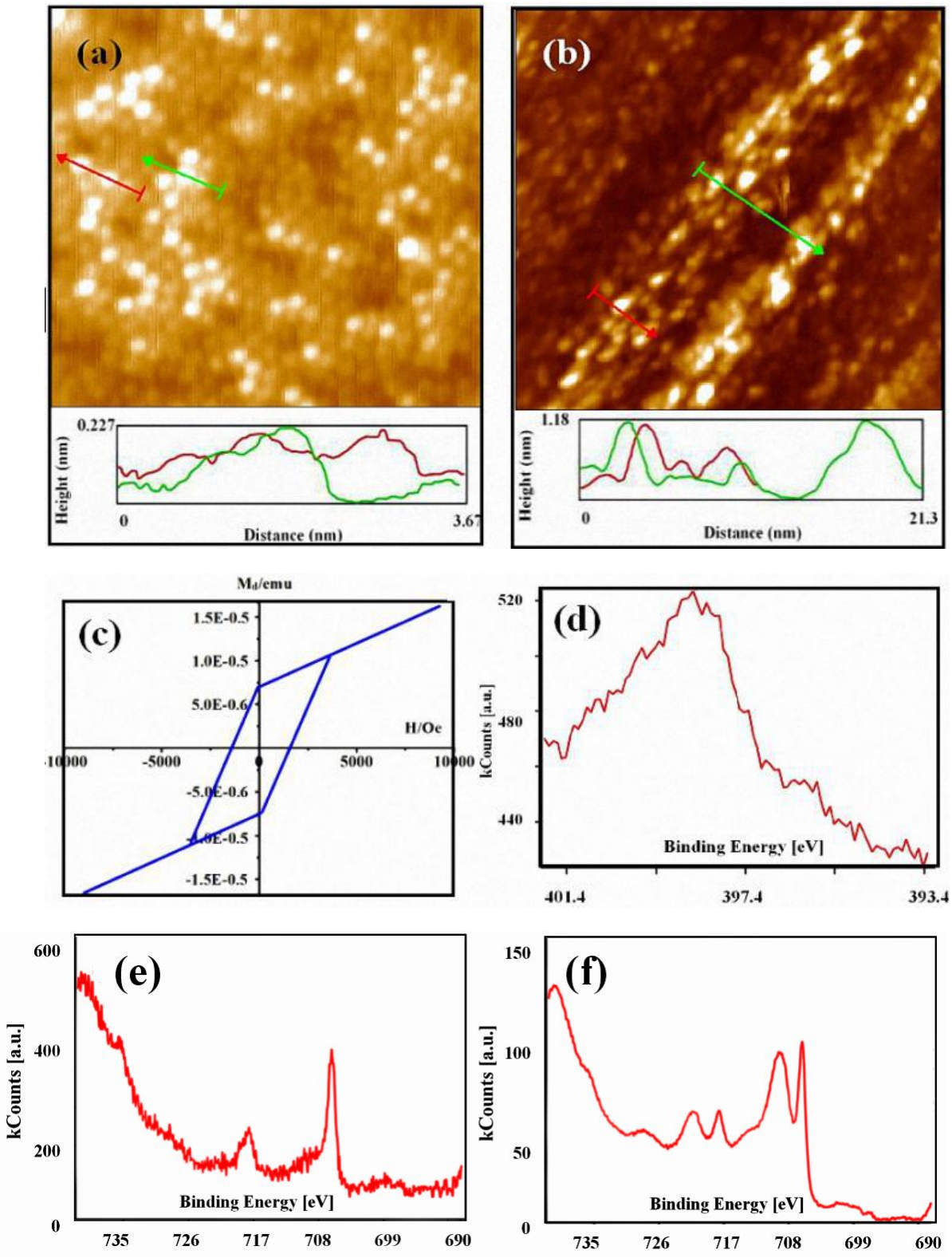

Fig. 4.13 (a) STM image of the Si(111)-7×7-CH_3OH surface steamed with thin Fe layer, and its height measurement. (b) is the nitriding outcome based on the surface

of (a), the condition of NH_3 is the same of Fig. 4.6 (a). (c) The magnetization curve of the new iron-nitride sample, as Fig. (b). (d) XPS spectra of N_{1s} in the samples of (b). (e) and (f) are spectra of Fe $_{2p3/2}$ in the samples before and after optimization.

4.6.3 Improvement of dissociation efficiency

Fe dots are considered to improve the density of magnetic storage units. However, since the magnetic property of existing Fe compounds is weak, this study tried to nitride it with adsorption gas. Concerning the stability of the iron compound in the nitrogen and oxygen environment, this paper tends to focus on NH_3 gas. Firstly, using mass spectrometer and gas adsorption device, the previous hypothesis is confirmed. As discussed in a previous breaking gas, the ammonia synthesis reaction on Fe catalysts is catalyzed by a cyclic process consisting of the formation of the quasi-compound Fe_xNH_y and its rapid change to Fe_xN. When the concentration is relatively high, although FexN compounds continue to grow steadily on the surface of Si(111)-7×7-CH_3OH, the linearity of them is quite confusing. By adjusting the concentration of ammonia, the preliminary formation stage of iron-nitride compounds has been figured out. In particular, some specific classifications, including the concept of precursor compounds could to be verified and summarized. Different formation mechanism corresponds to different cluster shapes, the most suitable growth pattern could be found with the 3D images of STM. As a result, 2 typical Fe_3N_x models have promoted the formation rate of the stable structure greatly. Finally, considering the growth of each cluster, the interaction of N atom to Fe atoms would be explored.

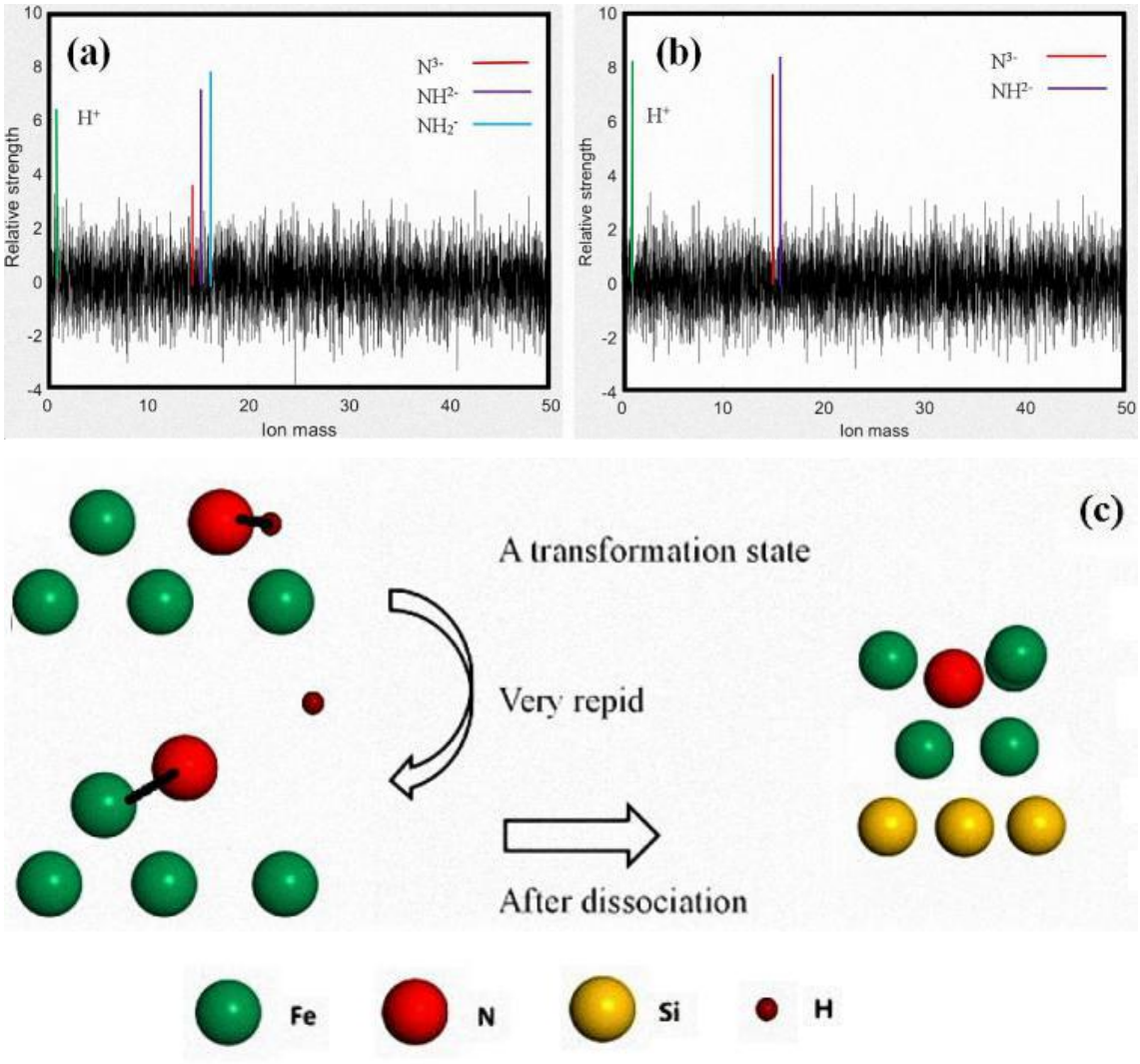

Fig. 4.14 (a) and (b): Mass spectra images of NH_3, detected in the nitriding process of Figs 4.6 and 4.10. (c) The model of adsorption process of NH_3, including a transformation state.

Aim to further enhance the magnetism of each iron compound, nitridation has become the key to the future development. The design of thin film magnetic materials capable of storing information at the atomic level represents one of the far reaching goals of nanotechnology. The driving force making one-dimensional linear structure might be the magnetic force of iron/iron nitride compound. If so, it can be predicted that magnetic storage unit will no longer be limited to the current level. According to the result of the magnetic testing equipment, the sensitivity of the sample to the

magnetic field is obviously different. The original weak magnetic (pure Fe compounds), after the initial nitriding, has been strengthened. All the facts indicated the possibility of a reaction between Fe clusters and N^{x-}. Utilizing the mass spectrometer, CH_3OH adsorption model was proved above. Now, in the process of the NH_3 adsorption on the Si(111)-7×7-CH_3OH-Fe, the similar data was detected:

$$CH_3OH = CH_3O^- + H^+ \quad (2)$$

$$NH_3 = NH_2^- + H^+ = NH^{2-} + 2H^+ = N^{3-} + 3H^+ \quad (3)$$

$$Fe_x \rightarrow Fe_xNH_2 \rightarrow Fe_xNH \rightarrow Fe_xN \quad (4)$$

Just as figures shown, the dissociation process/efficiency of ammonia can be detected gradually. The key to the formation of iron-nitride is sufficient N ions. When the iron layer is too thick (like Fig.4.9 (a)), we can only find a small number of N ions. The dissociation products of NH_3 are mainly NH_2^- or NH^{2-}. After adjusting the thickness, as the proportion of NH_2^- / NH^{2-} decreases obviously, the intensity of N ion and H ion increases. One of the most remarkable features is that there was almost no sign of the NH_2^-. It can be proved that a transformation state exactly divides the nitrification process of ammonia into two parts. That is, before and after the breaking of N-H bonds (Fig. 4.14 (c)) [17]. Ammonia does have a similar transformation model like methanol [18-21], that is, NH_3 first adsorbed at lower sites of Fe layer. Under the catalysis of the quasi-layer, ammonia is dissociated efficiently. After breaking the bond, N atom would rise to the top surface and be fixed with Fe-adatoms, forming iron-nitride.

4.7 Analysis of the relationship between magnetism and structure

4.7.1 Investigation on magnetism of nanoclusters

The chemical and physical properties of the atomic level materials have changed dramatically [22, 23]. Nevertheless, solid magnetic ordering theory has great reference value for explaining the magnetic properties of clusters. In 1936, Stoner used his energy band model to study the ferromagnetism of metals [24, 25]. He regarded 3d electrons as semi-local electrons and assumed that spin splitting takes place in the energy band under the exchange action. Thus, the stable conditions for ferromagnetism at absolute zero are given:

$$I \times D(E_F) > 1 \qquad (5)$$

Among them, I is the coulomb interaction energy between atoms. D (E_F) is the state density near the Fermi surface, which is inversely proportional to the bandwidth W of the band. If the state density in formula (4) is replaced by the local density of states, it can be used to determine the ferromagnetism of clusters. In general, the coulomb interaction energy between the transition metal atoms is around 1 eV. However, the state density near the Fermi surface depends largely on the local environment of the atom. The distribution of electron spin density near Fermi surface can be changed by changing the local environment of atoms, so that the magnetic properties of clusters can be controlled. For the local density of states, it can be roughly measured by $1/\sqrt{Z}$. Therefore, compared with bulk materials, low-dimensional systems such as surfaces and clusters are more likely to exhibit magnetic order.

Stoner criterion is derived from Pauli incompatibility principle [26]. It states that two electrons occupying the same orbit cannot have the same spin. It states that two electrons occupying the same orbit cannot have the same spin. Therefore, spin-parallel electrons should stay away from each other, which reduces the coulomb energy and

produces ferromagnetic alignment in atoms. Pauli incompatibility principle is also applicable to the interaction between atoms, resulting in the arrangement of ferromagnetic (FM) or antiferromagnetic (AFM) distances. There are many interesting performs of interaction between atoms, such as direct exchange, superexchange, double exchange and RKKY exchange. It can play a major role in the length range of several atoms or even several nanometers. At the same time, it can cause the transformation of ferromagnetic-antiferromagnetic state, the non-linear magnetic structure and the phenomena of domain or domain wall.

In clusters, d electrons and other electrons jump from atom to atom as their motion is limited by the space. This jump is equivalent to the hybridization of the electron wave function, which reduces the total energy of the system. Electrons are bound around a single atom, which is equivalent to electrons moving in an infinite deep potential well of length B. The kinetic energy is proportional to $1/b^2$. The hopping of electrons between adjacent atoms is equivalent to increasing the length of potential well b, thus reducing the kinetic energy of electrons. When the two atoms are far apart, the electron wave functions do not overlap. When two atoms are close to each other, the wave functions of them overlap, and the tight-bound Hamiltonian (H) produced is:

$$H = \begin{pmatrix} E_0, & t \\ t, & E_0 \end{pmatrix} \qquad (6)$$

Among them, E_0 is the orbital energy when there is no interaction between atoms. t is the hopping integral.

4.7.2 Study on the formation of magnetic units

As can be seen from the phase diagram of iron and nitrogen, various iron-nitride structures will be generated at different temperatures and nitrogen concentration. And they can change from one another to another. Reasonably, it can be found body-centered cubic, face-centered cubic and dense hexagonal structures at lower

temperature. In this experiment, nitrogen ions dissociated from ammonia gas are used to nitride-iron clusters, forming iron nitride. The specific process mainly includes the dissociation of ammonia, the interfacial reaction and the diffusion of nitrogen atoms. The ammonia gas on the surface of the Fe layer (atomic level) is very unstable. Like a catalyst, Fe atom further promotes the dissociation of ammonia. The process model is shown in the figure.

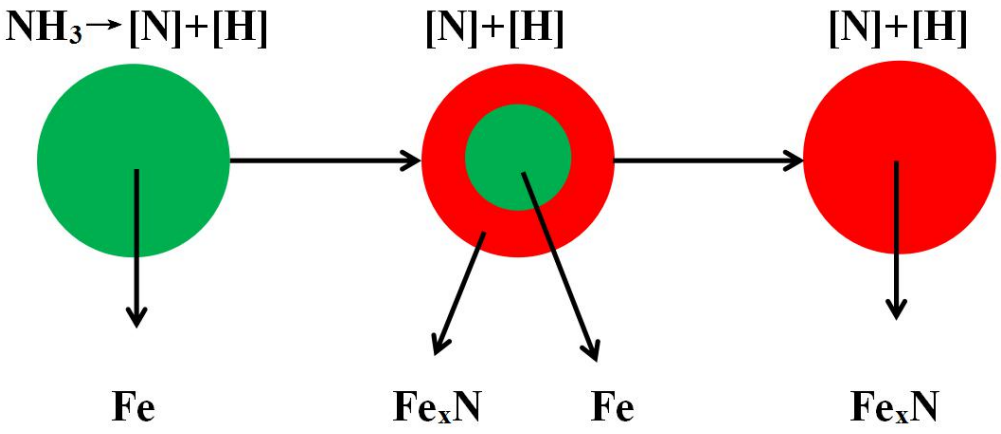

Fig. 4.15 The model of dissociation and nitridation processes of NH3.

(1) The dissociation of Ammonia

The dissociation of ammonia requires a high activation energy [27, 28], which can be greatly reduced under the catalysis of iron. So, iron is both reactant and catalyst in the whole reaction process.

(2) Interfacial reaction

Reactive nitrogen atoms dissociated from ammonia would react with iron at the interface:

$$Fe + [N] \rightarrow Fe(N) \quad (7)$$
$$4Fe + [N] \rightarrow Fe_4N \quad (8)$$
$$3Fe + [N] \rightarrow Fe_3N \quad (9)$$
$$2Fe + [N] \rightarrow Fe_2N \quad (10)$$

Whether the nitriding environment meets the dynamic conditions will determine

these reactions can be carried out or not. A certain nitrogen potential can be obtained by controlling the concentration of ammonia. This potential determines the dynamic of nitrogen at equilibrium, and well as the reaction product. Under the condition of different ammonia content, different structures of iron nitride can be obtained when the equilibrium is reached.

(3) The diffusion process

When nitrogen atom reaches the iron surface, it will cause a dynamic imbalance. Since there is already a difference in the concentration of nitrogen between the surface and inside of the iron, the N ion tends to move from higher concentration to the lower concentration. Whether the iron layer can be permeated completely is a key problem in the preparation of iron-nitride, which involves the relationship between the structure of iron clusters and the actual depth of the penetration.

4.7.3 Analysis of magnetic results

Ferromagnets consist of small magnets called domains. In a certain size range, magnetic domains are clustered by parallel or antiparallel magnetic units, so as to have magnetization spontaneously. However, the formation of metal compounds on the Si(111)-7×7 surface is a typical case, that is, if an elementary reaction involves a precursor state, the feature of chemical reaction is difficult to explain without the precursor state. Therefore, a quasi-compound process which enables the substitution of individual adsorbate metal atoms into the intrinsic adatom sites was explored in this paper. Each domain is separated by its domain wall. Due to the surface effect, interface effect and small size (dimension) effect, the properties of nano-scale metallic magnetic layers are obviously different from those of bulk magnetic materials. The source of magnetism is interpreted as the direct exchange interaction in the process of connecting adjacent Fe/FeN islands. It can be seen from the above reports that the thickness of nanoclusters must reach a certain critical value to form a stable magnetic structure. Therefore, the shape, size, structure and distribution of our Fe atoms have

important effects on the magnetization of thin films [29, 30].

As the main part of information industry, the research of magnetic recording materials has attracted much attention. Increasing the density and speed of magnetic recording is the common goal of researchers. Reducing the size of metallic clusters in magnetic recording medium is one of the effective ways to improve the density of magnetic storage. Therefore, the size of existing magnetic particles is developing from micron to nanometer. Research shows that iron-nitride can be used for magnetic storage materials because of its high coercivity and mild saturation magnetization.. Relative to the vertical direction of Figure 4.10 (b), Figure 4.16 (a) is the test result of the horizontal direction of Fe cluster. There is no obvious difference between the horizontal and the vertical in the sharp triangle structure. The magnetic intensity of Fe magnetic films nitrided in NH_3 atmosphere should be improved to a certain extent. It may be that the grain orientation has been optimized by nitriding process, and the magnetic moments of each domain are arranged in an orderly direction towards the external magnetic field. In addition, the nitrided Fe exhibits some characteristics of hard magnetic materials with high coercivity and remanence, which may be related to the orientation of grains in mesoporous channels. That is, there are obvious differences in growth patterns and speeds between the two directions. After nitriding, the symmetry of the magnetic unit was destroyed. There is a significant difference in magnetic intensity between the horizontal and vertical directions as shown in Fig. 4.16 (b). Further research on the nitrified iron film has found that it has a magnetic anisotropic. It tends to exhibit uniaxial anisotropy when the thickness is relatively thin. While the cubic anisotropic is found if the thickness increases.

More magnetic tests were performed, as shown in tables 4.2 and 4.3, we carried on the comparative analysis. On the one hand, the thickness of iron atom layer can obviously affect the nitriding efficiency. Thus, with the increase of nitriding efficiency, the magnetic strength increases. On the other hand, the magnetic durability of iron nitride is higher than that of iron clusters. With the increase of nitriding efficiency, the magnetic stability is also improved. Overall comparison, horizontal magnetism guarantees linearity and vertical magnetism guarantees practicability. In terms of

magnetic stability, there is a direct relationship between horizontal and vertical directions. In terms of remanence, there is no significant correlation between horizontal and vertical directions.

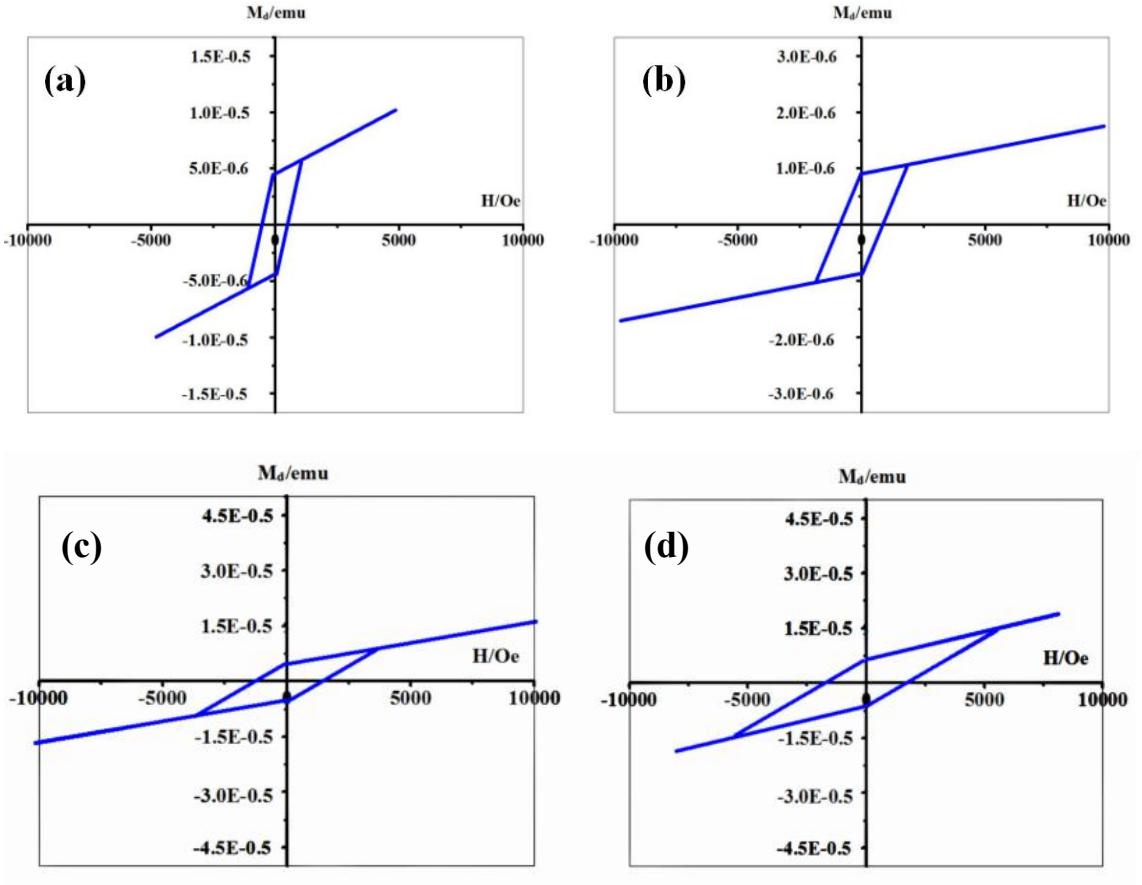

Fig. 4.16 The MPMS results of: (a) Si(111)-CH_3OH-Fe (10 ML), whose magnetic unit is symmetrical; (b) Si(111)-CH_3OH-FeN (4 ML), whose magnetic unit is asymmetric; (c) and (d) are two results of Si(111)-CH_3OH-FeN (2 ML): in horizontal direction and in vertical direction.

Table. 4.2 Comparison of magnetic parameters of different types of magnetic units (in horizontal direction)

	10 ML Fe	4 ML FeN	2 ML FeN
Brm (E-0.6 emu)	4.5	1.5	5
Hc ($\times 10^3$ Oe)	1.2	1.1	1.6

Table. 4.3 Comparison of magnetic parameters of different types of magnetic

units (in vertical direction)

	10 ML Fe	4 ML FeN	2 ML FeN
Brm (E-0.6 emu)	6	7	6.7
Hc ($\times 10^3$ Oe)	0.5	1.7	2

4.8 Stability verification for large-scale application

Mono-atom magnets represent the theoretical limit of current high density storage, that is, each atom represents a byte. Researchers mainly focus on how to optimize the magnetic properties of small atoms/clusters randomly distributed on the substrate. There is also much debate about which storage medium (i.e., which atom to use) and how to record them. As we mentioned above, different scientists choose to study different atoms, and it is impossible to define what is better or worse at present. Although atomic storage technology represents a big improvement of existing storage technology, it is still difficult to be popularized and applied at present. Specifically, the key challenge of using cluster arrays as data storage devices is to ensure magnetic stability. Secondly, the interaction between units should be avoided as far as possible, since it will lead to the confusion of data. In addition, due to the extreme instability of atomic-level function at room temperature and pressure, the cost of controlling atoms is much higher. The magnetic stability of existing clusters is limited below ultra-low temperature and is extremely sensitive to impurities [31, 32], so we have to complete the experiment in ultra-vacuum environment. In the future, we will further improve the structural properties of magnetic clusters. The researchers plan to increase the critical temperature for magnetic stability by finding the best combination of single atoms and substrates. If possible, we will use a coating to protect the atomic-level structure and ensure more stable magnetic atomic properties. Although atomic storage technology still has many constraints in application, compared with the current storage technology, it has made great progress in all aspects and pointed out the direction for the future development of storage technology. We look forward to further breakthroughs in atomic storage technology with the progress of science and

technology.

At last, the application of these magnetic clusters was verified. Some dimension measurements were carried out around the new linear structure. It can be found that heights of each cluster in the linear structure are basically maintained at a stable value. Besides, the width of linear structures was still controlled bellow 10 nm. After that, air was introduced into the observation chamber. Without the adverse effects of oxidation, the stability of iron-nitride clusters is surely better than that of pure iron clusters. After repeated scanning of XPS after air introduction, no peak represents N-O or Fe-O bond was found. From the viewpoint of Si peak (Fig. 4.17 (b)), in addition to the Si-Si bonds, some new Si-O bonds were newly found after exposed in the air environment. It can be proved that O_2 will react with Si rather than N or Fe. These interesting phenomena are worthy of our deep investigation and utilization, as well as the foundation for high-density magnetic storage application.

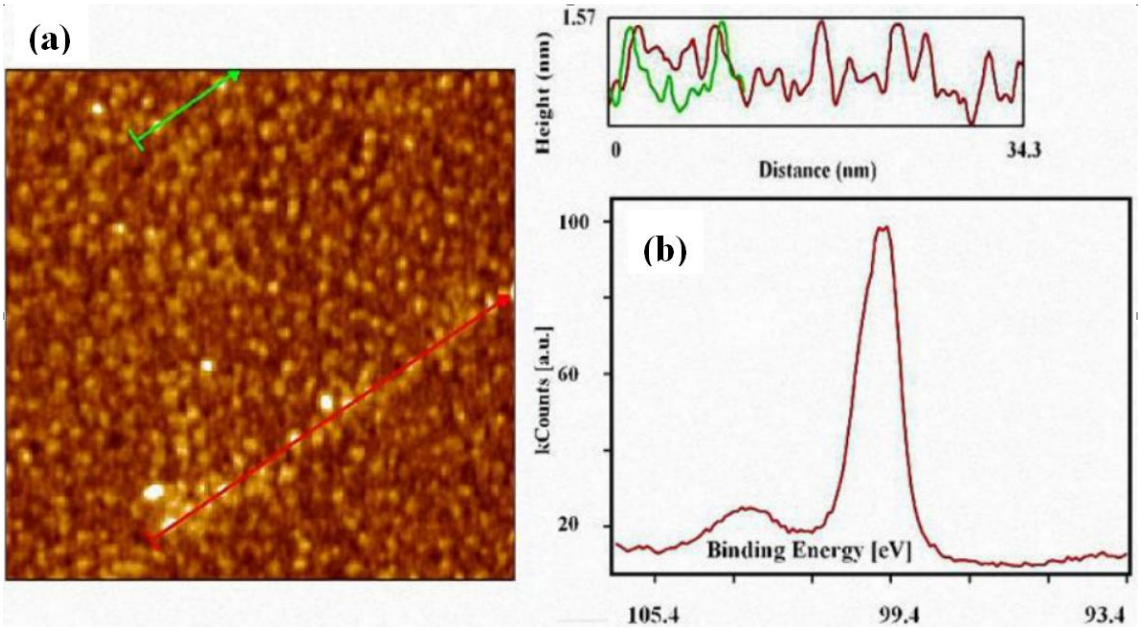

Fig. 4.17 (a) STM image of iron-nitride sample, exposed in air for 2 months, (b) is the XPS result of Si 2p after introduction of O_2.

Concluding remarks

In order to further enhance the magnetic strength, the samples were nitrided in this chapter. In the case of no obvious nitriding effect in the earlier stage, the dissociation efficiency of ammonia is greatly improved by reducing the thickness of Fe layer. With the deepening of nitriding degree, the nitriding structures of different stages were found and compared. In addition, compared with ordinary thin film materials, magnetic measurement of ultra-thin nanostructures must change from two-dimensional (unidirectional) to three-dimensional (bidirectional). The nitriding effect was verified by XPS experiment and magnetic comparison.

The results can be summarized as follows:

1. Two typical structures of iron-nitride have been proposed. With the increase of ammonia introduction time, the structure of the model changes, and the corresponding characteristics are also proposed.

2. Referring to the adsorption process of methanol, an intermediate model for ammonia is proposed.

3. The driving force making linear structures in Figures above should be the magnetic force (Fe or FeN). It is true that magnetic strength can be increased by nitriding.

4. In the vertical direction, the thickness still restricts the magnetic strength. How to maintain magnetic strength in thinner situation is our future expectation.

Reference

1 Le Roy, J. J., Ungur, L., Korobkov, I., Chibotaru, L. F., & Murugesu, M. (2014). Coupling Strategies to Enhance Single-Molecule Magnet Properties of Erbium–Cyclooctatetraenyl Complexes. Journal of the American Chemical Society, 136(22), 8003-8010.

2 Kauffmann-Weiss, S., Hamann, S., Gruner, M. E., Schultz, L., Ludwig, A., & Fähler, S. (2012). Enhancing magnetocrystalline anisotropy of the Fe70Pd30 magnetic shape memory alloy by adding Cu. Acta Materialia, 60(20), 6920-6930.

3 Tanaka, K. I., Yuan, Y., Xie, Z., Oyama, S. T., & He, H. (2019). A mini-review on the role of quasi-compounds in catalysis—The ammonia synthesis reaction on metals. Surface Science, 679, 264-272.

4 R. Raccichini, A. Varzi, S. Passerini, et al.The role of graphene for electrochemical energy storage, NAT MATER (2017) 14(3), 4170

5 P. P. Shi, Y. Y. Tang, P. F. Li , et al. Discovery of BF4 Molecular Ferroelectric Thin Film for Nonvolatile Low-Voltage Memories, J AM CHEM SOC (2017) 139(3): 1319-1324.

6 I. Buttinoni, J. Bialké, F. Kümmel, et al.Dynamical clustering and phase separation in suspensions of self-propelled colloidal particles, PHYS REV LETT (2013) 110(23), 238301.

7 D. Harvey, R. Massey, T. Kitching, et al. The nongravitational interactions of dark matter in colliding galaxy clusters, SCIENCE (2015) 347(6229): 1462-1465.

8 Lindley, M. W., Elias, D. P., Jones, B. F., & Pitman, K. C. (1979). The influence of hydrogen in the nitriding gas on the strength, structure and composition of reaction-sintered silicon nitride. Journal of Materials Science, 14(1), 70-85.

9 Musil, J., Vlček, J., & Růžička, M. (2000). Recent progress in plasma nitriding. Vacuum, 59(4), 940-951.

10 Hudis, M. (1973). Study of ion‐nitriding. Journal of Applied Physics, 44(4), 1489-1496.

11 Ritter, M., Stindtmann, M., Farle, M., & Baberschke, K. (1996). Nanostructuring of the Cu (001) surface by ion bombardment: a STM study. Surface science, 348(3), 243-252.

12 Girard, J. C., Samson, Y., Gauthier, S., Roussel, S., & Klein, J. (1994). STM study of the nucleation and annealing of ion bombardment induced defects on Cu (100). Surface science, 302(1-2), 73-80.

13 Gupta, M., Gupta, A., Chaudhari, S. M., Phase, D. M., Ganesan, V., Rao, M. R., ... & Dasannacharya, B. A. (2001). Microstructural study of iron nitride thin films deposited by ion beam sputtering. Vacuum, 60(4), 395-399.

14 Jiang, M., Li, Y., Lu, Z., Sun, X., & Duan, X. (2016). Binary nickel–iron nitride nanoarrays as bifunctional electrocatalysts for overall water splitting. Inorganic Chemistry Frontiers, 3(5), 630-634.

15 Meskinis, S., Andrulevicius, M., Kopustinskas, V., & Tamulevicius, S. (2005). XPS study of the ultrathin aC: H films deposited onto ion beam nitrided AISI 316 steel. Applied surface science, 249(1-4), 295-302.

16 Miola, E. J., de Souza, S. D., Nascente, P. A., Olzon-Dionysio, M., Olivieri, C. A., & Spinelli, D. (1999). Surface characterisation of plasma-nitrided iron by X-ray photoelectron spectroscopy. Applied surface science, 144, 272-277.

It shows different stages of nitriding process.

17 Xin Xu, C. Wang, Z-X. Xie, X. Lu, M. Chen, and K-I. Tanaka, Chem. Phys. Lett. 388 (2004) 190.

14 K-I. Tanaka, Y. Nomoto, and Z-X. Xie, J. Chem. Phys. 120 (2004) 4486

15 K-I. Tanaka and Z-X. Xie, J. Chem. Phys., 122 (2005) 054706

16 Z-X. Xie, Y. Uematsu, X. Lu, and K-I. Tanaka, Phys. Rev., B 66 (2002) 125306.

17 H-J. Liu, Z-X. Xie, H. Watanabe, J. Qu, and K.I. Tanaka, Phys. Rev. B 73 (2006) 165421

18 Yang, X. H., Wang, Y. F., Liu, A. P., Xin, H. Z., & Liu, J. C. (2005). Studies on magnetic nanomaterials by atomic force microscopy with high resolution. Modern Physics Letters B, 19(09n10), 469-472.

19 Chang, C., Wang, X., Bai, Y., & Liu, H. (2012). Applications of nanomaterials in enantioseparation and related techniques. TrAC Trends in Analytical Chemistry, 39, 195-206.

20 Stoner, E. C. (1936). Collective electron specific heat and spin paramagnetism in metals. Proc. R. Soc. Lond. A, 154(883), 656-678.

21 Stoner, E. C. (1938). Collective electron ferronmagnetism. Proc. R. Soc. Lond. A, 165(922), 372-414.

22 ZHANG, L. H., & AN, Y. (2005). The Qualitative Analysis of the Structure of the Magnetism Farmland as Source of the Minimum Energy Principle [J]. Journal of Hebei Institute of Technology, 3, 026.

23 Mocuta, D., Ahner, J., & Yates Jr, J. T. (1997). Adsorption and electron-stimulated dissociation of ammonia on Cu (110): an ESDIAD study. Surface science, 383(2-3), 299-307.

24 Liu, R., Shen, W., Zhang, J., & Li, M. (2008). Adsorption and dissociation of ammonia on Au (1 1 1) surface: A density functional theory study. Applied Surface Science, 254(18), 5706-5710.

25 Jensen, P. J., & Bennemann, K. H. (1990). Direction of the magnetization of thin films and sandwiches as a function of temperature. Physical Review B, 42(1), 849.

26 Ramesh, R., & Spaldin, N. A. (2010). Multiferroics: progress and prospects in thin films. In Nanoscience And Technology: A Collection of Reviews from Nature Journals (pp. 20-28).

31 Navio, C., Alvarez, J., Capitan, M. J., Yndurain, F., & Miranda, R. (2008). Nonmagnetic γ″-FeN thin films epitaxially grown on Cu (001): Electronic structure and thermal stability. Physical Review B, 78(15), 155417.

32 Houari, A., Matar, S. F., Belkhir, M. A., & Nakhl, M. (2007). Structural stability and magnetism of FeN from first principles. Physical Review B, 75(6), 064420.

Chapter 5 Conclusions and recommendation

5.1 Conclusions

The development of high density magnetic memory (film) materials undoubtedly has a significant value in the application market. On the surface of Si(111)-7×7, a great deal of work is required to promote the structural properties of magnetic storage unit. Scientists have known that atoms on the ladder region are particularly active. Since not completely surrounded by atoms that make up a flat terraced structure, they are more likely to interact with themselves. Although the previous linear structures were very attractive, most of them appeared accidentally in the ladder region of surface. Originally, CH_3OH was used as an intermediate layer to prevent the Fe atoms from reacting with silicon, reserving their strong magnetic property. In this paper, the comparative analysis of various compounds is very important. The formation of metallic compound on the Si(111) substrate is a typical case, that is, different metal atoms will form different types of compounds. Although previous metallic clusters were very attractive, there was still much room for improvement after the intermediate layer was introduced. Since the study of gas adsorption was still in the initial stage, the specific models of alcohols were put forward in this paper. From a perspective of stereoscopic thinking, the characteristics of methanol were explored in two directions. In the vertical direction, the effect of methanol is mainly displayed by CH_3O^-. As can be seen from the data of the height measurement and XPS, methanol can exactly prevent the iron atom forming Fe-Si compound. However, for some dynamic atoms (like Sn and Zn), CH_3O^- can only play an effective limiting role. In the horizontal direction, the temperature parameter was introduced. After a series of preheating experiments at low temperature, the importance of the horizontal characteristic (represented by H^+) was proposed. Using the dual characteristics of CH_3OH, our emphasis was further placed on the changes in the adsorption positions of metal atoms. Accordingly, several metal-H^+ models were derived to promote the

most favorable formation process of metallic compounds. Meanwhile, some complicated questions (like Sn before) were explained. In fact, only when the vertical and horizontal characteristics are combined can regular atomic structures be formed better.

The more regularity, the higher probability of application. The question of how to improve the stability of linear Fe cluster structure has become the focus of our work in recent years. Firstly, the thermal stability of methanol was used to adjust the adsorption ratio of center/corner sites. Afterwards, an intermediate layer model could be established to find the most favorable adsorption sites of Fe clusters. Furthermore, with the increase of evaporation temperature, a double-layer cluster model was successfully found. In the corresponding temperature range, a new structural model of the Fe clusters is basically consistent with the situation of face centered cubic unit cell. The Fe cluster is stabilized by the interaction with Si ad-atoms with a dangling bond remained on the Si(111)-7×7-CH_3OH surface. Specific adsorption positions often correspond to specific cluster structures. The XPS results showed that the Fe clusters were stable in the thin-air condition at room temperature. When the deposition of Fe atoms was increased, linear Fe clusters were formed and underwent one-dimensional self-assembly crossing the step onto the upper or lower terrace. The driving force making one-dimensional linked straight chain structure might be the magnetic force of Fe clusters. If so, the Fe cluster takes single magnetic domain with about 5 nm of critical size, and we could expect to lower the single magnetic domain to ca. 10 nm without a change to the super paramagnetic property. With the help of MPMS-7T, the magnetization was measured as an important application parameter. Although not strong, the ferromagnetism does exist with the easy magnetization axis in the horizontal direction of the substrate. Moreover, the relationship between linearity and magnetic intensity should be deduced.

As a periodic result, the stability and linearity of iron clusters on silicon surface have been greatly improved, accelerating the pace of the application of nanoscale magnetic storage. On this basis, utilizing STM device and several functional measurements (like magnetic intensity measurement), we will further improve the

application property of storage units on Si(111)-7×7 surface. Some nitriding experiments have been explored on the existing Fe clusters, thus greatly enhancing the magnetic properties of the storage units. Inspired by the first breaking mechanism of alcohols, NH_3 was selected as the nitrogen gas. With the increasing of ammonia concentration, the new linear iron-nitride clusters can also be formed. During nitriding process, a great deal of work was required to promote the structural properties of iron-nitride. As an important exploration, the concept of transition state in the adsorption process was proposed. The relevant model not only explains the detailed process of methanol adsorption, but also provides an important reference for the nitriding process. In order to solve the problems of poor linearity and weak magnetic intensity, this paper mainly carried on the optimization from the thickness of Fe layer. By introducing Ar into the steaming stage, the efficiency of NH_3 dissociation was greatly increased as well as the linearity. After that, two typical models of iron-nitride are proved. So, the weak interaction of N atom on the iron atoms in each model is also investigated. When the number of iron atoms is fixed, N^{3-} will effectively play its weak role, which is directly represented by the change of cluster’s shape. Finally, to speed up the pace of application, the regularity of these linear structures was investigated. Results show that the stability of iron-nitride cluster is perfect. Even in the condition of thin air, the performance of our samples is perfect. Overall, metal nitride has robust bonding between metal and nitrogen atoms. Based on the current results, the Fe cluster is hopefully to synthesize the strong magnetic FeN_X particles with less than 10 nm of critical size in the future.

5.2 Recommendation

The study of nanostructures, especially magnetic low-dimensional systems, is one of the most interesting problems in modern condensed matter physics. Because of its unique properties, magnetic nanoparticles have become one of the promising next generation ultra-high density magnetic storage media. At the same time, it can also be used as an excellent candidate for magnetic sensors. In recent years, people have made extensive research on the theory of micromagnetism, preparation methods and properties of materials. Magnetic storage has become an important means of modern information storage. Accordingly, increasing the surface density of magnetic memory and shortening the reading and writing reaction time have become the problems that need to be solved continuously in the research of magnetics and magnetic materials. In terms of improving storage density, metal steaming technology is the most promising next generation breakthrough technology after vertical recording mode. The basic unit of storage medium is selected and prepared as nano magnetic particles. In this paper, iron clusters and their nitrides are chosen as research objects, and the transformation state of them is mainly studied. The influence of shape anisotropy on magnetization inversion is studied by analyzing and establishing various models, hoping to provide useful guidance for future lattice medium technology. On this basis, a variety of magnetic particle arrays have been extensively studied. With the preparation and scanning of the atomic level microscopic systems, the unique magnetic properties of magnetic nanoparticle arrays have been found. In this field, not only high basic research value, but also wide practical application value can be found, such as high density magnetic storage, magnetic catalysis and sensors. Based on the current results, the Fe_3N_x cluster is hopefully to synthesize the strong magnetic unit with 5 nm of critical size in the future. Finally, from the point of higher-density magnetic storage, it is interesting to prepare the linear Fe_4N_x clusters with a critical size lower than 10 nm. The present work reveals a simple way to realize it as well as the physicochemical mechanism behind it.

Related publications

1. Li, W., Ding, W., Ju, D., Tanaka, K. I., & Komori, F. (2018). Study on Formation Process and Models of Linear Fe Cluster Structure on a Si (111)-7×7-CH3OH Surface. Materials, 11(9), 1593.
2. Li, W., Ju, D. (2019). Explore the dual characteristics of alcohols to the metallic compounds on Si(111)-7×7 surface. International Journal of Science, accept.
3. Li, W., Ding, W., Ju, D., & Tanaka, K. I. (2017). Study on the formation of Fe ultrathin nanostructure on Si(111)7×7 surface, Taiwan Association for Coatings and Thin films Technology (TACT) 2017 International Thin Films Conference, B-O-517.
4. Li, W., Ding, W., Ju, D., & Tanaka, K. I. (2018). The effect of reactant gas on the atom adsorption of Si (111) substrate, 25th Congress of International Federation for Heat Treatment and Surface Engineering (IFHTSE), P-402.

Acknowledgments

I would like to express my sincere appreciations to Prof.Dr. Dongying Ju, for taking me as his student and giving me the opportunity to pursue the Ph.D. degree at Saitama Institute of Technology. I want to express my sincere thanks for his support, encouragement and guidance throughout my study. Without his support I could not have achieved so much.

I would like to appreciate the exchange program between Saitama Institute Technology in Japan and Hangzhou Dianzi University, China. And I would like to express my sincere gratitude to all the people who have provided information to me for giving me the chance to study abroad.

I would like to thank Prof. Komori, Prof. Negishi, Prof. Uchida and Prof. Sato for sparing time from their busy schedules in reviewing my dissertation and their advisable comments for revising the paper. Without their help, I couldn't have understood the research deeply.

I would also like to thank Prof. Komori and Prof. Iimori for helping me complete the experiments about LEED, XPS and MPMS. With their help, the research reached to a higher level. What's more, I would also like to express my acknowledgement to Pro.f Tanaka for the most important instruction and discussion of the issues.

My thanks also go to all the members of Ju laboratory. I would like to sincerely gratitude all the relatives who have encouraged and supported me to pursue the Ph.D.. Especially, I would like to thank our five visiting scholars (G., D., X., Z. and L.) for give me precious suggestions.

Finally, my deep appreciation is due to my parents for their love, support and encouragement throughout my study and graduate work.